SINTEF

SINTEF A17561 - Unrestricted

Report

SECOMAS

Final report from the project Spectral Efficient Communications for Aeronautical Services (SECOMAS) - Technical

Author(s)
Jan Erik Håkegård
Tor Andre Myrvoll, Bengt Holter

SINTEF ICT
Communication Systems
2011-01-07

SINTEF ICT
Address:
Postboks 4760 Sluppen
7465 Trondheim

Telephone: 73593000
Direct line: 73597541
Telefax: 73591039

postmottak.IKT@sintef.no
www.sintef.no
Enterprise /VAT No:
NO 948 007 029 MVA

Report

SECOMAS

Final report from the project Spectral Efficient Communications for Aeronautical Services (SECOMAS) - Technical

KEYWORDS:
Aeronautical communication

VERSION
1.0

DATE
2011-01-07

AUTHOR(S)
Jan Erik Håkegård
Tor Andre Myrvoll, Bengt Holter

OPPDRAGSGIVER(E)
Norwegian Research Council

OPPDRAGSGIVERS REF.
180018

PROJECT NO:
90F246

NUMBER OF PAGES/APPENDICIES:
67+ Appendicies

ABSTRACT

Abstract

SECOMAS was a research project running from January 2007 to December 2010 targeting spectral efficient communications for aeronautical services. The Research partners of the project were SINTEF and NTNU, and the project was funded by the Norwegian Research Council and members of the Norwegian ATM industry (AVINOR, Jotron, KDC, Thales Norway and NGPAS).

This report contains three technical notes written during the project period and three conference papers. Together these notes and papers encompass the work done by SINTEF as part of SECOMAS. The work done by the Ph.D. student will be included in the Ph.D. report which is scheduled for June 2011.

The topics covered by this report are:

- An overview of current aeronautical CNS (Communications, Navigation, Surveillance) systems.
- HEO satellite communications for ATM in high latitudes
- Airport Surface Datalink Communications (Appendix A)
- MIMO techniques for air/ground communications (Appendix B)
-MIMO techniques for aeronautical satellite communications (Appendix C)

PROJECT MANAGER
Jan Erik Håkegård

SIGN

CHECKED BY
Vidar Ringset

SIGN

APPROVED BY (name, position)
Erik Kampenhøy

SIGN

REPORTNO. SINTEF A17561
ISBN 978-82-14-04969-5
CLASSIFICATION Unrestricted
CLASSIFICATION THIS PAGE Unrestricted

Document history

VERSION	DATE	VERSION DESCRIPTION
1.0	2011-01-07	Final version

Table of contents

APPENDICIES

Appendix A J.E. Håkegård, T.A. Myrvoll, "*Evaluation of downlink IEEE802.16e communications at airports*," in Proc. of Integrated Communications, Navigations and Surveillance Conference 2008, (ICNS 2008), Bethesda 5-7 May, 2008.

Appendix B B. Holter, J. E. Håkegård, and T. A. Myrvoll, *"On the use of MIMO in aeronautical communications,"* in Proc. 2nd ENRI International Workshop on ATM/CNS (EIWAC2010), Tokyo, Japan, November 2010.

Appendix C T. A. Myrvoll, J. E. Håkegård, and B. Holter, *"Aeronautical satellite propagation channel characteristics using multiple antennas,"* in Proc. 2nd ENRI International Workshop on ATM/CNS (EIWAC2010), Tokyo, Japan, November 2010.

SECOMAS

1 Introduction

SECOMAS was a four year project running from January 2007 until end of December 2010. It was a *Kompetansebyggende prosjekt med brukermedvirkning (KMB)* project funded partly by the Norwegian Air Traffic Management (ATM) industry and partly by the Norwegian Research Council. Active partners, i.e. partners doing research funded by the project, were SINTEF and NTNU. The industrial partners funding the project were Jotron, Northrop Grumman Park Air Systems, Thales Norway, Kongsberg Defence Communications and AVINOR. The industrial partners, except AVINOR and KDC, are members of ATM Forum Norway, and SECOMAS was the first project mounted by this interest organisation.

According to the project proposal, the main research goal of SECOMAS was to analyze and design key system components for use in promising transmission and networking schemes which can enable future spectrum-efficient aeronautical communications. This includes aeronautical satellite communications as well as aeronautical terrestrial communications when the aircraft is in air and on ground. The timing of the project was in line with the definition phase of the European SESAR (Single European Space ATM Research) program. This goal was kept during the execution of the project, which can be broadly divided into three phases.

The first phase consisted of research of existing aeronautical communication systems. This study included all frequency bands, and for completeness also navigation systems and surveillance systems were included. The results from this study are included in Chapter 2 and Chapter 3 of this report.

The second phase of the project targeted the three new datalink communication systems that are currently developed by SESAR. These systems are the L-band Digital Aeronautical Communication System (LDACS) for air/ground communications, satellite communications, and airport surface datalink communications. This stage started before the respective SESAR projects were initiated, and the goal was to achieve relevant and sufficient knowledge to participate in the definition phases of these projects. As a result of this phase, SINTEF has succeeded in participating in several SESAR and ESA projects related to future aeronautical communications. Chapter 4 of this report contains a study of the use of highly elliptical orbit (HEO) satellites to obtain good coverage in the high north, which is of particular interest for Norway. Chapter 5 (Appendix A) includes a publication evaluating the use of WiMAX technology for airport surface communication.

When the second phase activities of the project were continued in SESAR and ESA projects, SECOMAS went into a third phase that may be called “beyond SESAR”. In this phase, advanced techniques not included in SESAR were considered. The rationale for this was that the world will not end after the SESAR systems are implemented sometime around 2020-2025. The advanced topics considered in the third phase were all linked to the use of multiple antennas. The introduction of multiple antennas is seen in all kinds of wireless communication systems, as existing advanced coding and signal processing techniques exploit the frequency domain close to the theoretical limit. The only way to increase the capacity on physical level is then to add antennas and to exploit the spatial domain. Traditionally, the use of multiple antennas on aircraft was strongly opposed to by aircraft manufacturers like Airbus, as they would like to limit the number of holes to drill in the fuselage. However, lately multiple antenna techniques have started to emerge in the planning and

development of the future aeronautical communication systems. In Chapter 6 (Appendix B), the use of multiple antenna techniques for air/ground aeronautical communications is considered for a typical line-of-sight (LOS) air-to-ground propagation channel. In Chapter 7 (Appendix C), the use of multiple antennas for satellite communications at low elevation angles is assessed.

The work of the Ph.D. student at NTNU includes scheduling techniques. Hence, as the work presented in this report only considers one point-to-point connection, the NTNU work expands this to include the multi-link case. When several aircraft, each requiring a certain guarantee for successful communication, compete for limited bandwidth resources, new scheduling techniques are needed. The results of this work will be presented in the Ph.D. report due in June 2011.

2 Overview of current aeronautical communication systems

The purpose of this chapter is to give an overview of which frequency bands that are allocated to aeronautical services, and what they are used for. The services include communication, navigation and surveillance. A list of the frequency bands and systems is provided in Table 1.

	Band	Service	Type
1	90-110 kHz	Loran-C	Navigation
2	130-526.5 kHz	NDB	Navigation
3	2.850-22 MHz	HF COM	Communication
4	74.8-75.2 MHz	Marker Beacon	Navigation
5	108-111.975 MHz	ILS LOC/VOR +[GBAS]	Navigation
6	111.975-117.975 MHz	VOR + [GBAS]	Navigation
7	117.975-137 MHz	VHF COM	Communication
8	328.6-335.4 MHz	ILS GP	Navigation
9	406-406.1 MHz	ELT	Surveillance
10	960-1215 MHz	DME/GNSS	Navigation
11	1025-1040 MHz	SSR GA/ACAS	Surveillance
12	1084-1093 MHz	SSR AG/ACAS	Surveillance
13	1215-1400 MHz	PSR	Surveillance
14	1545-1555 MHz	SAT COM	Communication
15	1559-1610 MHz	GNSS + PSR	Navigation/Surveillance
16	1646.5-1656.5 MHz	SAT COM	Communication
17	2700-3100 MHz	PSR	Surveillance
18	4200-4400 MHz	RadioAlt	Navigation
19	5030-5150 MHz	MLS	Navigation
20	5091-5150 MHz	AeroMACS	Communication
20	5350-5470 MHz	Radar – weather	Surveillance
21	8750-8850 MHz	Radar – Doppler	Surveillance
22	9000-9500 MHz	ASDE	Surveillance
23	13.25-13.4 GHz	Radar - Doppler	Surveillance
24	15.4-16.6 GHz	ASDE	Surveillance
25	31.8-33.4 GHz	ASDE	Surveillance

Table 1 Aviation Frequency Bands

Aeronautical communication services are currently limited to three frequency bands:

- The HF band between 2850 kHz and 22 MHz
- The VHF band between 117.975 MHz and 137 MHz
- The L-band 960-1164 MHz for air-ground communications (LDACS)
- The L-bands 1545-1555 MHz and 1646.5-1656.5 MHz for satellite communications
- The C-band 5091-5150 MHz for airport surface datalink communications (AeroMACS)

The frequency bands 960-1164 MHz and 5091-5150 MHz were allocated to aeronautical mobile (R) services at WRC-07 (Resolution 417 and Resolution 418, respectively).These decisions have lead to considerable activity both in Europe and in the U.S. to develop new systems for these bands. LDACS is currently under development for air-ground communication in the L-band, and AeroMACS is under development for airport

communication in the C-band. In addition, the development a new satellite communication system for ATM is under consideration. All these three systems are currently under development within the SESAR program in Europe, in cooperation with other regions.

Frequency bands not allocated to aeronautical services may still be used by aeronautical communication services. Examples are unlicensed bands such as the 2.4 ISM band around airports, and leased capacity in communication satellites operating on other frequencies.

Navigation services can be grouped into radio beacons for *en route*, navigation aids for approach around airports, and satellite navigation with correction/augmentation signals.

- Radio beacons:
  - Non-directional beacons (NDBs) operate in the 130-526.5 kHz band
  - VHF Omnidirectional Radio (VOR) operates in the 111.975-117.975 MHz band.
  - Distance Measuring Equipment (DME) operates in the 960-1215 MHz band
- Approach:
  - Instrument landing system (ILS) with beacon markers operates in several bands between 74.8 MHz and 335.4 MHz
  - Microwave landing system (MLS) operates in the 5030-5150 MHz band
- Satellite navigation:
  - Correction messages for GPS is transmitted in the 90-110 kHz band using Loran-C
  - Ground Based Augmentation Systems (GBASs) transmit correction signals in the 108-118 MHz band
  - Satellite navigation systems transmit in the 960-1215 MHz and 1559-1610 MHz bands.

The following surveillance systems exist:

- Primary surveillance radar (PSR) transmitting in the 1215-1400 MHz, 1559-1646.5 MHz and 2700-3100 MHz bands
- Secondary Surveillance radar (SSR) transmitting in the 1025-1040 MHz and 1084-1093 MHz bands
- Airborne Collision Avoidance System (ACAS) operating in the same bands as SSR.
- Airport Surface Detection Equipment (ASDE) and weather and Doppler radars operating in bands between 5350 MHz and 33 GHz.

In the remaining parts of this chapter, the different aeronautical systems are briefly described.

2.1 Loran-C (90-110 kHz)

LORAN Data Channel (LDC) is a project underway between the FAA and the U.S. Coast Guard to send low bit rate data using the LORAN system. Messages to be sent include station identification, absolute time, and position correction messages. In 2001, data similar to Wide Area Augmentation System (WAAS) GPS correction messages were sent as part of a test of the Alaskan LORAN chain. As of November 2005, test messages using LDC were being broadcast from several U.S. LORAN stations.

For several years, LORAN-C has been used to send differential GPS and other messages using a similar method of transmission known as EUROFIX in Europe and 9th pulse in the US. This is done using enhanced Loran, also called eLoran. The most fundamental enhancement of eLoran compared to the traditional Loran is the ability to broadcast data to users.

2.2 NDB (30-526 kHz)

A Non-Directional Beacon (NDB) is a radio broadcast station in a known location, used as an aviation or marine navigational aid. Even with the advent of VOR systems (see Sec. 2.6) and GPS navigation, NDBs continue to be the most widely-used navigational aid worldwide. NDBs have one major advantage over the more sophisticated VOR: NDB signals follow the curvature of the earth, so they can be received at much greater distances at lower altitudes. However, the NDB signal is affected more by atmospheric conditions, mountainous terrain, coastal refraction and electrical storms, particularly at long range.

NDB navigation actually consists of two parts – the Automatic Direction Finding (ADF) equipment on the aircraft that detects an NDB's signal, and the NDB transmitter itself. ADF equipment determines the direction to the NDB station relative to the aircraft. This may be displayed on a relative bearing indicator (RBI). This display looks like a compass card with a needle superimposed, except that the card is fixed with the 0 degree position corresponding to the centreline of the aircraft.

NDBs may designate the starting area for an ILS (see Sec. 2.5) approach or a path to follow for a standard terminal arrival procedure (STAR). In the United States, an NDB is often combined with the outer marker beacon in the ILS approach (called a Locator Outer Marker (LOM)). In Canada, low-powered NDBs have replaced marker beacons entirely.

Apart from Morse Code Identity of either 400Hz or 1020Hz, the NDB may broadcast Airfield Terminal Information Service (ATIS), Airfield Weather Information Service (AWIS), or, in an emergency i.e. Air-Ground-Air Communication failure, an Air Traffic Controller using a Press-To-Talk (PTT) function, may modulate the carrier with voice. The pilot uses their ADF receiver to hear instructions from the Tower.

2.3 HF COM (2.85-22 MHz)

Within the high frequency (HF) band, both analogue voice and digital data services are available. Services are operated on 3 kHz wide channels in the frequency bands between 2.85 MHz and 22 MHz.

HF single side band (SSB) voice is among the oldest forms of aeronautical mobile radio communications. It supports ATS voice communication exchanges in oceanic and remote regions between aircraft and air traffic control centres or flight service stations. In addition it is used for aeronautical operational control (AOC) between aircraft and airline operations centres. HF SSB voice enables very long-range communications extending up to several thousand kilometres, but it is affected by solar activity and other natural phenomena. Range and intelligibility may vary, and at times some frequencies are unusable. In general, specially trained radio operators and experienced pilots are needed to make effective use of this system. Service providers in the various regions typically share families of frequencies distributed among sub-bands to provide frequency and range diversity, and to vary capacity and provide redundant communications paths. HF SSB voice remains the primary communications link for long-range procedural air traffic control.

In the 1990s, the airline industry sought ways to improve HF communications. A successor to a military design, the HF data link (HFDL) was developed for use in the aeronautical HF band and thus makes use of the same frequencies and equipment as HF voice. It operates in the same 3 kHz channels with a single side band digital modulation scheme, providing up to 2.4 kilobits per second data throughput. HFDL is less sensitive to varying propagation conditions than is HF voice because it is automatically adaptive both in radio frequency and data rate and it includes extensive error detection and correction algorithms in the protocol. This system uses a bit-oriented data protocol designed to function as a sub-network of the ATN. In order to be compatible with present airline data communications infrastructures, it also supports character oriented ACARS messages. HFDL provides an average transfer delay of 75 seconds and a 95th percentile delay of 200 seconds. It is presently used for AOC applications globally. It is also being used in pre-operational trials for ATS applications in the North Pacific and North Atlantic. Several studies indicate that

HFDL can also be a backup to satellite communications, notably in Polar Regions where geostationary satellites have reduced or no coverage.

2.4 Marker beacon (74.8-75.2 MHz)

A marker beacon is a beacon used in conjunction with an ILS (see Sec. 2.5) to give pilots a means to determine distance to the runway. There are three types of marker beacons on an ILS.

2.4.1 Outer marker

The Outer Marker, which normally identifies the Final Approach Fix, is situated on the same line with the localizer and the runway centreline, four to seven miles before the runway. It is typically located about 1 nautical mile inside the point where the glide slope intercepts the intermediate altitude and transmits low-powered (3 W), 400 Hz tone signal on a 75 MHz carrier frequency. Its antenna is highly directional, and is pointed straight up. The valid signal area is 2,400 ft by 4,200 ft ellipse (as measured 1000 ft above the antenna.) When the aircraft passes over the outer marker antenna, its marker beacon receiver detects the signal. The system gives the pilot a visual (blinking blue outer marker light) and aural (continuous series of audio tone Morse code 'dashes') indication. Some countries, such as Canada, have abandoned marker beacons completely, replacing the outer marker with a NDB. In the United States, the outer marker will often be combined with an NDB to make a LOM. Some ILS approaches have no navigation aid at all situated at the outer marker, but use other means, such as radial intersections or DME fixes, to identify the position.

2.4.2 Middle marker

A middle marker works on the same principle as an outer marker. It is normally positioned 0.5 to 0.8 miles before the runway. When the aircraft is above the middle marker, the receiver's yellow middle marker light starts blinking, and a repeating pattern of audio Morse code dot-dashes at a frequency of 1,300 Hz in the headset. This is intended as an annunciator for the pilot, an alert that the missed approach point (typically 200 feet above ground level (AGL) on the glide slope) has been passed and should have already initiated the missed approach if one of several visual cues has not been spotted. Middle Markers are typically associated with Category II or III approaches.

2.4.3 Inner marker

Similar to the outer and middle markers; located at the beginning (threshold) of the runway on some ILS approach systems (Category II and III) having decision heights of less than 200 feet AGL. Triggers a flashing white light on the same marker beacon receiver used for the outer and middle markers; also a series of audio tone 'dots' at a frequency of 3,000 Hz in the headset.

2.4.4 Fan marker

A fan marker can be used for a final approach fix on an ILS back course. It is located in a location similar to the outer marker only on the back course or opposite end of the runway. A fan marker on a back course lights the white light and emits a series of audio tone 'dots' at a frequency of 3,000 Hz in the headset.

DMEs (see Sec. 2.10) are replacing markers in many installations. This provides more accurate and continuous monitoring of correct progress on the ILS to the pilot, and does not require an installation outside the airport boundary. The DME is frequency paired with the ILS so that it is automatically selected when the ILS is tuned. It gives pilots the exact measurement of distance to the runway usually in miles.

2.5 ILS (LOC:108-111.975 MHz and GP:328.6-335.4 MHz)

The Instrument Landing System (ILS) is an instrument approach system which provides precise guidance to an aircraft approaching a runway and in the case of one type of Category III approach, it also provides guidance along the runway surface.

An ILS consists of two independent sub-systems, one providing lateral guidance (Localizer), the other vertical guidance (Glideslope or GlidePath) to aircraft approaching a runway. The emission patterns of the localizer and glideslope signals are as follows.

2.5.1 Localizer (LOC in the U.S. and LLZ in Europe)

A localizer (LOC, or LLZ in Europe) antenna array is normally located beyond the departure end of the runway and generally consists of several pairs of directional antennas. Two signals are transmitted on a carrier frequency between 108 MHz and 111.975 MHz. One is modulated at 90 Hz, the other at 150 Hz and these are transmitted from separate but co-located antennas. Each antenna transmits a fairly narrow beam, one slightly to the left of the runway centreline, the other to the right. The localizer receiver on the aircraft measures the Difference in the Depth of Modulation (DDM) of the 90 Hz and 150 Hz signals. For the localizer, the depth of modulation for each of the modulating frequencies is 20 percent. The difference between the two signals varies depending on the position of the approaching aircraft from the centreline. If there is a predominance of either 90Hz or 150Hz modulation, the aircraft is off the centreline. In the cockpit, the needle on the Horizontal Situation Indicator, or HSI (The Instrument part of the ILS), will show that the aircraft needs to fly left or right to correct the positional error to fly down the centre of the runway. If the DDM is zero the receiver aerial and therefore, the aircraft, is on the centreline of the localizer coinciding with the physical runway centreline.

2.5.2 Glide Path (GP)

A glide slope or glide path (GP) antenna array is sited to one side of the runway touchdown zone. The GP signal is transmitted on a carrier frequency between 328.6 MHz and 335.4 MHz using a technique similar to that of the localizer, the centreline of the glide slope signal being arranged to define a glide slope at approximately 3° above the horizontal. Localizer and glide slope carrier frequencies are paired so that only one selection is required to tune both receivers. These signals are displayed on an instrument in the cockpit. The pilot controls the aircraft so that the indications on the instrument remain centred on the display. This ensures the aircraft is following the ILS centreline. Some aircraft possess the ability to route signals into the autopilot, which allows the approach to be flown automatically by the autopilot.

2.6 VOR (111.975-117.975 MHz)

VHF Omni-directional Radio Range (VOR) broadcasts a VHF radio composite signal including the station's Morse-code identifier (and sometimes a voice identifier), and data that allows the airborne receiving equipment to derive the magnetic bearing from the station to the aircraft (direction from the VOR station in relation to the earth's magnetic North). This line of position is called the "radial" in VOR parlance. The intersection of two radials from different VOR stations on a chart allows for a "fix" or specific position of the aircraft.

VORs provides considerably greater accuracy and reliability than NDBs due to a combination of factors in their construction such as less course bending around terrain features and coastlines, and less interference from thunderstorms. Although VOR transmitters are more expensive to install and maintain (as was the airborne equipment, initially), today VOR has almost entirely replaced the low/medium frequency ranges and beacons in civilian aviation. It is also in the process of being supplanted by GPS. Because of their VHF frequency, VOR stations rely on line-of-sight. This limits VOR (and DME) range to the horizon or closer if mountains intervene. This means that an extensive network of stations is needed to provide reasonable coverage along main air routes. The VOR network is a significant cost in operating the current airway system, although the modern solid state transmitting equipment requires much less maintenance than the older units.

In many cases the VOR stations have co-located DME or military TACAN (TACtical Air Navigation, which includes both the distance feature, DME, and a separate TACAN azimuth feature that provides military pilots data similar to the civilian VOR). A co-located VOR and TACAN beacon is called a VORTAC. A VOR

with co-located DME only is called a VOR-DME. A VOR radial with DME distance allows a one-station position fix. Both VOR-DMEs and TACANs share the same DME system.

2.7 GBAS (108-118 MHz)

Augmentation of a Global Navigation Satellite System (GNSS) is a method of improving system attributes such as accuracy, reliability, and availability through the integrated of external information into the calculation process. There are many such systems in place. Ground Based Augmentation System (GBAS) describe a system that supports augmentation through the use of terrestrial radio messages. Such systems are commonly composed of one or more ground stations, which take measurements concerning the GNSS, and one or more radio transmitters, which transmit the information directly to the end user.

The Local Area Augmentation System (LAAS) is an GBAS landing system based on real-time differential correction of the GPS signal. Local reference receivers send data to a central location at the airport. This data is used to formulate a correction message, which is then transmitted to users via a VHF data link. LAAS's VHF uplink signal is currently slated to share the frequency band from 108 MHz to 118 MHz with existing ILS localizer and VOR navigational aids. Some existing navaids will need to be turned off because of congestion in the band. Additionally, before LAAS is fully implemented, users may be required to have multiple sets of radio equipment to support all possible situations.

2.8 VHF communication (117.975-137 MHz)

Double side band - amplitude modulation (DSB-AM) analogue voice is the primary line-of-sight service for ATS and AOC.

During the 1980s the airline industry saw the need for a data communications system to supplement AOC voice services. Originally intended as a management tool, the VHF aircraft communication, addressing and reporting system (ACARS) was developed by the Airlines Electronic Engineering Committee (AEEC) to transmit automatically messages between aircraft and ground stations to indicate when an aircraft departed and arrived at its assigned gate. The industry standard is known as the *ARINC Specification 618-5 Air-Ground Character-Oriented Protocol Specification*. As the use of AOC data communications grew it became apparent that ATS benefits could also be realised through the use of VHF data communications.

The ACARS data link provides character oriented data services at 2.4 kbps rate on shared 25 kHz wide channels. The channels may be assigned in AOC sub-bands or on specific frequencies in the VHF band as determined by local administrations. The ACARS radio signal uses a minimum shift keying (MSK) modulation scheme that allowed for early use in the band in compliance with the Radio Regulations. Channel access is shared on a contention basis known as carrier sense multiple access (CSMA) and there are limits to the efficiency of spectrum use. These limits are offset to a great degree by the efficiency of the information exchanges, which greatly exceeds that of voice. The ACARS protocol is not compliant with ICAO standards, but it does support a number of ATS applications in addition to many AOC applications. Communications services are offered by commercial operators around the world and several million messages are handled by ACARS each month. Approximately ten thousand airline transport and business aircraft are equipped with VHF ACARS.

ICAO saw the need to adopt a data link system in the VHF band that would be bit oriented, would offer greater message integrity, and would be suitable for ATS. The AMCP developed the VHF digital link (VDL) Mode 1 based on the ACARS physical layer (modulation scheme, data rate and channel access protocol) to enable the early introduction of VHF data services into Annex 10. These standards became applicable in 1996 but were later withdrawn from Annex 10, as no plans for implementation of VDL Mode 1 existed, whereas implementation of VDL Mode 2, with a higher level of performance, was already underway.

2.8.1 VDL Mode 2

The VDL Mode 2 digital link is an evolution from Mode 1 that uses a digital, 8-phase shift keying (D8PSK) modulation scheme at a data rate of 31.5 kilobits per second. It is ATN compliant, providing a bit oriented protocol that may also handle character oriented messages that are compatible with non-ATN infrastructures. It has limitations in its support of time critical applications in high air traffic density areas because of its CSMA channel access protocol that exhibits a non-deterministic behaviour. It does not support message priorities and it cannot guarantee the message transfer time. VDL Mode 2 employs a globally dedicated common signalling channel at 136.975 MHz.

The Eurocontrol LINK 2000+ Programme aims to plan and co-ordinate the implementation of operational air/ground data link services for ATM in the core area of Europe in the timeframe 2000 – 2007. It co-ordinates ATS data link implementation in the EUROCONTROL EATM framework and has recognised VDL Mode 2 as the first requested sub-network for the same reasons of availability, commonality with the AOC communications needs and suitability for supporting ATN and ICAO CNS/ATM concept. Statistics per January 2006 show that a total of 155 aircraft from 20 are equipped with VDL2**Error! Reference source not found.**.

2.8.2 VDL Mode 3

VDL Mode 3 uses the same physical layer as Mode 2 with a time division multiple access (TDMA) technique. This enables up to four 4.8 kbps circuits for voice or data on each 25 kHz channel that may be assigned anywhere in the band. The data capability provides a mobile sub-network that is compliant with the ATN.

Frequency assignment planning criteria are still under development by the Aeronautical Communications Panel (ACP). There is currently no operational use of VDL Mode 3, and a future implementation looks uncertain although there are implementation plans in the United States (NEXCOM programme.

2.8.3 VDL Mode 4

VDL Mode 4 is a VHF data link technology, standardised by ICAO, and designed to support CNS/ATM digital communications services, including time and safety critical broadcast applications as well as point to point communications. This is based on a self-organizing time division multiple access (STDMA) scheme, using 19.2 kilobit per second Gaussian frequency shift keying (GFSK) modulation. VDL Mode 4 requires a DSP radio architecture with ultra-linear RF stages to transmit and receive data.

VDL Mode 4 also supports navigation and surveillance applications. WRC2003 approved operation of VDL Mode 4 in the ARN band (108 MHz - 117.975 MHz) for surveillance applications. Frequency allocations in this band are conditional on the capacity studies demonstrating that sufficient capacity is available for the current navigation services in this band, which have priority in assignments.

VDL Mode 4 is considered in EUROCONTROL in the following two Domains:

- Communications Domain (COM) as a candidate point-to-point datalink in support of advanced applications with stringent Quality of Service (priority, time critical etc.), when such applications will be operationally required.
- Surveillance Domain (SUR) as a candidate ADS-B datalink (in complement to 1090 ES) to support Package 1+ type of applications.

2.8.4 8.33 kHz channels

In 1994, ICAO decided to introduce channel split from 25 kHz to 8.33 kHz **Error! Reference source not found.**. Subsequently, 8.33 kHz channel-spacing was introduced above FL245 in the ICAO EUR Region from October 1999.

In 2002, the ICAO agreed on relevant conclusions concerning the requirement for 8.33 kHz channel spacing below FL245. In accordance with EUROCONTROL Permanent Commission Recommendation 05/06, the mandatory carriage and operation of 8.33 kHz capable radio equipment above FL195 in the ICAO EUR Region will be effective from 15 March 2007.

The use of 8.33 kHz channels below FL195 is under consideration. EUROCONTROL has developed a business case in order to support the decision making process. The ICAO EANPG48 meeting, held 28-30 November 2006, agreed to proceed with a full 8.33 kHz implementation below FL195.

2.9 ELT (406-406.1 MHz)

Emergency Locator Transmitters (ELTs) were the first emergency beacons developed and most U.S. civil aircraft are required to carry them. ELTs were intended for use on the 121.5 MHz frequency to alert aircraft flying overhead. Obviously, a major limitation to these is that another aircraft must be within range and listening to 121.5 MHz to receive the signal.

Different types of ELTs are currently in use. There are approximately 170,000 of the older generation 121.5 MHz ELTs in service. Unfortunately, these have proven to be highly ineffective. They have a 97% false alarm rate, activate properly in only 12% of crashes, and provide no identification data. In order to fix this problem 406 MHz ELTs were developed to work specifically with the Cospas-Sarsat system**Error! Reference source not found.**. These ELTs dramatically reduce the false alert impact on SAR resources, have a higher accident survivability success rate, and decrease the time required to reach accident victims by an average of 6 hours.

Presently, most aircraft operators are mandated to carry an ELT and have the option to choose between either a 121.5 MHz ELT or a 406 MHz ELT. Due to the obvious advantages of 406 MHz beacons and the significant disadvantages to the older 121.5 MHz beacons, the International Cospas-Sarsat Program have made a decision to phaseout 121.5 MHz satellite alerting on February 1st, 2009.

2.10 DME (960-1215 MHz)

Distance Measuring Equipment (DME) is a transponder-based radio navigation technology that measures distance by timing the propagation delay of VHF or UHF radio signals. DME is similar to Secondary Radar, except in reverse. The system was a post-war development of the IFF (Identification Friend or Foe) systems of World War II. To maintain compatibility, DME is functionally identical to the distance measuring component of TACAN.

Aircraft use DME to determine their distance from a land-based transponder by sending and receiving pulse pairs - two pulses of fixed duration and separation. The ground stations are typically colocated with VORs. A typical DME ground transponder system for enroute or terminal navigation will have a 1 kW peak pulse output on the assigned UHF channel. A low power DME can also be colocated with an ILS localizer where it provides an accurate distance function, similar to that otherwise provided by ILS Marker Beacons.

The aircraft interrogates the ground transponder with a series of pulse-pairs (interrogations). The ground station replies with an identical sequence of reply pulse-pairs with a precise time delay (typically 50 microseconds). The DME receiver in the aircraft, searches for pulse-pairs with the correct time interval between them. The correct time between pulse pairs is determined by each individual aircraft's particular

interrogation pattern. The aircraft interrogator locks on to the DME ground station once it understands that the particular pulse sequence is the interrogation sequence it sent out originally. Once the receiver is locked on, it has a narrower window in which to look for the echoes and can retain lock.

DME frequencies are paired to VOR frequencies. A DME interrogator is designed to automatically tune to the corresponding frequency when the associated VOR is selected. An airplane's DME interrogator uses frequencies from 1025 to 1150 MHz. DME transponders transmit on a channel in the 962 to 1150 MHz range and receive on a corresponding channel between 962 to 1213 MHz. The band is divided into 126 channels for interrogation and 126 channels for transponder replies. The interrogation and reply frequencies always differ by 63 MHz. The spacing of all channels is 1 MHz with a signal spectrum width of 100 kHz.

DME facilities identify themselves with a 1350 Hz morse code three letter identity. If collocated with a VOR or ILS it will have the same identity code as the parent facility. Additionally, the DME will identify itself between those of the parent facility. DME identity is 1350 Hz to differentiate itself from the 1020 Hz tone of the VOR or the ILS localizer.

2.11 GNSS (960-1215 MHz and 1559-1610 MHz)

There are three Global Navigation Satellite Systems (GNSSs) that are fully operational or under development: GPS, Galileo and GLONASS.

2.11.1 GPS

The Global Positioning System (GPS) is currently the only fully-functional GNSS. More than two dozen GPS satellites are in medium Earth orbit, transmitting signals allowing GPS receivers to determine the receiver's location, speed and direction.

Aircraft navigation systems usually display a moving map and are often connected to the autopilot for *en route* navigation. Aviation-certified GPS receivers using technologies such as WAAS or LAAS to increase accuracy may also be used for some final approach and landing operations. Hand-held aviation-certified GPS receivers are often used in smaller general aviation aircraft. Glider pilots use GNSS Flight Recorders to log GPS data verifying their arrival at turn points in gliding competitions. Flight computers installed in many gliders also use GPS to compute wind speed aloft, and glide paths to waypoints such as alternate airports or mountain passes, to aid en route decision making for cross-country soaring.

2.11.2 Galileo

The Galileo positioning system, referred to simply as Galileo, is built by the European Union and the European Space Agency (ESA) as an alternative to GPS.

Galileo is tasked with multiple objectives including to provide a higher precision to all users than is currently available through GPS, to improve availability of positioning services at higher latitudes, and to provide an independent positioning system upon which European nations can rely even in times of war or political disagreement. The current project plan has the system as operational by 2010, two years later than originally anticipated.

There will be four different navigation services available:

- The Open Service (OS) will be free for anyone to access. The OS signals will be broadcast in two bands, at 1164–1214 MHz and at 1563–1591 MHz. Receivers will achieve an accuracy of less than 4 m horizontally and less than 8 m vertically if they use both OS bands. Receivers that use only a single band will still achieve less than 15 m horizontally and less than 35 m vertically, comparable to what the civilian GPS C/A service provides today. It is expected that most future mass market

receivers, such as automotive navigation systems, will process both the GPS C/A and the Galileo OS signals, for maximum coverage.
- The encrypted Commercial Service (CS) will be available for a fee and will offer an accuracy of better than 1 m. The CS can also be complemented by ground stations to bring the accuracy down to less than 10 cm. This signal will be broadcast in three frequency bands, the two used for the OS signals, as well as at 1260–1300 MHz.
- The encrypted Public Regulated Service (PRS) and Safety of Life Service (SoL) will both provide accuracy comparable to the Open Service. Their main aim is robustness against jamming and the reliable detection of problems within 10 seconds. They will be targeted at security authorities (police, military, etc.) and safety-critical transport applications (air-traffic control, automated aircraft landing, etc.), respectively.

In addition, the Galileo satellites will be able to detect and report signals from Cospas-Sarsat search-and-rescue beacons in the 406 MHz band, which makes them a part of the Global Maritime Distress Safety System.

2.11.3 GLONASS

Global'naya Navigatsionnaya Sputnikovaya Sistema (GLONASS) is the former Soviet and now Russian counterpart to GPS and Galileo. Formerly operated for the Russian government by the Russian Space Forces, it is now being jointly developed by Russia and India.

The GLONASS system was intended to be operational in 1991, it was announced to be operational in September 1993, but the constellation was not completed until December 1995. Due to the economic situation in Russia there were only eight satellites in operation in April 2002 rendering it almost useless as a global navigation aid. The situation changed on August 20, 2001, when the Federal Target Program Global Navigation System was accepted by the Russian government. According to it, GLONASS system should be fully deployed (i.e. with 24 satellites in orbit and the global continuous coverage) by 2011. On January 24, 2007, there were 16 satellites in the GLONASS system, of which 11 were in operation and five "temporarily switched off". Additional 3 satellites were launched on December 25, 2006. They have not yet been activated, but are in Commissioning Phase. In total since 1992 Russia launched 44 GLONASS satellites. Six are scheduled for launch in 2007. Five are scheduled for launch in 2008.

As of January 24, 2007, GLONASS availability in Russia was 50.8% and the global availability was 39.8%. Meaning that at least 4 satellites are visible 39.8% of time everywhere on the Earth.

2.12 SSR/ACAS (AG:1025-1040 MHz, GA: 1084-1093 MHz)

2.12.1 SSR

Secondary Surveillance Radar (SSR) is a radar system that not only detects and measures the position of aircraft but also requests additional information from the aircraft itself such as its identity and altitude. Unlike primary radar systems, which measure only the range and bearing of targets by detecting reflected radio signals, SSR relies on its targets being equipped with a radar transponder, which replies to each interrogation signal by transmitting its own response containing encoded data.

The purpose of SSRs is to improve the ability to detect and identify aircraft while it additionally provides automatically the Flight Level (pressure altitude) of a flight. An SSR continuously transmits interrogation pulses as its antenna rotates, or is electronically scanned in space. A transponder on an aircraft that is within line-of-sight range 'listens' for the SSR interrogation signal and sends back a reply that provides aircraft information. The reply depends on the mode that was interrogated (see below). The aircraft is then displayed as a tagged icon on the controller's radar screen at the calculated bearing and range. An aircraft without an

operating transponder still may be observed by primary radar, but would be displayed to the controller without the benefit of SSR derived data.

For military flights there are defined five modes (Mode 1 to Mode 5). For civilian flights, there are three modes A, C and S:

- Mode A - provides a 4-digit octal identification code for the aircraft, known as a squawk code, assigned by the air traffic controller.
- Mode C - provides a 10-bit binary Gray Code for the aircraft's pressure altitude read automatically from the aircraft altimeter.
- Mode S - originally envisioned as a data packet standard in both uplink data and downlink data formats. Extended squitter is an addition to the Mode S system designed to support ADS-B (see Sec. 2.12.3), which will also allow enhancements to the ACAS (see Sec. 2.12.2). The extended squitter consists of a set of broadcast messages that provide information regarding, inter alia, the aircraft position, velocity, and identification. It uses the same format as the current mode S data link.

For modes A and C, all aircraft receiving the interrogation signal will reply, whereas mode S allows aircraft to be addressed individually.

2.12.2 ACAS

Airborne Collision Avoidance System (ACAS) is an ICAO standard which provides pilots with a system independent of air traffic control to detect the presence of other aircraft which may present a threat of collision. Where the risk of collision is imminent, the system provides an indication of a manoeuvre that will reduce the risk of collision. As of 2006, the only implementation that meets the ACAS II standards set by ICAO is Version 7.0 of TCAS II (Traffic Alert and Collision Avoidance System).

TCAS involves communication between all aircraft equipped with an appropriate transponder. Each TCAS-equipped aircraft "interrogates" all other aircraft in a determined range about their position (via the 1030 MHz radio frequency), and all other craft reply to other interrogations (via 1090 MHz). This interrogation-and-response cycle may occur several times per second. Through this constant back-and-forth communication, the TCAS system builds a three dimensional map of aircraft in the airspace, incorporating their bearing, altitude and velocity. Then, by extrapolating current position data to anticipated future positions, it determines if a potential collision threat exists.

The next step beyond identifying potential conflicting aircraft is automatically negotiating a mutual avoidance manoeuvre between the two conflicting aircraft. These avoidance manoeuvres are communicated to the flight crew by a cockpit display and by synthesized voice instructions.

TCAS has the following versions:

- Passive: Collision Avoidance systems which rely on transponder replies triggered by ground and airborne systems are considered passive. Ground and airborne interrogators query nearby transponders for mode C altitude information, which can be monitored by third-party systems for traffic information. Passive systems display traffic similar to TCAS, however generally have a range of less than 7 nautical miles.
- TCAS I is the first generation of collision avoidance technology. It is cheaper but less capable than the modern TCAS II system, and is mainly intended for general aviation use. TCAS I systems are able to monitor the traffic situation around a plane (to a range of about 40 miles) and offer information on the approximate bearing and altitude of other aircraft. It can also generate collision warnings in the form of a Traffic Advisory (TA). The TA warns the pilot that another aircraft is in near vicinity, announcing "traffic, traffic", but does not offer any suggested remedy. It is up to the

pilot to decide what to do, usually with the assistance of Air Traffic Control. When a threat has passed, the system announces “clear of conflict”.

- TCAS II is the second and current generation of TCAS, used in the majority of commercial aviation aircraft. It offers all the benefits of TCAS I, but will also offer the pilot direct, vocalised instructions to avoid danger, known as a Resolution Advisory (RA). The suggestive action may be corrective, suggesting the pilot change altitude by announcing “descend, descend” or “climb, climb”. By contrast, a preventive RA may be issued which simply warns the pilots not to deviate from their present altitude, announcing “monitor vertical speed”. TCAS II systems coordinate their resolution advisories before issuing commands to the pilots, so that if one aircraft is instructed to descend, the other will typically be told to climb and thus maximising the separation between the two craft.
- TCAS III is the next generation of collision avoidance technology which is currently undergoing active development by aviation companies such as Honeywell. TCAS III incorporates technical upgrades to the TCAS II system, and will have the capability to offer traffic advisories and resolve traffic conflicts using horizontal as well as vertical manoeuvring directives to pilots. For instance, in a head-on situation, one aircraft might be directed “turn right, climb” while the other would be directed “turn right, descend”. This would act to further increase the total separation between aircraft, in both horizontal and vertical aspects.

Although the system occasionally suffers from false alarms, pilots are now under strict instructions to regard all TCAS messages as genuine alerts demanding an immediate, high-priority response. (Only Ground Proximity Warning System warnings have higher priority than the TCAS.) The FAA and most other country’s authorities’ rules state that in the case of a conflict between TCAS RA and air traffic control (ATC) instructions, the TCAS RA always takes precedence. (If one aircraft follows a TCAS RA and the other follows conflicting ATC instructions, a collision can occur, such as the July 1, 2002 Überlingen disaster. In this mid-air collision, both airplanes were fitted with TCAS II systems which functioned properly, but one obeyed the TCAS advisory while the other ignored the TCAS and obeyed the controller; both aircraft descended into a fatal collision.)

2.12.3 ADS-B

Automatic Dependent Surveillance-Broadcast (ADS-B) messages are transmitted from aircraft equipped with suitable transponders, containing information such as identity, location, and velocity. TCAS equipment which is capable of processing ADS-B messages may use this information to enhance the performance of TCAS, using techniques known as “hybrid surveillance”. As currently implemented, hybrid surveillance uses reception of ADS-B messages from an aircraft to reduce the rate at which the TCAS equipment interrogates that aircraft. This reduction in interrogations reduces the use of the 1030/1090 MHz radio channel, and will over time extend the operationally useful life of TCAS technology. The ADS-B messages will also allow low cost (for aircraft) technology to provide real time traffic in the cockpit for small aircraft.

Hybrid surveillance does not include the use any of the aircraft flight information in the TCAS conflict detection algorithms; ADS-B is used only to identify aircraft that can safely be interrogated at a lower rate.

In the future, prediction capabilities may be improved by using the state vector information present in ADS-B messages. Also, since ADS-B messages can be received at greater range than TCAS normally operates, aircraft can be acquired earlier by the TCAS tracking algorithms. The identity information present in ADS-B messages can be used to label other aircraft on the cockpit display (where present), improving situational awareness.

The major demonstrated problem of the ADS-B protocol integration is this added verbosity of the extra information transmitted, which is unnecessary for collision avoidance purposes. The more data transmitted from one aircraft in accordance with the system design, the lesser the number of aircraft that can participate in the system, due to the fixed and limited channel data bandwidth. The ADS-B “fix” proposal is to increase

the packet length from 64 bit to 128 bit to reduce the impact of overhead, which is not an accepted international standard.

Three link solutions are being proposed as the physical layer for relaying ADS-B position reports:

- 1090 MHz Mode S Extended Squitter (ES) (see Sec. 2.12.1)
- Universal Access Transceiver (UAT) (see below)
- VDL Mode 4 (see Sec. 2.8.3)

2.12.4 UAT

ADS-B messages are also carried on a Universal Asynchronous Transmitter (UAT) in the 900 MHz band. UAT was designed specifically for ADS-B with no constrains from legacy systems. It also supports Traffic Information Service -Broadcast (TIS-B), Flight Information Service – Broadcast (FIS-B) and Weather uplink.

Currently UAT based traffic uplinks are provided in Alaska and in regions of the East coast of the U.S.

2.13 PSR (1215-1400 MHz, 1559-1610 MHz and 2700-3100 MHz)

Unlike secondary surveillance radar systems, primary surveillance radars (PSRs) measure only the range and bearing of targets by detecting reflected radio signals.

2.14 AMS(R)S (1545-1555 MHz and 1646.5-1656.5 MHz)

The only satellite service provider offering communications for ATS purposes in Europe is Inmarsat. In the late 1980s Inmarsat offered the aeronautical community the possibility of using its satellite infrastructure, which was initially developed to support the marine community. All aeronautical uses ranging from passenger communications to safety related ATS communications could use the system and special provisions were included in the design of the system to ensure safety uses has priority over other uses. With such a wide customer base, the service was considered financially viable and allowed communication costs to be reduced to a level that was considered acceptable. The Inmarsat system became the basis of the existing Aeronautical Mobile Satellite Service (AMSS).

There exist other satellite systems that are capable of communication with aircraft. These include Iridium and Globalstar.

2.14.1 Inmarsat

The original investment in the specific aeronautical infrastructure deployed at the Ground Earth Stations (GESs) was justified on the basis of expected returns through the use of passenger cabin telephony. Over the ensuing years it started to become apparent that the expected passenger telephony business was unlikely ever to materialise primarily due to the perceived cost of the service to the passenger. This consequentially reduced the motivation of the GES operators to continue to invest in maintaining and upgrading the GES aeronautical infrastructure.

The Inmarsat system is based on a constellation of satellites in geostationary orbit. There are three classes of satellite in use:

- Inmarsat-2 satellites provide only global beam coverage in L-band and are generally used for leased services. There are four Inmarsat-2 satellites in operation.
- Inmarsat-3 satellites provide global beam coverage and also regional spot beam coverage to specific areas, such as the North Atlantic allowing operation of services such as Swift-64. There are five Inmarsat-3 satellites in operation.

- Inmarsat-4 satellites provide global beam coverage, regional beam coverage, and narrow spot beam coverage. Unlike the Inmarsat-3 satellites, the Inmarsat-4 satellites provide regional beam coverage to the entire visible earth's surface, resulting in increased geographical coverage for services such as Swift-64. The Inmarsat-4 narrow spot beams also cover virtually the entire visible earth's surface. The narrow spot beams allow the use of BGAN based services such as SwiftBroadband. The first two Inmarsat-4 satellites were launched in 2005 and the third in 2008.

Swift64 provides a basic speed of 64kbps per channel, which can be boosted to 256kbps and higher by proven techniques such as channel bonding and data acceleration. It supports ISDN and Inmarsat's Mobile Packet Data service (MPDS), which permits the use of TCP/IP (Internet packet data). Swift64 targets use of e-mail, Internet and corporate intranet access, large file transfer, videoconferencing, confidential communications and multi-channel telephony.

SwiftBroadband is a new aeronautical mobile communication satellite service that provides a channel rate of 432 kbps, and which is supported by Inmarsat 4 satellites. SwiftBroadband is the aeronautical service part of the generic Global Broadband Area Network previously known as Aero-BGAN. SwiftBroadband offers improved services compared to those available via Inmarsat 3 satellites. The driver for SwiftBroadband equipage will most likely be the passenger demand for broadband capability in the cabin. SwiftBroadband has two basic classes of service:

- A basic, or default class supporting 'background' and 'interactive' classes (defined in 3GPP). This has no guaranteed bandwidth assigned to the connection. It is typically used for file transfer, internet access and email. Users will see a nominal maximum of 432kbps data rate. This will be the class of service assigned to any connection where no QoS is declared in the connection establishment.
- Guaranteed bit rate class for 'streaming' services with guaranteed bandwidth for the duration of the session. Data rates are between 32 kbps and 256kbps. This requires a defined QoS end-to-end in order to deliver service. The on-board server will be responsible for the management of the connectivity and class of connection so this should be transparent to the user.

The ATM service providers and relevant International Organisations are currently considering enhancing the current mobile communication infrastructure to provide more capacity, in particular in the areas suffering from VHF frequency congestion (i.e. Europe and North America), and to support enhanced capabilities. The use of satellite systems offers great potential to complement the current communication infrastructure, which is based on terrestrial systems - VHF in continental airspace, and HF in oceanic regions.

EUROCONTROL let a contract to a consortium to assess how Inmarsat's SwiftBroadband system could be used to provide satellite based ATM service in Europe. The conclusions were that without the availability of a hot-standby satellite, SwiftBroadband can not be the primary means of communication for critical applications anywhere but in low-density, en-route airspace. It may however serve as a supplement to other forms of communication, i.e. VDL Mode 2 that is expected to be mandated in Link2000+ airspace from circa 2010. SwiftBroadband could therefore be used to reduce congestion in the VDL band.

Inmarsat has several plans for new systems:

- Alphasat will provide advanced mobile voice and data communication services and is developed in the frame of ESA's ARTES-8 program. It will operate in the additional 2x7 MHz L-band spectrum allocated at WRC-03. The target date of launch is early 2012.
- Global Xpress consists of a constellation of three Ka-band (Inmarsat-5) satellites. The first constellation is scheduled for completion in 2013, and full global coverage is expected by the end of 2014. Each satellite will carry a payload of 89 small Ka-band beams.

- EuropaSat is an S-band system providing mobile broadcast and two-way communication services in Europe. The satellite was scheduled for launch early 2011, but the project was put on hold in 2009.

2.14.2 Iridium

The Iridium satellite constellation is a system of 66 active communication satellites and spares around the Earth. The system was originally to have 77 active satellites, and as such was named for the element iridium, which has atomic number 77.

The system is being used extensively by the U.S. Department of Defense for its communication purposes through the DoD Gateway in Hawaii. The commercial Gateway in Tempe, Arizona provides voice, data and paging services for commercial customers on a global basis. Typical customers include maritime, aviation, government, the petroleum industry, scientists, and frequent world travellers. Iridium Satellite LLC claims to have approximately 175,000 subscribers as of December 31, 2006, a 23.2% increase from the total as of December 31, 2005.

Iridium was proposed as the basis of one of the first next generation satellite systems (NGSSs) by ICAO in the mid-1990s until the Iridium Company ceased operation due to financial difficulty. However the Iridium system is now back in operation and a sub-group of ICAO Working Group M has been formed to develop a technical and implementation manual for the Iridium system as part of the ICAO assessment process for aeronautical safety services. At the moment Iridium supports some ATS related trials in Alaska as part of the FAA Capstone project.

2.14.3 MTSAT

The Japanese Multi-function Transport Satellite (MTSAT) was launched in February 2005 and is in orbit over Japan between the Inmarsat Indian and Pacific Ocean satellites locations. Part of its mission is to support AMS(R)S and it therefore complements the Inmarsat coverage in that region. MTSAT is fully compliant with the AMS(R)S SARPs and is expected to be used for ATS purposes in that area as well as AOC. However, it does not support a broadband capability.

2.14.4 Connexion by Boeing

Connexion by Boeing was an in-flight online connectivity service from Boeing. This service allowed travellers to access a high-speed internet connection while on board a plane in flight through a wired Ethernet or a wireless 802.11 Wi-Fi connection. The infrastructure used a phased array antenna or a mechanically steered Ku-band antenna on the aircraft, leased satellite transponders, and ground stations. The service coverage included North America, North Atlantic, Europe, the Middle East, Northern Pacific, Australia, and Asia.

Connexion by Boeing was first launched as a service May 17, 2004 with Lufthansa German Airlines. Later in 2004, ANA, Japan Airlines, and SAS signed on to the service. Other airlines which launched Connexion by Boeing service in 2005 include China Airlines, Singapore Airlines, Asiana Airlines, and Korean Air. In the later months of 2005, El-Al Israel Airlines and Etihad Airlines offered the service. In 2005 Connexion by Boeing launched the first in-flight live TV on an international route on Singapore Airlines, to be expanded to all current airlines in the first quarter of 2006. Flying out of Germany, the service provided access to live TV for CNBC (Europe), EurosportNews, BBC World and Euronews.

The prices varied from airline to airline, but were typically $9.99 for one hour of access, $14.95 for two hours of access, $17.95 for 3 hours of access and $26.95 for flat-rate access. Various payment options were allowed. The service could be paid with major credit cards, mobile phone, hotspot accounts and even frequent flyer miles.

In June 26, 2006 it became public that Boeing was exploring selling or shutting down Connexion by Boeing, having failed to attract sufficient customers. On August 17, 2006, Boeing announced that it would discontinue its Connexion service, stating that, "the market for this service has not materialized as had been expected". Boeing offered free service starting on October 2, 2006 as part of its plan to discontinue the service on December 31, 2006.

2.14.5 Globalstar

Globalstar is a low Earth orbit (LEO) satellite constellation for telephone and low-speed data communications, similar to (and competing with) the Iridium satellite system.

In 2005, some of the satellites began to reach the limit of their operational lifetime of 7.5 years. In December of 2005, Globalstar began to move some of its satellites into a graveyard orbit above LEO. In December 2006, Globalstar announced that Alcatel Alenia Space has been awarded a € 661 million contract for the 2nd generation 48 satellite constellation.

In July 2009, Globalstar, Inc. announced that it has received complete financing for its second-generation satellite constellation and signed an amendment to the initial contract, specifying in particular the adjusted conditions for production and the new satellite delivery timetable. The first six second-generation satellites were launched in October 2010 and are expected to provide Globalstar customers with satellite voice and data services until at least 2025. Eighteen more satellite launches are scheduled in February, April and June 2011.

2.15 Radio Altimeter (4400-4600 MHz)

A radar altimeter measures altitude above the terrain presently beneath an aircraft or spacecraft. This type of altimeter provides the distance between the plane and the ground, as opposed to a barometric altimeter which only provides altitude above sea level.

Radar altimeters are critical for flying very low over terrain. Radar altimeters are frequently used by commercial aircraft for approach and landing, especially in low-visibility conditions, and are incorporated in terrain avoidance warning systems, warning the pilot if the aircraft is flying too low, or if rising terrain ahead is a hazard to be avoided. Radar altimeters are also used in military aircraft flying extremely low over terrain to avoid radar detection and targeting by anti-aircraft artillery or Surface-to-air Missiles. Radar altimeter technology is also used in terrain-following radar allowing fighter aircraft to fly at very low altitude.

2.16 MLS (5030-5150 MHz)

The Microwave Landing System (MLS) is an all-weather, precision landing system originally intended to replace or supplement the Instrument Landing System (ILS). MLS has a number of operational advantages, including a wide selection of channels to avoid interference with other nearby airports, excellent performance in all weather, and a small "footprint" at the airports.

Although some MLS systems became operational in the 1990s, the widespread deployment initially envisioned by its designers never came to be. GPS-based systems, notably WAAS, allowed the same level of positioning detail with no equipment needed at the airport. GPS/WAAS dramatically lowers the cost of implementing precision landing approaches, and since its introduction most existing MLS systems in North America have been turned off.

MLS continues to be of some interest in Europe, where concerns over the availability of GPS continue to be an issue. A widespread installation in England is currently underway, which included installing MLS receivers on most British Airways aircraft, but the continued deployment of the system is in doubt.

The development of Category II/III GBAS systems will probably be decisive for the future of MLS. Multi-constellation multi-constellation GBAS will be considered within SESAR, and it is expected that MLS will only be widely deployed if it proves unfeasible to develop such GBAS systems with accuracy and reliability satisfying the ATM requirements.

The system may be divided into five functions: Approach azimuth, Back azimuth, Approach elevation, Range and Data communications.

2.16.1 Approach azimuth guidance

The azimuth station transmits MLS angle and data on one of 200 channels within the frequency range of 5031 to 5091 MHz and is normally located about 1,000 feet (300 m) beyond the stop end of the runway, but there is considerable flexibility in selecting sites. For example, for heliport operations the azimuth transmitter can be collocated with the elevation transmitter. The azimuth coverage extends:

- Laterally, at least 40 degrees on either side of the runway centreline in a standard configuration.
- In elevation, up to an angle of 15 degrees and to at least 20,000 feet (6 km), and in range, to at least 20 nautical miles (37 km).

2.16.2 Elevation guidance

The elevation station transmits signals on the same frequency as the azimuth station. A single frequency is time-shared between angle and data functions and is normally located about 400 feet from the side of the runway between runway threshold and the touchdown zone.

Elevation coverage is provided in the same airspace as the azimuth guidance signals: In elevation, to at least +15 degrees; Laterally, to fill the Azimuth lateral coverage and in range, to at least 20 nautical miles (37 km).

2.16.3 Range guidance

The MLS Precision Distance Measuring Equipment (DME/P) functions the same as the navigation DME, but there are some technical differences. The beacon transponder operates in the frequency band 962 to 1105 MHz and responds to an aircraft interrogator. The MLS DME/P accuracy is improved to be consistent with the accuracy provided by the MLS azimuth and elevation stations. A DME/P channel is paired with the azimuth and elevation channel. A complete listing of the 200 paired channels of the DME/P with the angle functions is contained in FAA Standard 022 (MLS Interoperability and Performance Requirements). The DME/N or DME/P is an integral part of the MLS and is installed at all MLS facilities unless a waiver is obtained. This occurs infrequently and only at outlying, low density airports where marker beacons or compass locators are already in place.

2.16.4 Data communications

The data transmission can include both the basic and auxiliary data words. All MLS facilities transmit basic data. Where needed, auxiliary data can be transmitted. MLS data are transmitted throughout the azimuth (and back azimuth when provided) coverage sectors. Representative data include: Station identification, Exact locations of azimuth, elevation and DME/P stations (for MLS receiver processing functions), Ground equipment performance level; and DME/P channel and status.

2.17 AeroMACS

The new airport surface datalink system AeroMACS is currently under development within the SESAR project 15.2.7 in collaborations within the U.S. It will operate in the 5091-5150 MHz band, and is based in IEEE802.16 (WiMAX) technology. A realistic estimation is that the first AeroMACS systems will become operative around 2020-2025.

2.18 Weather radar (5350-5470 MHz)

These radars are used for weather detection, wind shear and turbulence detection, and ground mapping.

2.19 Doppler radar (8750-8850 MHz and 13.25-13.4 GHz)

In the sub-band 8750-8850 MHz, the aeronautical radionavigation service has secondary status. The military services operate numerous radars for such operations as airborne multimode weapons fire-control; airborne search and interception radars; mobile and portable battlefield radars for air search and surveillance; artillery, rockets, and mortar locating radars; airborne anti-submarine warfare radar; shipborne weapons fire-control radars; submarine surface navigation and search radars; and airborne maritime Doppler surveillance radars. Non-military radars are supported in this band for such search and tracking of airborne test/experimental manned and unmanned vehicles; tracking radars supporting nuclear reactor test activities and limited nuclear test band treaty; mobile meteorological radars; and land-based planetary radars.

The aeronautical radionavigation service is primary in the 13.25-13.4 GHz band. The predominant users in this band are the military services. Airborne radar applications support multimode Doppler navigation and search radars; and navigation and sea search radars. Non-military applications include airborne ocean wave spectrometer radars that measure ocean surface characteristics.

2.20 ASDE (9000-9500 MHz, 15.4-16.6 GHz and 31.8-33.4 GHz)

Airport Surface Detection Equipment (ASDE) is used for tracking ground targets moving on an airport surface. ASDE-X (9.0-9.2 GHz) is designed for small/medium airports, while ASDE-3 (15.7-16.2 GHz) is designed for large airports.

3 Aeronautical surveillance systems

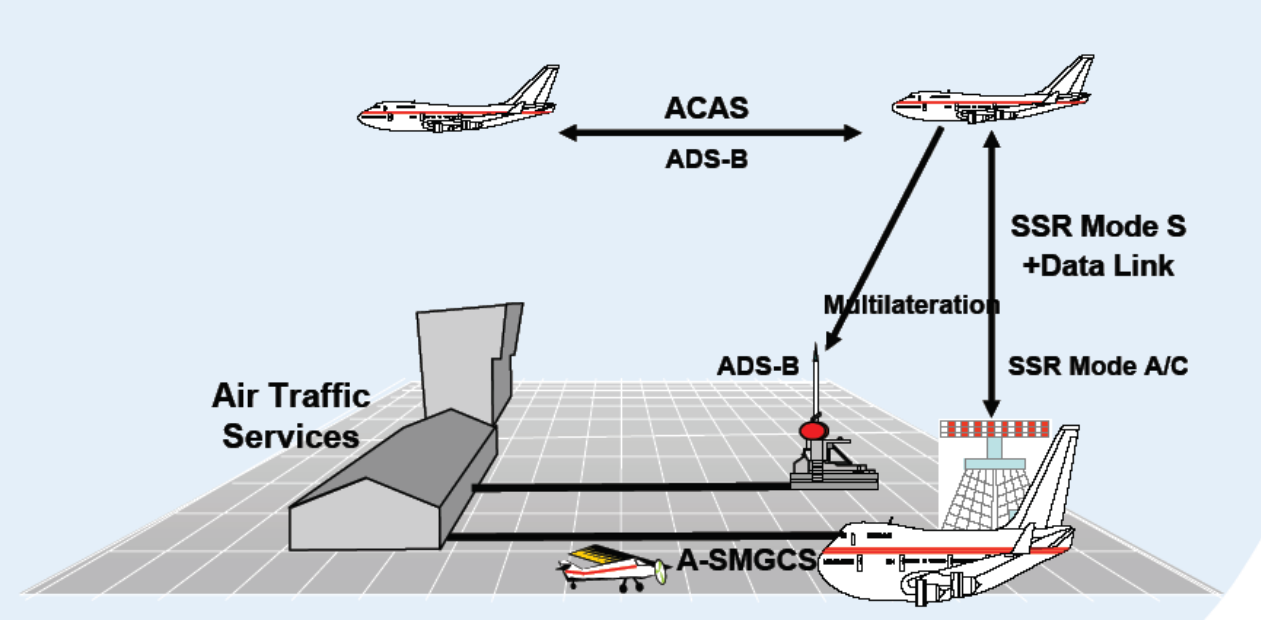

Figure 1 Illustration of aeronautical surveillance system 1

The principal parts of the aeronautical surveillance system including communications to and from aircrafts are illustrated in Figure 1. For airborne aircrafts those are:

- Secondary surveillance radar (SSR)
- Aircraft Collision Avoidance System (ACAS)
- Automatic Dependent Surveillance-Broadcast (ADS-B)

For surface movements, the main system is:

- Advanced Surface Movement and Guidance Control System (A-SMGCS)

These systems have that in common that they operate at 1030 MHz and 1090 MHz (although ADS-B messages can be transmitted in the VHF band using VDL Mode 4 and in the 900 MHz band using Universal Access Transceiver (UAT)).

In this document a brief overview of these systems is provided. The intent is obviously to provide an insight in aeronautical surveillance. In addition, due to the probable allocation of bandwidth to aeronautical communication services in the 960-1164 MHz band at WRC-07, it is of interest to know what systems are operating in this band today and the characteristics of these systems with respect to signal transmission.

ICAO Annex 10 aeronautical telecommunications is the document laying down the standards of civil aviation technical infrastructure. Volume IV is specifically for SSR systems.

3.1 Secondary surveillance radar

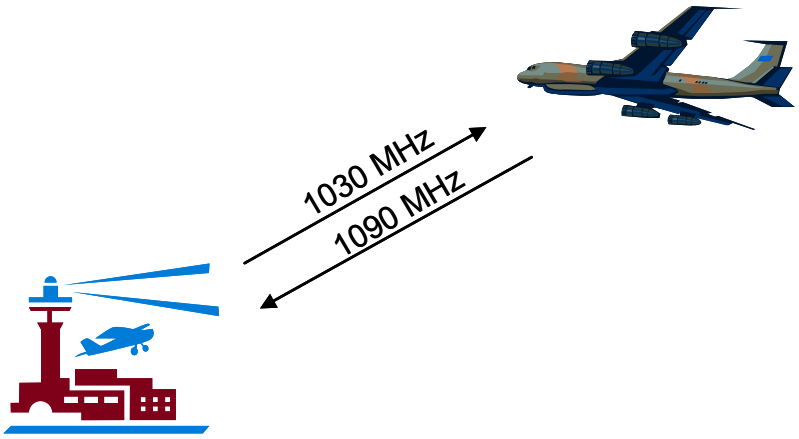

Figure 2 Illustration of a SSR system

The principle of a SSR is as follows. A ground system transmits an interrogation signal via the directional beam of a rotating antenna at 1030 MHz. When a transponder at an aircraft detects the signal, it responds by transmitting a signal at 1090 MHz. The response is detected at the ground station and displayed on the radar display.

There are three civilian transponder modes:

- Mode A provides a 4-digit octal identification code for the aircraft assigned by the air traffic controller
- Mode C provides a 10-bit binary Gray Code for the aircraft's pressure altitude
- Mode S provides transponder responds to selective interrogations (each aircraft can be assigned a fixed 24-bit address for selective interrogation purposes). The downlink data format can be utilized independently to squitter information such as position and velocity.

The ground station uses two principal beams: the interrogate beam with high gain and narrow main lobe, and the control beam which is broader and hence has a lower peak gain. The control beam is used to prevent the aircraft from replying to signals from the interrogate beam side lobes (as the control beam signal is stronger than the interrogation beam signal in all directions except that of the interrogation beam main lobe). This is called Interrogation Path Side Lobe Suppression (ISLS).

3.2 Mode A and Mode C

3.2.1 Signal formats

The interrogation signal format is shown in Figure 3. The pulses P1 and P3 are transmitted by the interrogation beam, and P2 by the control beam.

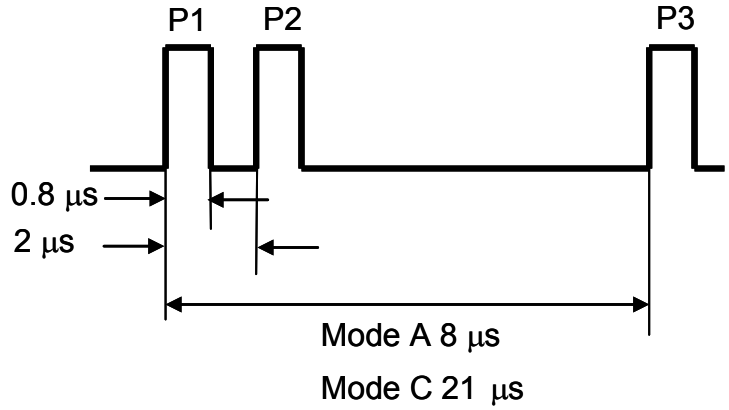

Figure 3 Interrogation signal format

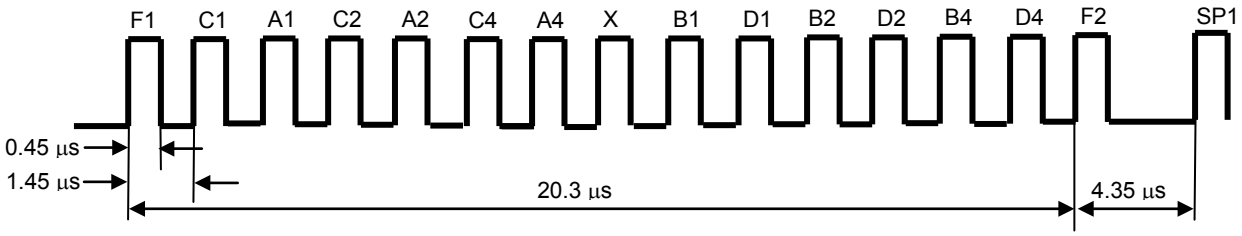

Figure 4 Reply signal format

The reply signal format is shown in Figure 4. The pulses F1 and F2 are framing pulses. The middle pulse X is never used. The twelve A-, B-, C- and D-pulses provides the possibility to encode 4096 codes. The last pulse SP1 may be added in the Mode A, usually on request from the ground air traffic controller who uses it for further identification.

Mode A is used for general identification. Hence, 4096 IDs can be supported. The IDs are assigned by the ground ATC.

Mode C is used for height. The pulse D1 is omitted so that 2048 codes can be used to indicate height in 100 ft increments -1000 ft to 121000 ft. Above a transition altitude, normally 6000 ft, the height is based on a standard barometric pressure of 1013.2 mbar. Multiple modes (A/C) can be accommodated by alternating the modes according to some preset interlace program.

Maximum range	250 n miles
Target capacity	400 aircraft
Interrogation rate	50- 450 Hz 120 Hz typically (12 rpm antenna scan rate)
Interrogator	
Transmit power	Typically 1000 W
Frequency	1030 +/- 0.01 MHz
Out-of-band emission	+/- 60 MHz: -50 dBr max +/- 100 MHz: -70 dBr max 1250-1350 MHz: -115 dBr max

Table 2 SSR signal parameters

3.3 Mode S

3.3.1 Levels of functionality

There are 2 levels of Mode S functionality: Elementary Surveillance (ELS) and Enhanced Surveillance (EHS). The latest date for aircraft compliance with Mode S ELS/EHS is 31 March 2007. In the case of EHS this is subject to operators applying for an exemption from the Mode S Exemption Coordination Cell (ECC). Exceptionally, an exemption may be granted for a small proportion of an operators' EHS applicable fleet until 31 March 2009. Separate comparable exemption arrangements apply for State aircraft.

3.3.1.1 Mode S Elementary Surveillance (ELS)

ELS is initially being implemented by Belgium, France, Germany, Luxembourg, the Netherlands, Switzerland and the United Kingdom.

The fundamental concept of Mode S ELS is the assignment to each aircraft of a unique ICAO 24-bit address. The addresses are allocated in blocks by ICAO to the state of registry, or common mark registering authority, for assignment to aircraft according to their country of registration. Mode S ELS uses this unique 24-bit aircraft address for selective interrogation and to acquire downlinked Aircraft Identification (commonly referred to as Flight ID). Among other attributes associated with Mode S ELS is the ability to acquire altitude in 25 foot increments.

Mode S requires each interrogator to have an Identifier Code (IC), which can be carried within the uplink and downlink transmissions.

The benefits of Mode S ELS are:

- Selective addressing of aircraft in order to overcome garbling[1], fruiting[2] and over-interrogation (which together constitute RF congestion).
- Automatic acquisition of Aircraft Identification (Flight ID), which enhances radar identification and has the capability to relieve the shortage of Mode A codes.
- Backwards compatibility with Mode A/C.

3.3.1.2 Mode S Enhanced Surveillance (EHS)

EHS is initially being implemented by France, Germany and the United Kingdom.

Mode S EHS consists of Mode S ELS supplemented by the extraction of downlink aircraft parameters (DAPs) for use in the ground ATM systems. Some parameters are for display to the controller, known as controller access parameters (CAPs) and others are for ATM system function enhancements, known as system access parameters (SAPs).

Mode S EHS is the first stage in making use of air derived data in the form of downlink aircraft parameters, either directly to the controller or to ATM systems. EHS permits improved situation awareness and eases R/T congestion, thus enhancing safety and also capacity.

3.3.2 Interrogation Methods

A Mode S sensor has two methods of interrogation: *All-Call* and *Selective*. A typical ratio between all call and selective is:

[1] Garbeling is interference due to responses from several aircraft to one interrogation
[2] Fruiting is interference due to replies triggered by other interrogations

- 1/3 all call
- 2/3 selective

The all call repetition frequency is normally between 40 Hz and 150 Hz. The maximum value defined by ICAO is 250 Hz.

3.3.2.1 All-call interrogations

All-call interrogations are transmitted regularly at a steady rate in a similar way to conventional SSR. Any Mode S transponder that is not 'locked out' will reply to an all-call interrogation, transmitting its unique 24-bit aircraft address. In this way, the interrogator acquires targets not previously detected. Once a transponder is known to the interrogator and its track has been established, it can be 'locked out'. This prevents the transponder from replying to any more all-call interrogations from that or any other Mode S sensor with the same identifier code, and it will then only respond to Selective interrogations. However, it will continue to respond to interrogations from other Mode S sensors with a dissimilar Identifier Code and also to Mode A/C sensors.

Lockout is a new concept for SSR and is one of the major factors in radically reducing reply rates and, thus, reducing interference. To prevent the potential for undesirable, uncontrolled lockout of targets, a number of safeguards have been built into the international standards for both interrogators and transponders to ensure that lockout is handled in a fail-safe manner.

3.3.2.2 Selective interrogations

Selective interrogations make use of the unique 24-bit aircraft address and can be sent out close to the azimuth where the aircraft is expected to be. No other aircraft that happens to be in the radar beam at that time will reply. The aircraft addressed will reply with its Mode A code (assuming one has been assigned), aircraft identification and altitude. The type of reply is controlled by the interrogator, but in either case only a single reply is required because there is no ambiguity as to which aircraft the reply belongs. Extra interrogations can be made to ensure that at least one reply is received and that the azimuth performance is maintained.

3.3.3 Signal formats

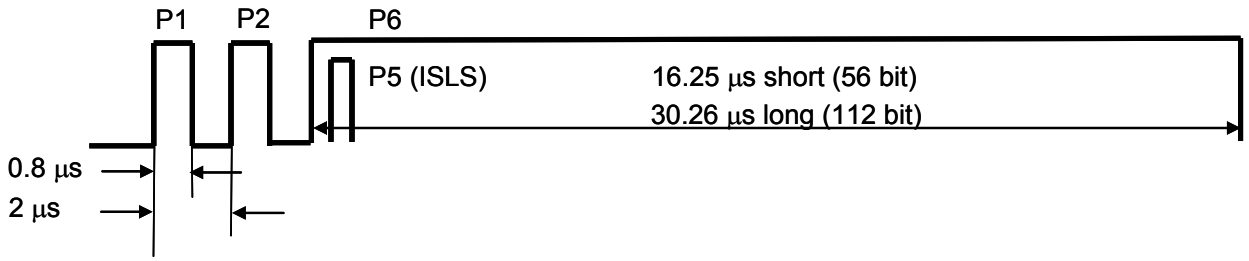

Figure 5 Mode S interrogation signal format

The Mode S uplink interrogation format starts with two pulses, P1 and P2, which are solely for the purpose of suppressing existing Mode A/C only transponders so that they are not aware of the main Mode S information. The Mode S interrogation data contained in the P6 data block is phase modulated. The first phase reversal is the timing point for the subsequent bits (chips) of information. The Mode S interrogation may be of short (56 bits) or long (112 bits) format.

The Mode S side lobe suppression pulse P5 is transmitted from the control beam like the P2 ISLS in the Mode A/C system. If P5 is of more power than P6 it has the effect of overwhelming the sync phase reversal of P6 so that the Mode S transponder cannot read the subsequent information.

Mode S Uplink interrogations use in the P6 pulse Differential Phase Shift Keying (DPSK) to modulate the data. The P6 begins with an initial phase reversal at the start of the P6 pulse with a length of 1.25 μs. This is known as the sync phase reversal. After the sync phase reversal, all subsequent phase reversals indicate the 56 or 112 bit P6 information. All subsequent timing is taken from the point of the first phase reversal. Each phase has duration of 0.25 μs and is known as a "chip". The series of chips starts 0.5 μs after the sync reversal.

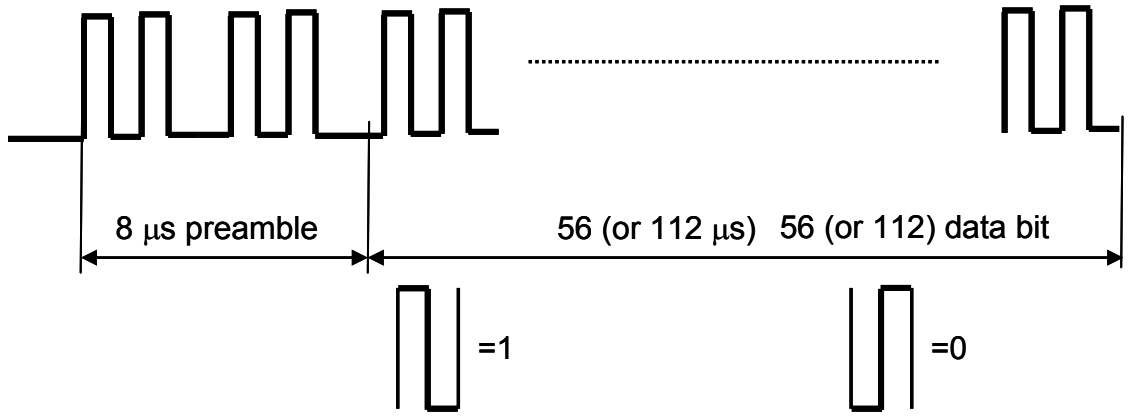

Figure 6 Mode S Reply signal format

Mode S replies consist of a certain number of pulses at one μs spacing providing a 1 Mbps data rate during the pulse. The modulation format is Pulse Position Modulation (PPM).

A downlink broadcast frame is resent at regular intervals by the aircraft for a specific period time. It includes the transmission of *Extended Squitter* - the unsolicited downlink broadcast of positional reports. This report can include:

- aircraft type and aircraft ID
- altitude
- encoded latitude and longitude (both coarse)
- airborne velocity

The extended squitter is enabler of ADS-B (see Sec. 3.5).

3.4 ACAS

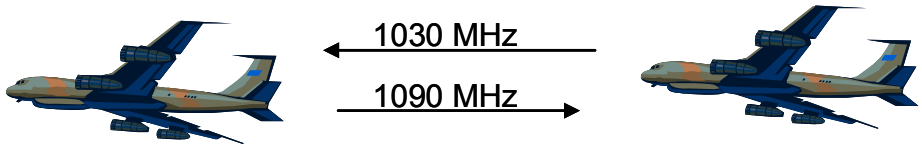

Figure 7 Illustration of ACAS

TCAS involves communication between all aircraft equipped with an appropriate transponder. Each TCAS-equipped aircraft "interrogates" all other aircraft in a determined range about their position (via the 1030 MHz radio frequency), and all other craft reply to other interrogations (via 1090 MHz). This interrogation-and-response cycle may occur several times per second.

Through this constant back-and-forth communication, the TCAS system builds a three dimensional map of aircraft in the airspace, incorporating their bearing, altitude and velocity. Then, by extrapolating current position data to anticipated future positions, it determines if a potential collision threat exists.

ACAS can issue two types of alert:

- Traffic Advisories (TAs), which aim at helping the pilot in the visual search for the intruder aircraft, and by alerting him to be ready for a potential resolution advisory;
- Resolution Advisories (RAs), which are avoidance manoeuvres recommended to the pilot. When the intruder aircraft is also fitted with an ACAS system, both ACAS' co-ordinate their RAs through the Mode S data link, in order to select complementary resolution senses.

ACAS-II implementation has been organised in 2 phases:

- Phase 1, with effect from 1 January 2000 for all civil fixed-wing turbine-engine aircraft having a maximum take-off mass exceeding 15 000 kg, or a maximum approved passenger configuration of more than 30.
- Phase 2, with effect from 1 January 2005, but with a transition phase until 31 March 2006, for all civil fixed-wing turbine-engine aircraft having a maximum take-off mass exceeding 5 700 kg, or a maximum approved passenger configuration of more than 19.

3.4.1 ACAS with Mode S

TCAS surveillance of Mode S equipped aircraft is based on the selective address feature of the Mode S transponder. TCAS listens for the spontaneous transmissions (squitters) sent once per second by Mode S transponders. The individual address of the sender is contained inside the squitter. Following receipt of a squitter, TCAS sends a Mode S interrogation to the Mode S address contained in the message. TCAS uses the reply received to determine range, bearing and altitude of the intruder aircraft. TCAS tracks the changes in range, bearing, and altitude of each Mode S aircraft within cover. This data is provided to the collision avoidance logic to determine the requirement for TAs or RAs.

3.4.2 ACAS with Mode A/C

TCAS uses a modified Mode C interrogation to interrogate Mode A/C transponders. This interrogation is known as the 'Mode C only all call'. Note: TCAS does not know the Mode A code of the intruder aircraft because it does not interrogate Mode A.

The replies from Mode A/C transponders are tracked in range, bearing and altitude. This data is provided to the collision avoidance logic to determine the requirement for TAs or RAs. In some cases, the Mode A/C transponders can reply to the 'Mode C only all-call', without providing any altitude information. TCAS then uses the synchronisation pulse of the reply to initialise and maintain tracking but provides only the range and the bearing for such aircraft. This data is provided to the collision avoidance logic to determine the requirement for TAs. This data is insufficient for the provision of RAs.

Synchronous and non-synchronous garbling problems, and ground-reflected replies, make it more complicated for TCAS to monitor Mode A/C equipped aircraft than those equipped with Mode S transponders.

3.4.3 RA downlink

Using the Mode S Data Link, TCAS can downlink RA reports to Mode S ground sites. Also, during an RA, every eight seconds TCAS generates a spontaneous message containing information on the current advisory.

3.5 ADS-B

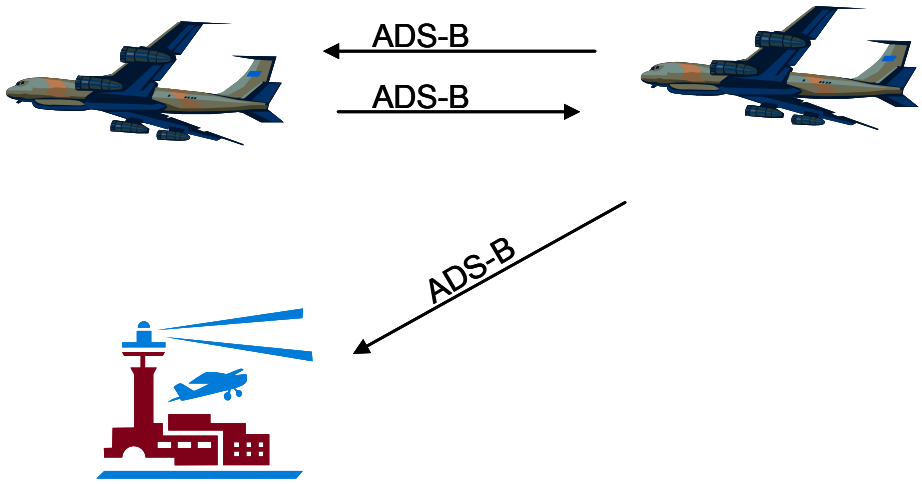

Figure 8 Illustration of ADS-B

Three link solutions are being proposed as the physical layer for relaying ADS-B position reports:

- Mode S Extended Squitter
- Universal Access Transceiver
- VDL Mode 4

An ADS-B transmitter periodically broadcasts its state vector (horizontal and vertical position, horizontal and vertical velocity) and other information, depending on the application.

3.5.1 Applications

The Core European 2010 scenario 3 assumes that the ADS-B applications to be implemented in the period of interest are those currently included in "Application Package 1". These applications are as follows:

- *Ground Surveillance (GS) Applications:* ATC Air to Ground Surveillance for *en route* and Terminal Manoeuvring Areas (TMA)
- *Airborne Surveillance (AS) Applications*
  - Airborne Traffic Situational Awareness (ATSAW)
- *Surface Enhanced Visual Acquisition (SEVA*)
- *Enhanced Visual Acquisition (EVA)*
  - Airborne Spacing and Merging for TMA and *en route*
- *Airborne Separation Assurance* in low-density remote and oceanic Airspaces

All the above applications, except for last bulleted item, are to be used in the Core European area, where ADS-B will be used in parallel with the existing ground surveillance infrastructure.

3.5.1.1 Ground Surveillance

Five GS applications are identified and are summarised below.

3.5.1.1.1 ATC surveillance for en-route air space (ADS-B-ACC)

This application will enhance ATC surveillance currently provided with radars. An example of many is the case of surveillance in areas where single radar coverage is provided.

3.5.1.1.2 ATC surveillance in terminal areas (ADS-B-TMA)

This application will enhance ATC surveillance currently provided with radars. An example of many is the case of surveillance at low altitude and close to the terrain and also in areas where single radar coverage is provided.

3.5.1.1.3 ATC surveillance in non-radar areas (ADS-B-NRA)

This application will provide ATC surveillance in non-radar areas; e.g. remote areas, offshore operation areas, any continental areas and certain oceanic areas, which, due to the level of traffic or the cost of the equipment, could not justify the installation of radars. The purpose is to enhance traffic information and separation services.

3.5.1.1.4 Airport surface surveillance (ADS-B-APT)

This application will provide a new source of surveillance information for a safer and more efficient ground movement management at airports with or without SMGCS. Airport ground vehicles can also be fitted with the necessary equipment and displayed on an airport map, together with aircraft.

3.5.1.1.5 Aircraft derived data for ground tools (ADS-B-ADD)

This application will provide additional aircraft derived data through ADS-B to be used by the ATC ground system for developing or enhancing ATC tools like displays, MTCD, AMAN, DMAN and ground based safety nets. CDM applications will also share the benefits.
It should be noted that this application does not encompass the ground tools themselves; it only provides additional input data for these tools.

3.5.1.2 Air Surveillance

Below a number of Air Separation Aid System (ASAS) applications belonging to the categories airborne traffic situational awareness and airborne spacing applications are listed.

3.5.1.2.1 Enhanced traffic situational awareness on the airport surface (ATSA-SURF)

This application provides the flight crews with an “enhanced traffic situational awareness” on the airport surface for both taxi and runway operations, in all weather conditions. The objectives are to improve safety (e.g. at taxiway crossings, before entering a runway, on pushback) and to reduce taxi time in particular during low visibility conditions or at night.

3.5.1.2.2 Enhanced traffic situational awareness during flight operations (ATSA-AIRB)

This application provides the flight crews with an “enhanced traffic situational awareness” irrespective of visual conditions. Additional data is provided to flight crews to supplement traffic information provided either by controllers or other flight crews. The objectives are to improve safety of flight and the efficiency of air traffic control. In all airspace, the flight crews will be better able to detect an unsafe situation.

3.5.1.2.3 Enhanced visual acquisition for see & avoid (ATSA-S&A)

This application is an aid for the flight crews to perform their collision avoidance task when separation service in not provided by ATC (e.g. IFR/VFR in class D and E airspace, class G airspace). The objective is safer flight operations.

3.5.1.2.4 Enhanced successive visual approaches (ATSA-SVA)

This application is an aid for the flight crews to perform successive visual approaches when they are responsible for maintaining visual separation from the aircraft they are following. The objectives are to perform successive visual approach procedures on a more regular basis to enhance the runway throughput, and to conduct safer operations especially in high-density areas.

3.5.1.2.5 Enhanced sequencing and merging operations (ASPA-S&M)

The objective is to redistribute tasks related to sequencing (e.g. in-trail following) and merging of traffic between the controllers and the flight crews. The controllers will be provided with a new set of instructions directing, for example, the flight crews to establish and to maintain a given time or distance from a designated aircraft. The flight crews will perform these new tasks using a suitable human-machine interface. The main expected benefit is increased controller availability, but increased capacity through better adherence to ATC separation minima is also expected especially in high-density areas.

3.5.1.2.6 In-trail procedure in oceanic airspace (ASPA-ITP)

The In-Trail Procedure in non-radar oceanic airspace is a procedure allowing in-trail ADS-B equipped aircraft, which may not be longitudinally separated from each other, to climb or descend through each other's flight levels. The objective is to improve the utilisation of the NAT oceanic airspace by facilitating a higher rate of flight level changes than is currently provided, yielding better flight efficiency (e.g. fuel savings, avoiding turbulent flight levels).

3.5.1.2.7 Enhanced crossing and passing operations (ASPA-C&P)

The objective is to provide the controller with a new set of instructions to solve conflicts directing, for example, the flight crews to cross or pass a designated traffic while maintaining a given spacing value. The flight crews will perform these new tasks using a suitable human-machine interface. The main expected benefit is increased controller availability through the reorganisation and the streamlining of tasks.

3.5.1.3 Future applications

Future packages are going to be built on the experience gained from Package I and data collected during the operation of Package I applications. It is too early to define the number and the content of the future packages because much R&D is required to better define the future applications and to validate these applications. Nevertheless, future applications can be split in two groups:

- Enhancement of applications already included in Package I
- New GS/AS applications.

3.5.1.3.1 Package I enhanced applications

Package I enhanced applications could be for example:

- For GS applications, to provide separation service in medium/high traffic density areas or to provide new aircraft derived data for enhancing ATC tools.
- For AS applications, to enhance spacing applications with new automated airborne spacing functions on board the aircraft which may require the exchange of aircraft intent parameters.

3.5.1.3.2 New GS/AS applications

For new GS/AS applications, the selection of applications belonging to the two last categories of the PO-ASAS document (i.e. Airborne separation and airborne self-separation applications) is, of course, envisaged. These applications are expected to bring further benefits in terms of capacity and flexibility. The following definitions for future packages are provided as an indication:

Package II:

- Enhanced GS/AS applications from Package I
- ADS-B as a sole mean of surveillance in high density airspace
- Airborne separation applications (i.e. PO-ASAS category III applications)
- Airborne self-separation application (i.e. PO-ASAS category IV applications) in low density airspace.

Package III:

- Enhanced GS/AS applications from Package II
- Airborne self-separation application (i.e. PO-ASAS category IV applications) in medium/high-density airspace.

3.6 A-SMGCS

An Advanced Surface Movement Guidance System (A-SMGCS) is needed to enhance safety and capacity of airport surface operations particularly under low visibility conditions. Surface surveillance is provided via several surveillance technologies (primary surface surveillance radar, ADS-B, and multilateration).

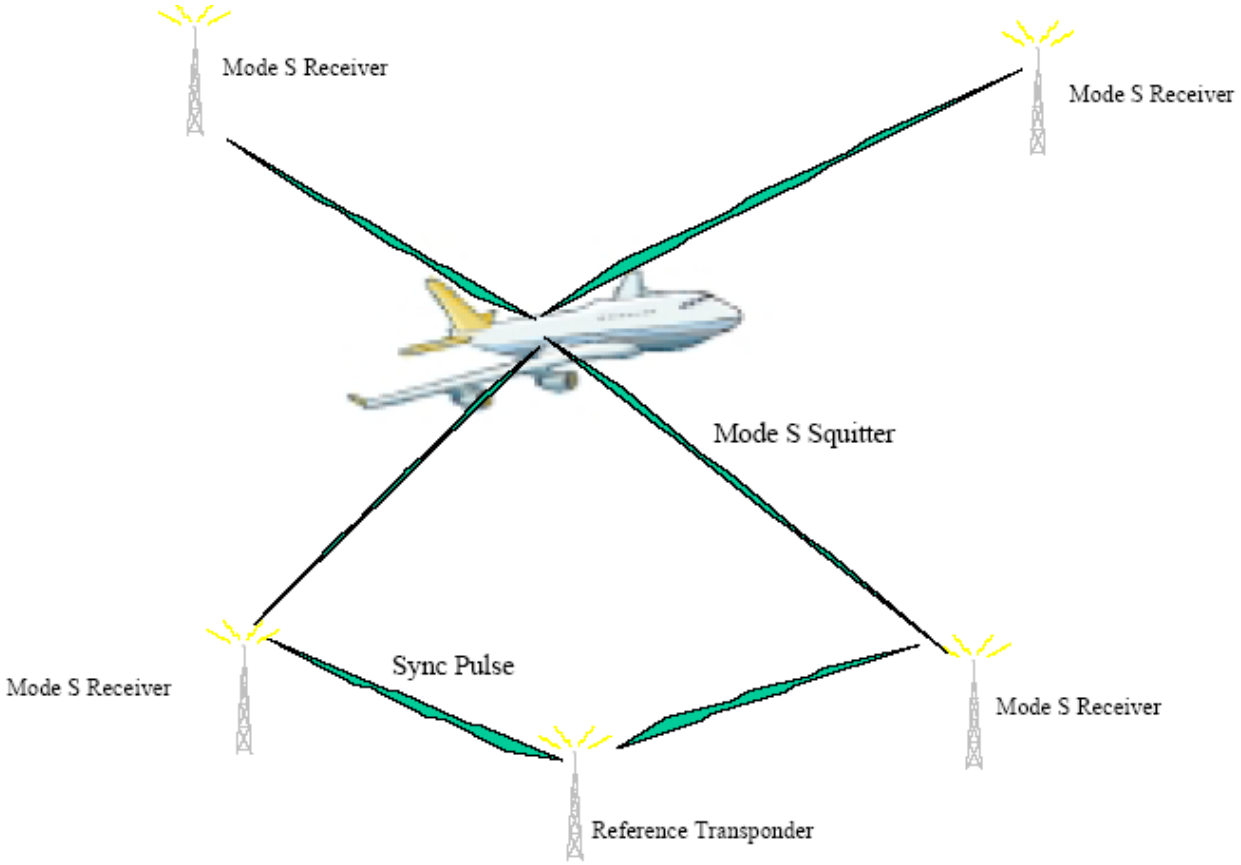

Figure 9 Illustration of multilateration at airports 4

Multilateration uses Time Difference Of Arrival (TDOA) to triangulate or multilaterate aircraft position. It determines position from Mode S and Mode A/C transponder transmissions, and supports update rates of once per second. It is more accurate than primary and secondary radar with accuracy less than 5 meters (RMS).

3.7 References

1. John Law, Presentation at Mode S & A-SMGCS Information Day, 14 June 2006. http://www.eurocontrol.int/msa/gallery/content/public/documents/Modes_Day.zip
2. M.C. Stevens, *Secondary Surveillance Radar*, Artech House, 1988.
3. CARE/ASAS Activity 5 Description of a first package of GS/AS applications, CARE/ASAS/EUROCONTROL/02-040 - Version 2.2 - September 30, 2002 - CA-02-040(2.2).doc

4. Evaluation of ADS-B at Heathrow for EUROCONTROL ADS Programme Report. EEC/ASTP/AIRP/003. http://www.eurocontrol.int/eec/gallery/content/public/documents/EEC_SSP_documents/ADS_B_Heathrow_Trial_1_0.pdf

4 HEO satellite communication for ATM in high latitudes

In the study reported in this chapter, an assessment of the effects of the propagation channel of a system for communication between aircraft and HEO satellites operating at 1.5 GHz is made. The work is done as part of a project investigating the requirements for a HEO satellite system providing ATM and AOC services to the aeronautical industry in northern latitudes and polar areas. Both Molniya and Tundra types of orbits are included. The objective is twofold. First, numeric results are given to be used in the communication system design, e.g. by being incorporated in link budget calculations. Secondly, the results are used to develop a software channel model that may be used to evaluate the bit level performance of a communication link.

The characteristics of the propagation channel are basically related to three factors. The first factor is the movements of the aircraft and the satellite. The highly elliptical satellite orbits lead to variations in distance between transmitter and receiver, and consequently to variations in free space path loss and two-way delay. As opposed to geostationary satellites, the satellite movements also introduce varying Doppler shifts and elevation angle. The second factor is atmospheric effects as the signal propagates through the ionosphere and the troposphere. Finally, the signal will experience multipath fading due to reflections both from the surface of the aircraft, and from the ground. The two first factors lead to relatively slow variations in the channel characteristics, and must be taken into account in the system design. The last factor leads to rapid variations of the channel conditions, and is included in the multi-tap channel model.

4.1 Effects of satellite movement

The propagation channel of HEO satellite communication has different characteristics than those of both GEO and LEO satellite communications. The effects of the orbital movements considered in this section are free space path loss, delay, elevation angle, Doppler shift and Doppler rate. Both Tundra orbit and Molniya orbit satellites are considered.

4.1.1 Calculations

For reference, the procedure used to calculate the channel parameters are given in this sub-section.

4.1.1.1 Free space path loss

The equation for the free space path loss is given by:

$$L_f = \left(\frac{4\pi d f_c}{c} \right)^2,$$

where d is the distance between the transmitter and the receiver, f_c is the carrier frequency and c is the speed of light. It is often more convenient to express L_f in dB:

$$L_f = 20\log_{10}(d) + 20\log_{10}(f_c) + 92.44,$$

where d is given in km and f_c in GHz.

4.1.1.2 Two-way delay

The two-way (ground-satellite-ground) delay τ_{2w} is simply given as:

$$\tau_{2w} = 2\frac{d}{c}$$

4.1.1.3 Elevation angle

In order to define the elevation angle ε it is convenient to define three vectors:

$\mathbf{r_c}$: the vector from the earth centre to the earth station

$\mathbf{r_e}$: the vector from the earth centre to the satellite

$\mathbf{d} = \mathbf{r_e} - \mathbf{r_c}$: the vector from the earth station to the satellite

The subscripts 'c' and 'e' denotes circular and elliptical orbits, respectively. The elevation angle is related to the zenith angle Ω in the following way:

$$\varepsilon = \frac{\pi}{2} - \Omega$$

The zenith angle is the angle between the vectors $\mathbf{r_c}$ and $\mathbf{d}$. The vectors are given in Cartesian coordinates by:

$$\mathbf{r_c} = R\left(\cos L \cos\theta_c \ \mathbf{i} + \cos L \sin\theta_c \ \mathbf{j} + \sin L \ \mathbf{k}\right),$$

$$\mathbf{r_e} = \frac{A\cos I}{1+e\cos\theta_e}\cos\theta_e \ \mathbf{i} + \frac{A\sin\theta_e}{1+e\cos\theta_e}\mathbf{j} - \frac{A\sin I}{1+e\cos\theta_e}\cos\theta_e \ \mathbf{k},$$

where R is the earth radius, the angle L is the latitude of the earth station, the angle I is the inclination angle of the satellite orbit, e is the eccentricity of the satellite orbit, and A is equal to b^2/a. The parameter a is the semi-major axis and b the semi-minor axis of the satellite orbit. The angle from the perigee longitude is denoted θ, where sub-script e denotes elliptical satellite orbit and sub-script c circular earth station orbit. The elevation angle can then be calculated using the scalar product between $\mathbf{d}$ and $\mathbf{r_c}$:

$$\varepsilon = \frac{\pi}{2} - \Omega = \frac{\pi}{2} - \arccos\left(\frac{\mathbf{d}\cdot\mathbf{r_c}}{|\mathbf{d}||\mathbf{r_c}|}\right)$$

4.1.1.4 Doppler shift

The Doppler shift is related to the radial velocity v_d between earth station and satellite:

$$f_d = -\frac{v_d}{c} f_c$$

The radial speed can be calculated using projection:

$$v_d = \mathbf{v} \cdot \frac{\mathbf{d}}{|\mathbf{d}|} = \left(\frac{d\mathbf{r}_e}{dt} - \frac{d\mathbf{r}_c}{dt} \right) \cdot \frac{\mathbf{d}}{|\mathbf{d}|}$$

4.1.1.5 Acceleration and Doppler rate

The Doppler rate is the variation in Doppler shift, and is related to the radial acceleration between the earth station and the satellite:

$$\frac{df_d}{dt} = -\frac{f_c}{c}\frac{dv_d}{dt}$$

4.1.2 Tundra orbit

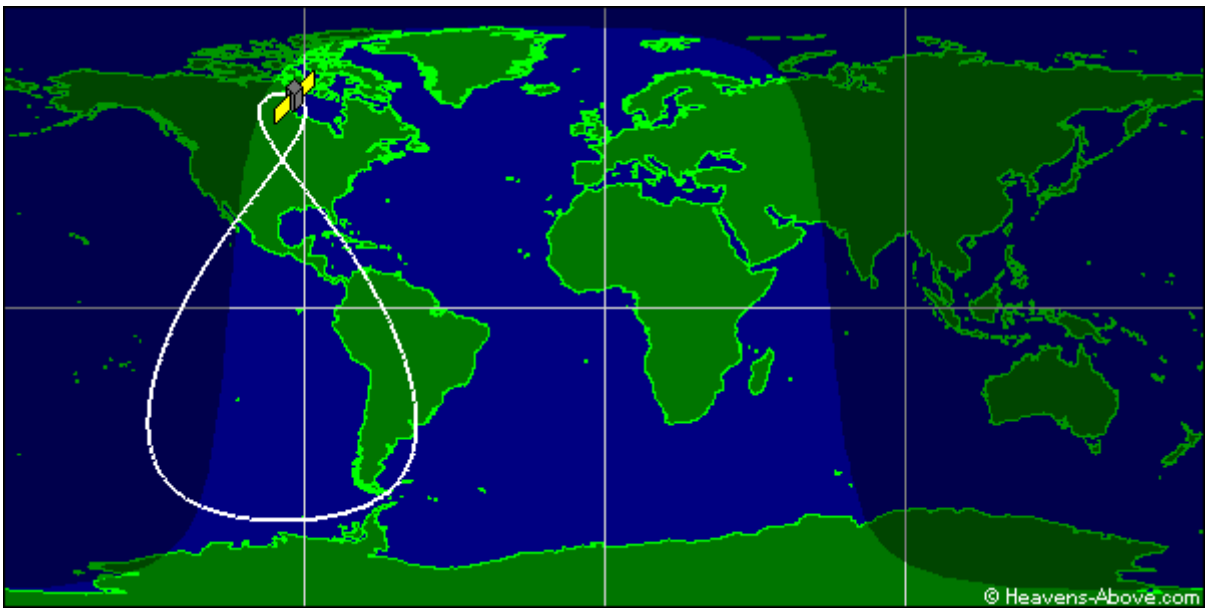

Figure 10 Sirius satellite ground track with apogee over Canada.

Table 3 Orbital parameters for Tundra orbit satellites.

	Sirius-1	Sirius-2	Sirius-3
Perigee height	24461.2 km	24574.7 km	24618.9 km
Apogee height	471225.9 km	47006.6 km	46964.5 km
Eccentricity e	0.27	0.27	0.26
Inclination i	61.8°	63.7°	63.9°
Argument of Perigee ω	270.3°	270.0°	270.0°
Period	1436.1 min	1435.9 min	1436.0 min

Examples of Tundra orbit satellites are the Sirius satellites providing satellite radio broadcasting over Northern America. Orbital parameters for the three Sirius satellites are given in Table 3. The parameters are very similar for the satellites, and for simplicity the parameters for the first satellite are used in the following.

4.1.2.1 Free space path loss

The equations used to calculate the free space path loss, elevation angle and Doppler shift permit to position the ground station anywhere on or above the earth surface. The curves included in this section correspond to locations on the apogee longitude and at latitudes from 60 degrees to 90 degrees.

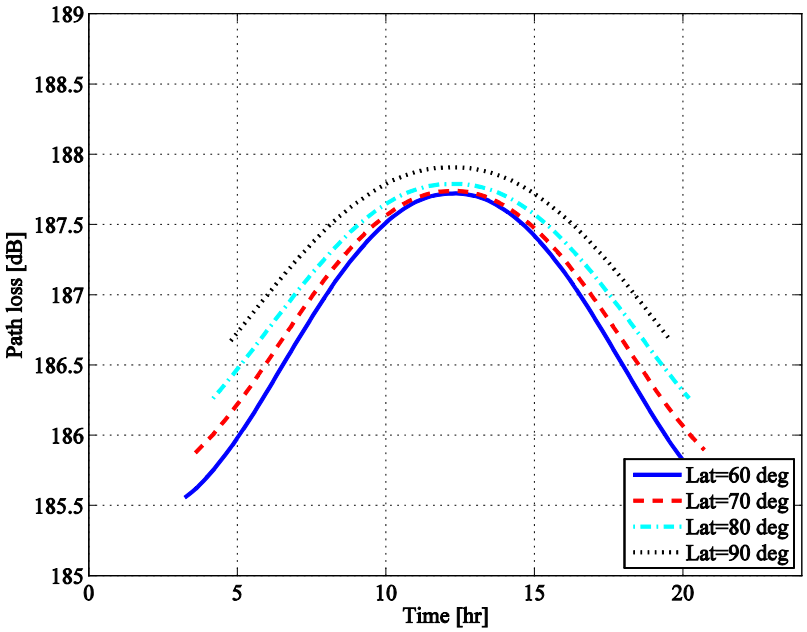

Figure 11 Free space path loss as function of time and latitude of ground station for perigee longitude zero.

The free space path loss varies from about 185.5 dB when the satellite appears above the horizon to almost 188 dB when the satellite reaches the apogee. For earth stations located 90 degrees to the east or to the west, the maximum path loss increases about 0.2 dB. The reduction in free space path loss for an airborne station at 10000 meters altitude compared to that of an earth station on ground is negligible.

4.1.2.2 Two-way propagation delay

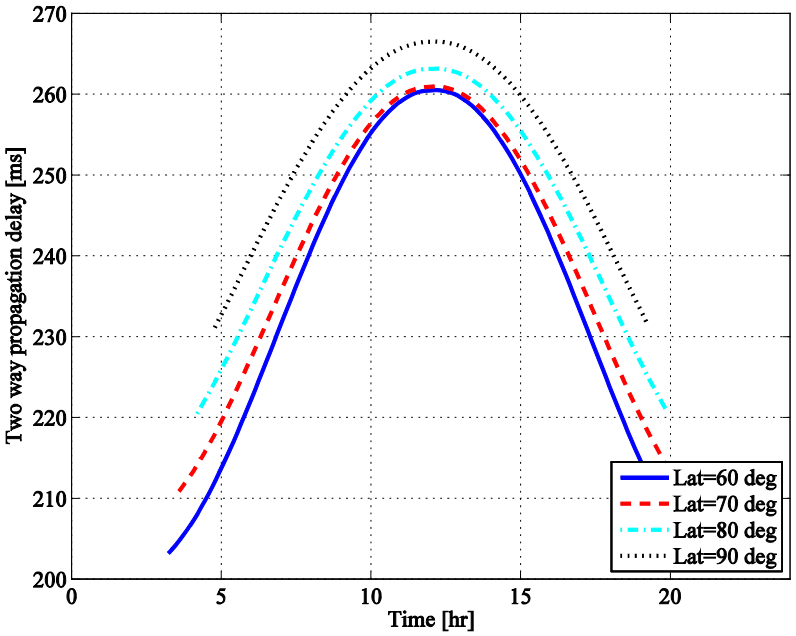

Figure 12 Two-way propagation delay as function of time and latitude of earth station for perigee longitude zero.

The maximum two-way propagation delay is between 260 ms and 270 ms, and it increases with the latitude.

4.1.2.3 Elevation angle

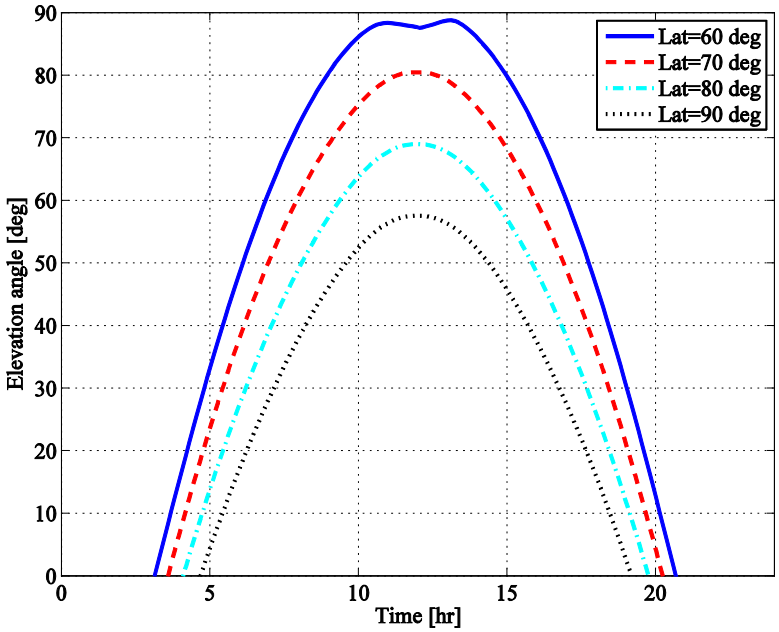

Figure 13 Elevation as function of time and latitude of earth station for perigee longitude zero.

Table 4 Time of visibility in hours per day at different latitudes and perigee longitude zero.

	Lat=60 deg	Lat=70 deg	Lat=80 deg	Lat=90 deg
e>80 deg	6	1.2	0	0
e>60 deg	10.1	7.9	5.2	0
e>40 deg	13	11.5	9.7	7.4
e>20 deg	15.4	14.4	13	11.4
e>0 deg	17.5	16.7	15.6	14.4

Table 5 Time of visibility in hours per day at different latitudes and perigee longitude 30 degrees.

	Lat=60 deg	Lat=70 deg	Lat=80 deg	Lat=90 deg
e>80 deg	0	0	0	0
e>60 deg	8.6	6.8	4.4	0
e>40 deg	12.4	11	9.5	7.4
e>20 deg	14.9	14	12.7	11.4
e>0 deg	17.3	16.4	15.5	14.4

Figure 13 illustrates how the elevation angle changes for an earth station at perigee longitude zero and different latitudes. As the period of the elliptic orbit is equal to the earth period, zero perigee longitude is optimal with respect to time of satellite visibility. The number of hours the satellite can be seen above different elevation angles is shown in Table 4. The time of visibility for an earth station with perigee longitude 30 degrees is shown in Table 5. Comparing the two tables illustrates that the time of visibility is not very sensitive to longitude position of the earth station.

4.1.2.4 Doppler shift

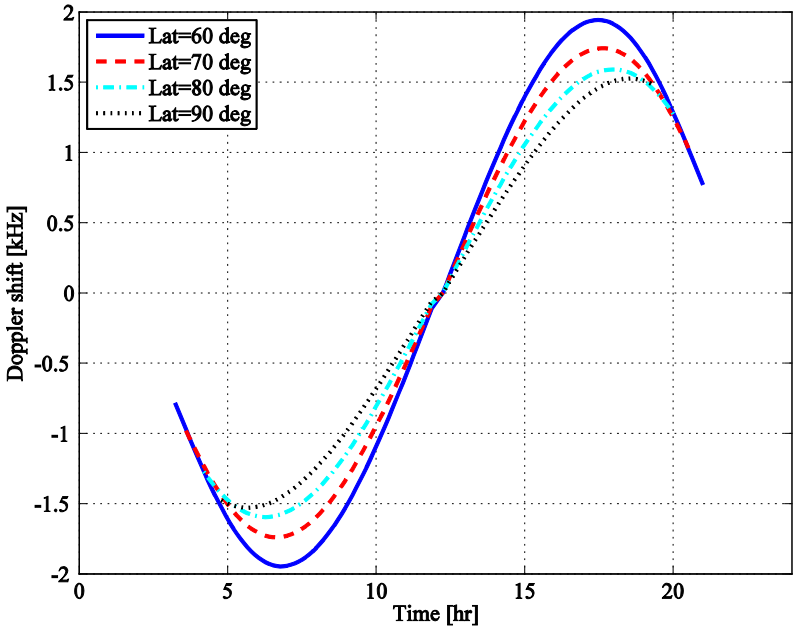

Figure 14 Doppler shift as function of time and latitude of earth station with perigee longitude zero.

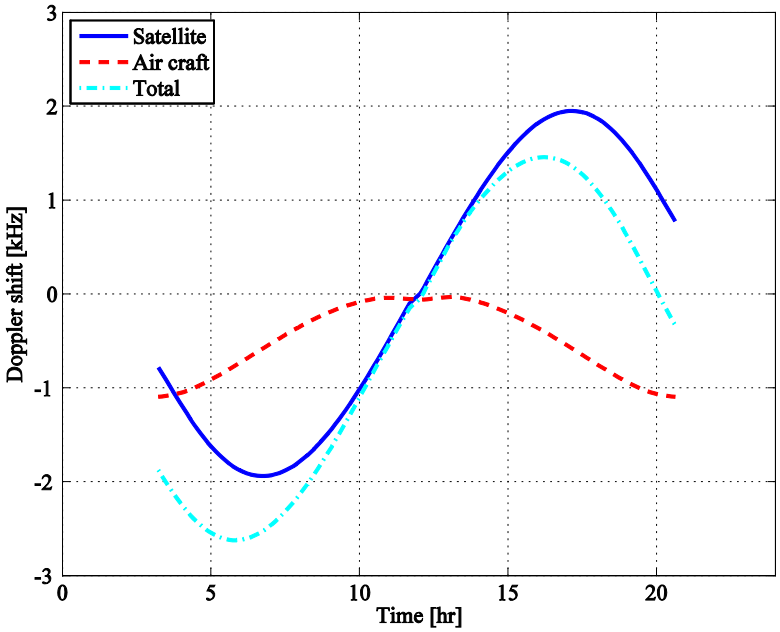

Figure 15 Doppler shift as function of time and latitude of an airborne station with perigee longitude zero, and with horizontal speed 800 km/h.

The Doppler shift is shown in Figure 14. The maximum Doppler shift occurs when the satellite is at the mid point between perigee and apogee, and is in the order of 2 kHz. As expected, the Doppler shift is zero when the satellite is at its apogee. Figure 15 compares the Doppler shift caused by the satellite movement with that caused by an aircraft with horizontal speed 800 km/h towards the satellite. The maximum Doppler shift caused by the aircraft movement is about 1 kHz. The total Doppler shift may therefore be up to about 2.5-3 kHz.

4.1.2.5 Doppler rate

The variation of Doppler shift is illustrated in Figure 16. It is less than 1 Hz/s for all times the satellite is visible.

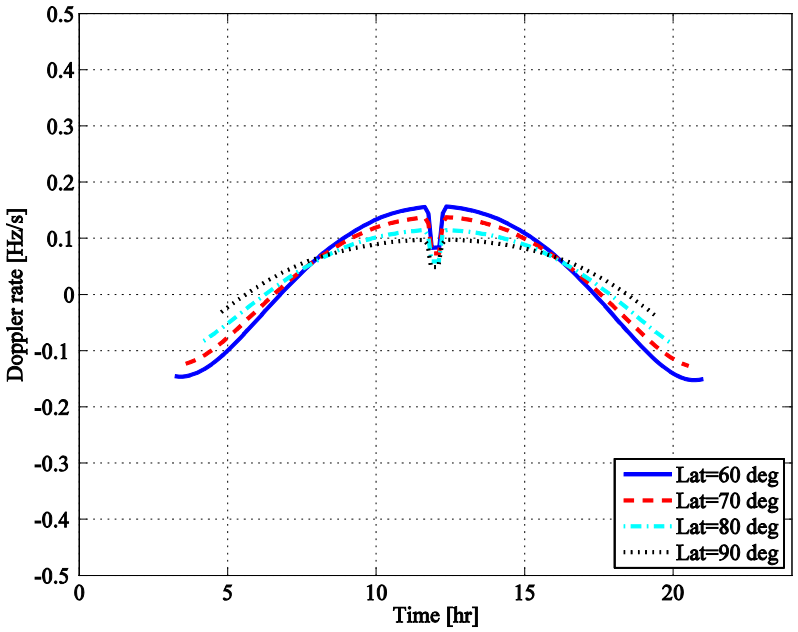

Figure 16 Doppler rate as function of time and latitude of earth station with perigee longitude zero.

4.1.3 Molniya orbit

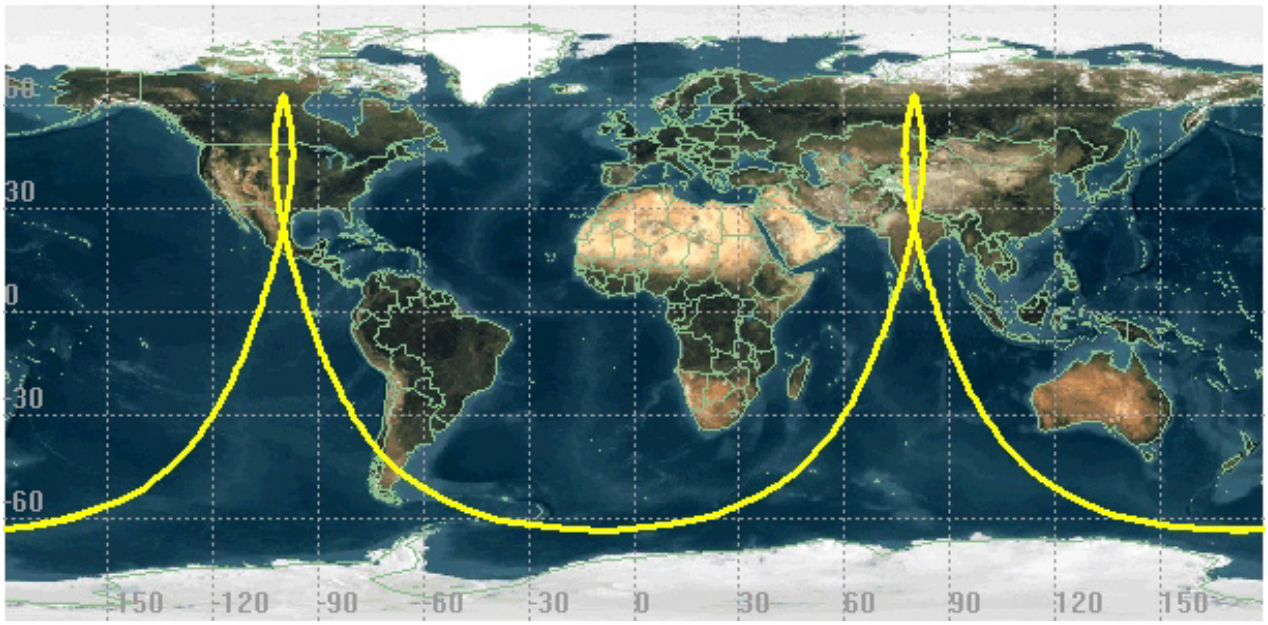

Figure 17 Molniya satellite ground track (from:http://en.wikipedia.org/wiki/Image:Molniya.jpg)

Russia currently has several satellites in Molniya orbits, both for military applications and for television broadcasting. Orbital parameters for three Molniya satellites are shown in Table 6.

The period of the Molniya satellites is 12 hours, which means that they reach apogee twice each 24 hours. For earth stations far to the north, the satellites are visible at both apogees, and at the geographical North Pole the satellites reach the same elevation angle both times.

Table 6 Orbital parameters for Molniya orbit satellites

	Molniya 1-92	Molniya 3-53	Molniya 1-93
Perigee height	1419.6 km	1417.1 km	792.3 km
Apogee height	38957.0 km	38953.2 km	39579.7 km
Eccentricity e	0.71	0.71	0.73
Inclination i	64.8°	64.8°	64.8°
Period	717.9 min	717.8 min	717.8 min

4.1.3.1 Free space path loss

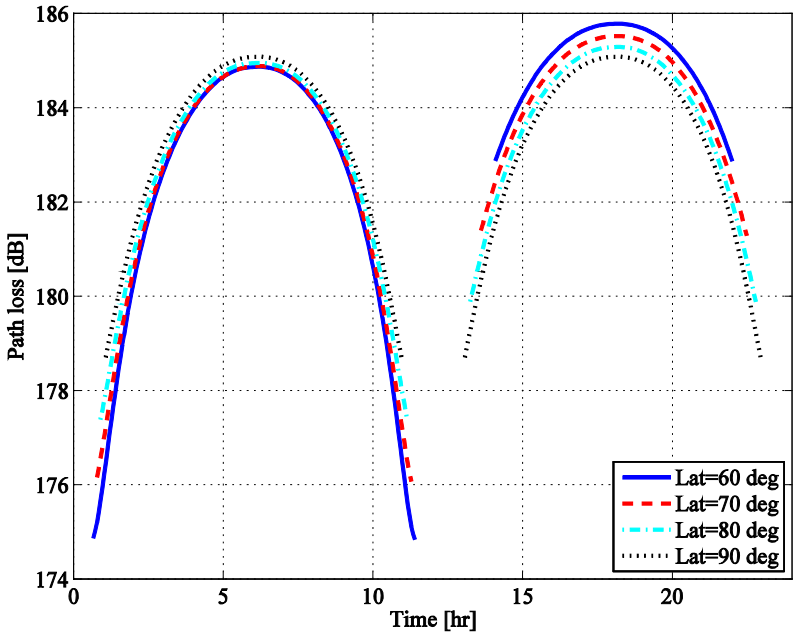

Figure 18 Free space path loss as function of time and latitude of earth station for perigee longitude 90 degrees.

The calculated free space path loss is shown in Figure 20. As the Molniya satellites rotate twice as fast as the earth, a perigee longitude of 90 degrees means that the satellite is at the same longitude as the earth station when it reach its apogee. (The earth station has rotated 90 degrees and the satellite 180 degrees). The maximum free space path loss is in the order of 185-186 dB.

4.1.3.2 Two-way propagation delay

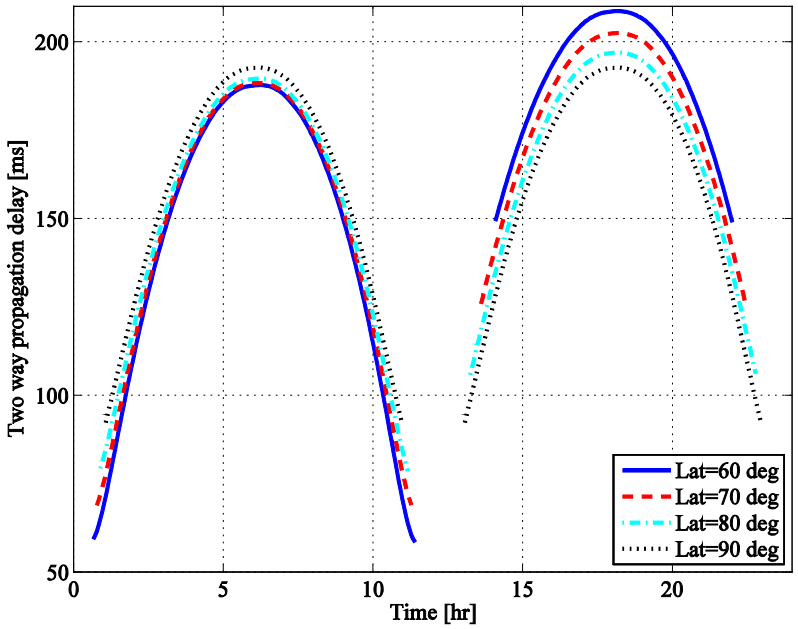

Figure 19 Two-way propagation delay as function of time and latitude of earth station for perigee longitude 90 degrees.

The maximum two-way propagation delay is in the order of 190 ms - 200 ms when the satellite is rising above the same hemisphere as the earth station is located, and 200 ms - 210 ms when the satellite is rising above the opposite hemisphere.

4.1.3.3 Elevation angle

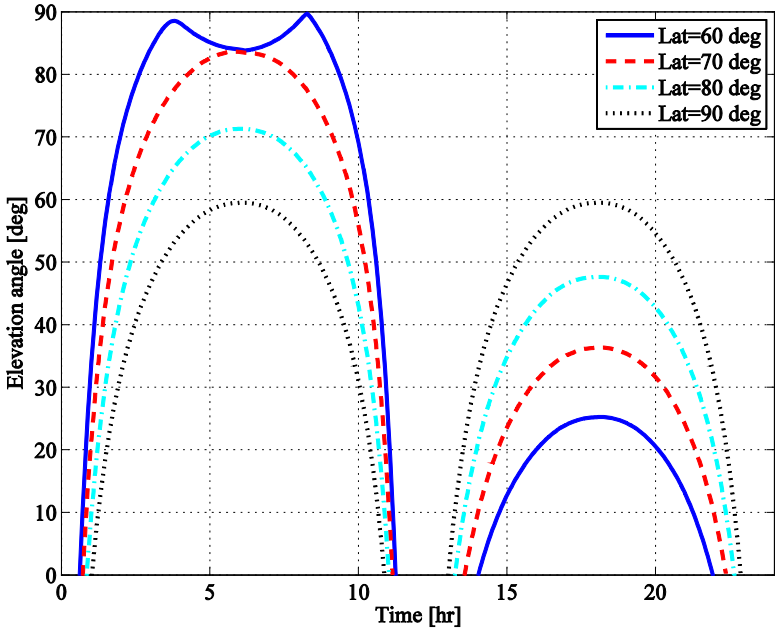

Figure 20 Elevation angle as function of time and latitude of earth station for perigee longitude 90 degrees.

Table 7 Time of visibility in hours per day at different latitudes and perigee longitude 90 degrees.

	Lat=60 deg	Lat=70 deg	Lat=80 deg	Lat=90 deg
e>80 deg	6.7+0	3.5+0	0+0	0+0
e>60 deg	8.8+0	7.6+0	5.8+0	0+0
e>40 deg	9.7+0	9.1+0	8.3+4.8	7.0+7.0
e>20 deg	10.3+4.1	10.0+6.7	9.5+8.0	8.9+8.9
e>0 deg	10.7+7.9	10.4+8.8	10.2+9.5	9.8+9.8

Table 8 Time of visibility in hours per day at different latitudes and perigee longitude 60 degrees.

	Lat=60 deg	Lat=70 deg	Lat=80 deg	Lat=90 deg
e>80 deg	0+0	0+0	0+0	0+0
e>60 deg	7.9+0	7.0+0	5.3+0	0+0
e>40 deg	9.4+0	8.9+0	8.2+5.1	7.0+7.0
e>20 deg	10.1+4.9	9.8+7.0	9.4+8.1	8.9+8.9
e>0 deg	10.6+8.2	10.3+8.9	10.1+9.5	9.8+9.8

Figure 20 shows how the elevation angle varies as function of time at different latitudes. The time durations the satellite is visible above a minimum elevation angle are listed in Table 7 for the optimal perigee longitude 90 degrees, and for 30 degrees off this longitude in Table 8.

4.1.3.4 Doppler shift

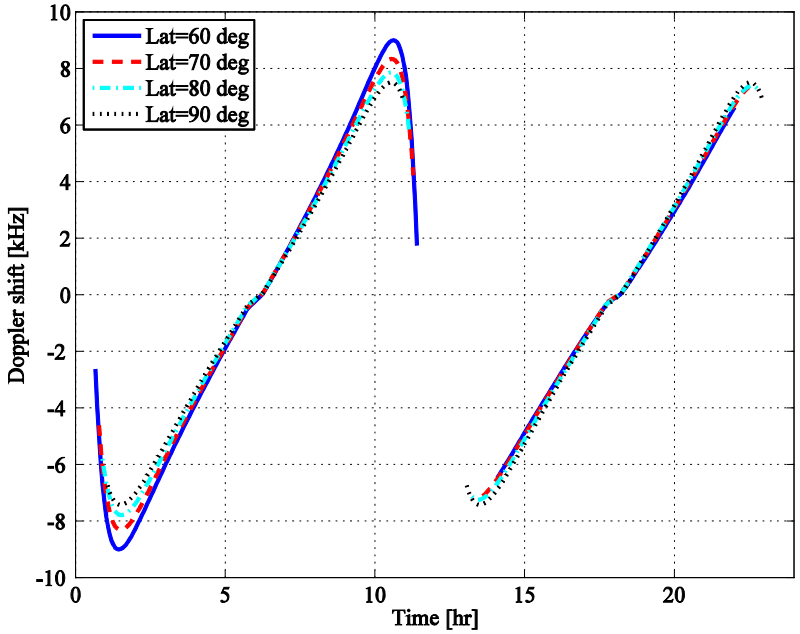

Figure 21 Doppler shift as function of time and latitude of earth station for perigee longitude 90 degrees.

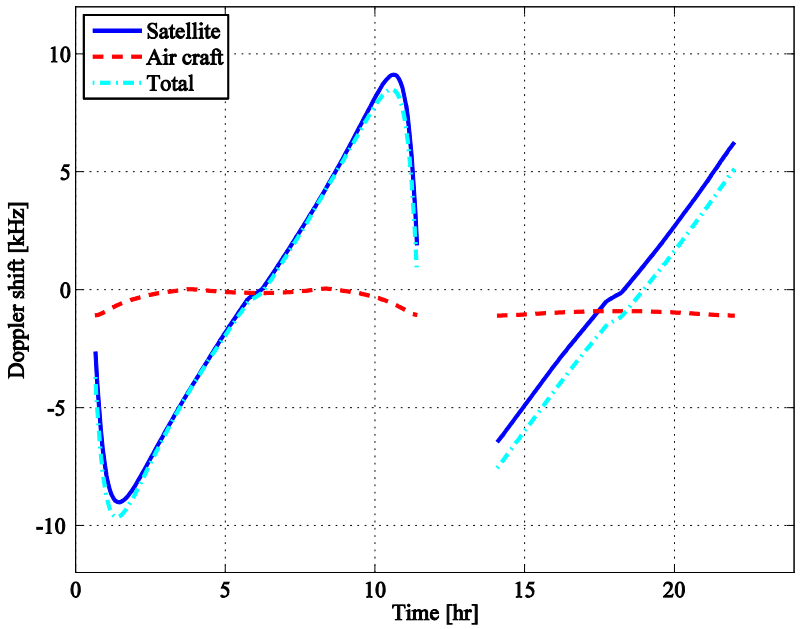

Figure 22 Doppler shift as function of time and latitude of an airborne station with perigee longitude zero, and with horizontal speed 800 km/h.

The Doppler shift as function of time is illustrated in Figure 21. The maximum Doppler shift is in the order of 8-9 kHz, and it does not change much as function of earth station position neither in latitude nor longitude. In Figure 22 the Doppler shift due to the satellite movement is compared to that of an aircraft with horizontal speed of 800 km/h towards the satellite. The effect of the aircraft's movement is small compared to that of the satellite.

4.1.3.5 Doppler rate

Finally, the variation of Doppler shift is illustrated in Figure 23. Its maximum value is in the order of 8 Hz/s at very low elevation angles. Most of the time the satellite is visible, the Doppler rate is below 1 Hz/s.

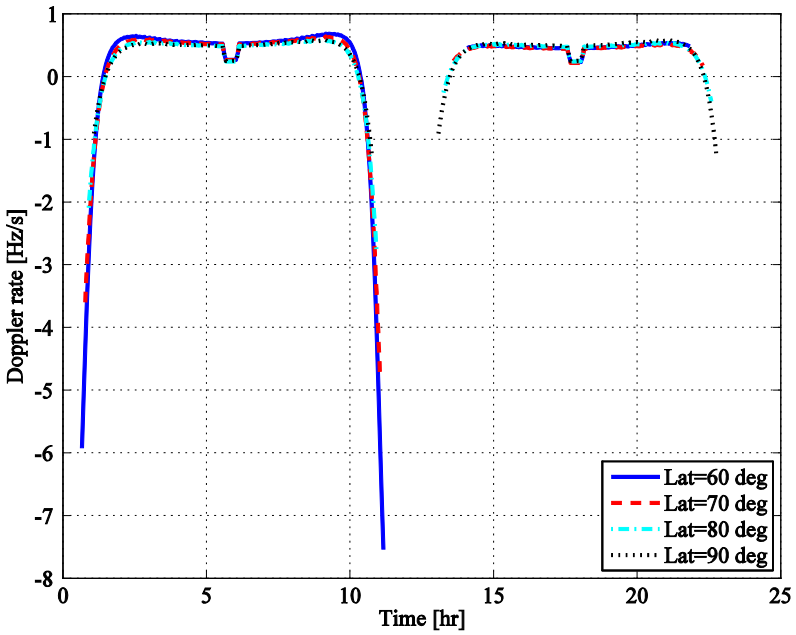

Figure 23 Doppler rate as function of time and latitude of earth station with perigee longitude zero.

4.1.4 Summary of the effects from satellite movement

The results of this section can be summarised as follows.

The maximum free space path loss is in the order of 187-188 dB for Tundra satellites, and in the order of 185-186 dB for Molniya satellites. It does not vary significantly with the altitude or position of the earth station.

The maximum two-way delay spread for Tundra orbit satellite communication is about 260 ms- 270 ms, while it is about 200 ms for Molniya orbit satellite communication. For voice communication, this is well above the maximum latency requirement given in e.g. [2]. It is however within the requirements for digital ATS and AOC services.

Both orbits provide good coverage on the North Pole. Molniya orbit satellites provide coverage with minimum elevation angle above 20 degrees almost 18 hours a day, which is 7 hours more then Tundra orbit satellites. For the far north, Molniya orbit satellites may therefore provide better coverage than Tundra orbit satellites, while the opposite is the case for lower latitudes (less than about 60 degrees).

The maximum Doppler shift is in the order of 2 kHz for Tundra satellites and 8-9 kHz for Molniya satellites. The Doppler shift caused by the aircraft may be up to about 1 kHz. It must therefore be taken into account for communications with Tundra orbit satellites, while it is less significant for communication with Molniya orbit satellites.

The Doppler rate may be significantly larger (in the order of 10 Hz/s) for Molniya orbit satellites for very low elevation angles, while the Doppler rate is always below 1 Hz/s for Tundra orbit satellites.

4.2 Atmospheric effects

A signal propagating between an aircraft and a satellite will be affected by the ionosphere and troposphere. In this section the impact of both the ionosphere and the troposphere on a 1.5 GHz signal is reviewed based on the relevant ITU-R recommendations.

4.2.1 Ionospheric effects

The impact of ionospheric effects on earth-space communications is considered in Rec. ITU-R P.531-9. A signal propagating through the ionosphere is degraded due to background ionizations and irregularities. Background ionizations lead to Faraday rotation, group delay and dispersion. Irregularities lead to scintillations of the signal.

4.2.1.1 Background ionizations

Background ionization depends on the total electron content (TEC) accumulated along the earth station-satellite signal path. One method used to estimate the TEC is based on the international reference ionosphere (IRI), another one is based on NeQuick.

- IRI-based method: A standard monthly median ionosphere (COSPAR-URSI IRI-95) is used to derive values for any location, time and heights up to 2000 km. A simplified and often sufficient method is to estimate electron content by multiplication of the peak electron density with an equivalent slab thickness value of 300 km. Problems using this method may arise under conditions of high solar activity.
- NeQuick-based method: A continuous function represents the electron density distribution. The TEC may be estimated along arbitrary ground to satellite paths. A computer program and associated data files are available from ITU-R.

The main impact of background ionization is Faraday rotation, which means that a linearly polarized signal will suffer a gradual rotation of its plane of polarization. The magnitude of the rotation is proportional to the average earth magnetic field strength B_{av} and the TEC N_T of the plasma, and inversely proportional with the square of the frequency *f*:

$$\Theta = 2.36 \cdot 10^{-14} \frac{B_{av} N_T}{f^2} \text{ [rad]}$$

At 1.5 GHz, the Faraday rotation may vary from 0.01 rad to about 10 rad (corresponding to a TEC between about 10^{16} and 10^{19} el/m^2). The cross-polarization discrimination XPD in dB is related to the Faraday rotation angle by:

$$XPD = -20 \log(\tan \Theta)$$

Another effect of background ionizations is the group delay which can be computed as follows:

$$t = 1.345 \cdot 10^{-7} \frac{N_T}{f^2}$$

The group delay will generally be a fraction of a microsecond.

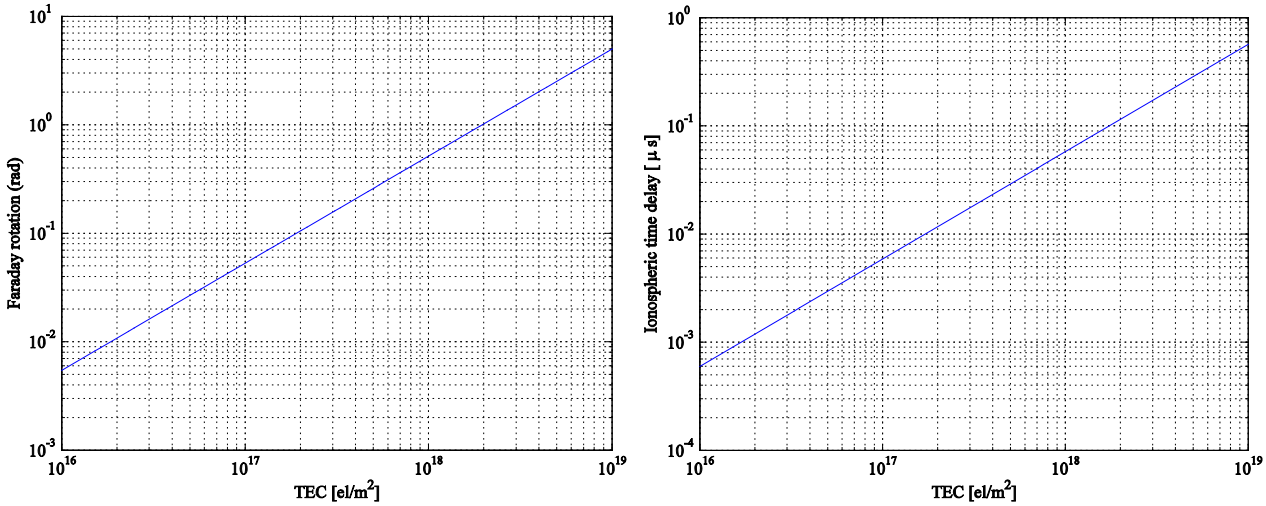

Figure 24 Effects of background ionizations on Faraday rotation (left) and group delay (right).

Dispersion due to background ionization will be small, less than 1 ns according to Figure 4 in Rec. ITU-R P531-9 assuming realistic signal bandwidths and TEC. It can consequently be neglected for realistic signal bandwidths.

The background ionization has relatively regular diurnal, seasonal and 11-year solar cycle variations. In the context of communications between aircrafts and satellites, the variations are slow and not considered further in this document.

4.2.1.2 Irregularities in ionization density

Small-scale irregular structures in the ionization density cause a steady signal to fluctuate in amplitude, phase and apparent direction of arrival. Such scintillations are particularly important at high latitudes and close to equator. Figure 5 in ITU-R P.531-9 indicates that the depth of fading may be as large as 5 dB in polar areas and larger than 15 dB close to equator at solar maximum. It is recommended that the global ionospheric scintillation model (GISM) is used to predict the intensity. GISM is used to predict the depth of amplitude fading and the rms phase and angular deviations as function of satellite and ground station position, date, time and operating frequency.

The effects of irregularities vary much faster than the background ionization. The corresponding Doppler spread is about 0.1 Hz to 1 Hz. Compared to channel variations shifts due to aircraft and satellite movement, which may be in the order of kilohertz, these variations are however still slow and will not be considered further in this document.

4.2.2 Tropospheric effects

Tropospheric attenuation is targeted in ITU-R P.618-9. Both large-scale reflections and scintillations induced by atmospheric turbulence may affect the signal, but the effects diminish at high altitudes.

Many of the tropospheric effects can be neglected for frequencies as low as 1.5 GHz. These effects include attenuation due to atmospheric gases and clear air effects. For elevation angles greater than 10 degrees, a number of other effects can be excluded as well. These include focusing and defocusing, decrease in antenna gain due to wave-front incoherence, and attenuation by sand and dust storm. For a constellation of Molniya or Tundra orbit satellites there should always be a satellite visible with elevation angle greater than 10 degrees. These effects are consequently not included in his document.

The one tropospheric effect that may be of importance is the attenuation by precipitation and clouds. A general method to predict the attenuation along a propagation path is given in ITU-R P.618-9, and is based on maps over rainfall rate provided in ITU recommendations.

Estimation of fading due to precipitation and clouds for different areas has not been done in this study. The variations will be slow compared to the channel variations due to aircraft and satellite movements, and therefore not included in the channel model. It should however be included in link budget calculations.

4.3 Multipath effects in aeronautical communications

Although other reflections may be imagined, the multipath components in a general aeronautical communications setting usually come from two sources:

- The aircraft itself
- The ground

These two sources will be treated separately in the next two sub-sections.

4.3.1 Aircraft reflections

The main source of information for this sub-section is Steingass *et al.* 2004 [8]. In this work the authors undertook a measurement campaign to determine the effect of multipath reflections from the plane and the ground on satellite navigation and positioning. In addition to the channel measurements a set of simulations were performed using 3D ray-racing techniques.

The conclusion from the work was that the reflections from the fuselage had an average delay of 1.5 ns, a relative power of -14.2 dB and a Doppler bandwidth of less than 0.1 Hz. The small average delay, which corresponds to an additional path length of about 50 cm, suggests that only reflections close to the antenna contribute to the received signal power.

In addition to the gross parameters just mentioned, the authors developed a parameterized model of the Doppler spectrum. Here the spectrum was assumed to correspond to an exponential process with three free parameters. These parameters were again expressed in terms of the elevation and azimuth of the observation direction.

4.3.2 Ground reflections

Ground reflections are in principle function of two parameters – the ground characteristics and the geometry of the problem at hand. These two parameters are clearly not independent.

As the ground is concerned, there is a wide variety of terrain to choose from, and it is infeasible to try to develop mathematical models for each and every case at hand. One type of terrain that has received some attention is the ocean surface. Before studying communication over oceanic regions, the grazing angle will be defined.

4.3.2.1 Grazing angle

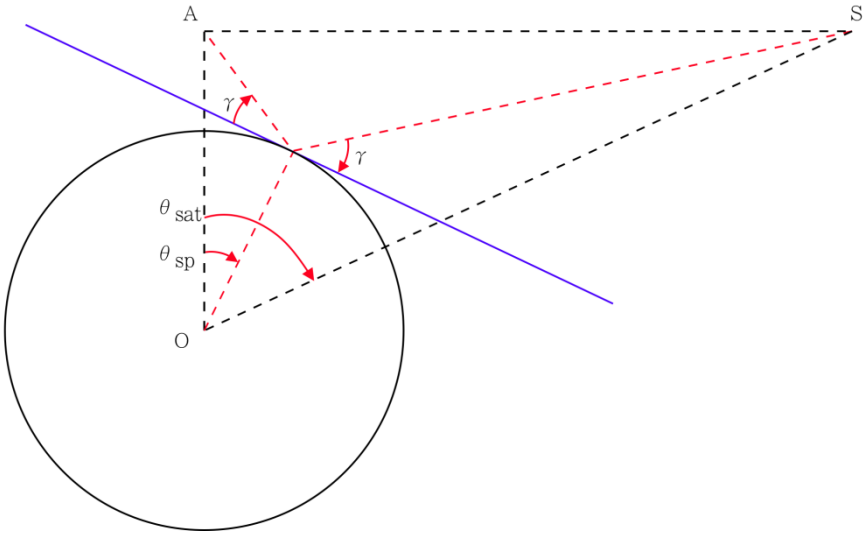

Figure 25 Simple geometric description of the grazing angle problem

The problem of calculating the grazing angle γ can be formulated from Figure 25. Let h_A and h_S be the heights of the aircraft and satellite respectively, and θ_{sat} the angle between direction vectors from the centre of the earth to the aircraft and satellite. If the two heights are equal there exists a closed form solution, but otherwise the solution needs to be obtained numerically. Using the law of sines the following iterative procedure can be formulated:

1. Initialize a guess at the grazing angle, γ_0.
2. Compute the following: $\gamma_{k+1} = \frac{1}{2}\left[\arccos\left(\frac{R}{R+h_A}\cos\gamma_k\right) + \arccos\left(\frac{R}{R+h_S}\cos\gamma_k\right) - \theta_{SAT}\right]$
3. Repeat until convergence

There exist however approximations for the grazing angle, such as the one referred to in ITU-R P.682-2. Their accuracy for different geometries needs however to be verified.

4.3.2.2 Specular reflection component

One of the earliest theoretical works specific to the oceanic region is (Bello 1973 [6]). Bello separates the ground reflection into two components – a specular reflection and a diffuse component. The specular component is modelled as following:

$$w_{sp}(t) = \Gamma G_{sp} z(t - \tau_{sp}) \exp(-i2\pi f_0 \tau_{sp}(t))$$

where:

- Γ is a complex gain that accounts for the roughness and electrical properties of the surface.
- G_{sp} is the product of the slowly varying complex antenna gains.
- z() is the signal of interest.
- τ_{sp} is the signal delay.
- f_0 is the carrier frequency.

The parameter that is of most interest here is the complex gain, Γ. Given that the wave heights have a Gaussian distribution we have

$$\Gamma = \Gamma_0 D \exp\left(-\frac{1}{2}\left[4\pi(\sigma/\lambda)\sin(\gamma)\right]^2\right)$$

Although the above formulation has been used for decades, it has been made clear from experiments that it under-estimates the gain for large grazing angles. In (Miller, Brown og Vegh 1984), a multiplicative correction term is added, yielding the following equation:

$$\Gamma = \Gamma_0 D \exp\left(-\frac{1}{2}\left[4\pi(\sigma/\lambda)\sin(\gamma)\right]^2\right) I_0\left(\frac{1}{2}\left[4\pi(\sigma/\lambda)\sin(\gamma)\right]^2\right)$$

where I_0 is a modified Bessel function of the first kind. The parameters are:

- γ is the grazing angle of the specular reflection
- Γ_0 is the reflection coefficient of a plane surface of the given material. Note that this parameter depends on the polarization of the EM-field and also to some degree on the grazing angle. However, at least for horizontal polarization, we can assume that Γ_0=-1. See Beckmann og Spizzichino 1963 [5] or [6] for plots that support these statements.
- σ is the root-mean-square of the surface height fluctuations.
- λ is the signal wavelength.
- D is the divergence of the surface and is used to compensate for the flatness assumption. From [5], we have that

$$D = \left[\left(1 + \frac{2h_1h_2}{R(h_1+h_2)\sin\gamma}\right)\left(1 + \frac{2h_1h_2}{R(h_1+h_2)}\right)\right]^{-\frac{1}{2}}$$

  where h_1 and h_2 are the respective heights of the objects, γ is the grazing angle and R is the radius of the earth.

We will now present some plots of D and Γ. For the plot of D assume that we have an aircraft cruising at 10000 meters altitude, and an HEO satellite at 39354 km altitude (its apogee in a Molniya orbit). The radius of the earth is 6378 km. From Figure 26 we see that the divergence is negligible for all but extremely small angles.

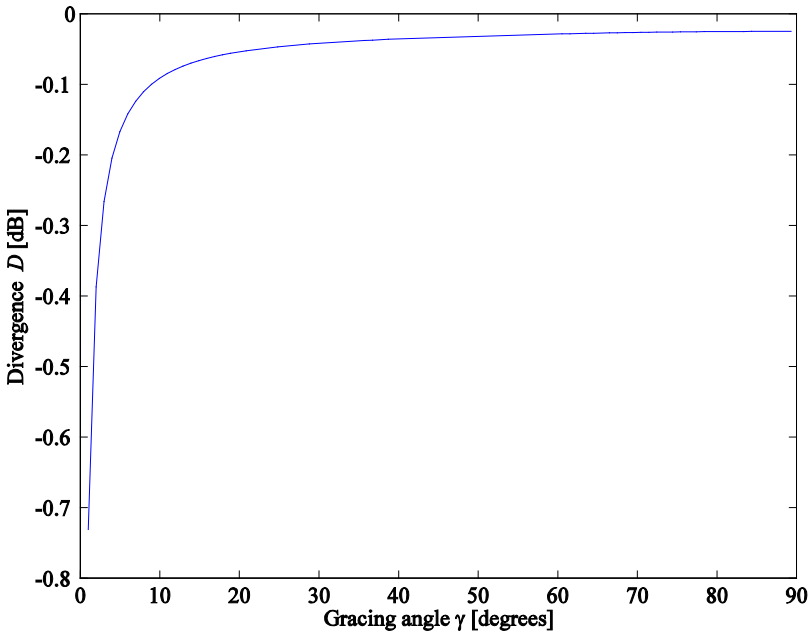

Figure 26 The divergence as a function of the gracing angle.

For the complex gain, Γ, we assume that the reflection coefficient for a flat, calm surface, Γ_0, has absolute value one. The electrical roughness is reproduced here from [6] in Table 9. We have plotted the absolute value of the gain in Figure 27 for several different weather conditions. Note that the results at low angles are less accurate, as the equations assume that:

$$\left(2\pi(\sigma/\lambda)(\sin(\gamma)+\sin(\theta))\right) >> 1$$

where θ is the incidental angle of the reflected wave.

RELATIONS BETWEEN ELECTRICAL ROUGHNESS AND SEA ROUGHNESS

			$\frac{4\pi\sigma}{\lambda} = \frac{g}{\sin\bar{\gamma}}$		$\bar{\gamma}$, in Degrees, for g = 1	
No.	Sea State	Wave Height Δh	150 MHz	1.5 GHz	150 MHz	1.5 GHz
0	Calm	0	0	0	-	-
1	Smooth	0 - 1 ft	0 - .47	0 - 4.7	-	> 12.3
2	Slight	1 ft - 3 ft	.47 - 1.41	4.7 - 14.1	> 45	12.3 - 4.1
3	Moderate	3 ft - 5 ft	1.41 - 2.35	14.1 - 23.5	45 - 25	4.1 - 2.4
4	Rough	5 ft - 8 ft	2.35 - 3.77	23.5 - 37.7	25 - 15.4	2.4 - 1.5
5	Very Rough	8 ft - 12 ft	3.77 - 5.64	37.7 - 56.4	15.4 - 10.2	1.5 - 1.0
6	High	12 ft - 20 ft	5.64 - 9.40	56.4 - 94	10.2 - 6.1	1.0 - .6
7	Very High	> 20 ft	> 9.40	> 94	< 6.1°	< .6

Table 9 Relations between electrical roughness and sea roughness (from [6])

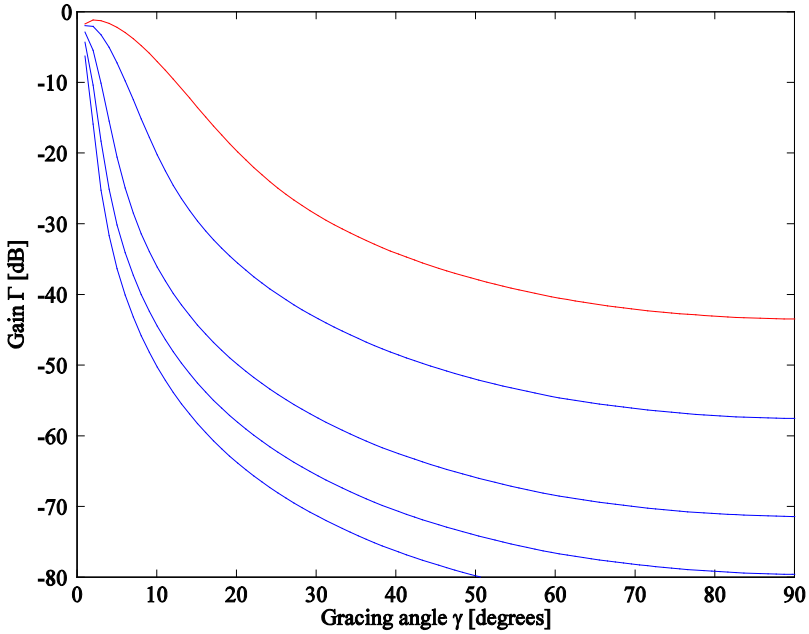

Figure 27 Reflection gain as a function of grazing angle. Surface roughness is 5 (red), 10, 20, 30 and 40, which ranges from smooth to very rough seas.

4.3.2.3 Diffuse reflection component

A method to calculate an approximation of the multipath power and fading depth of the diffuse component suitable for engineering applications is given in Rec. ITU-R P.682-2 with accompanying curves. Implementing the method gives not a perfect match to the curves, leading to the suspicion of errors in the equations provided in the recommendations. Still, the results are sufficiently close to provide some insights.

The power of the diffuse multipath component can also be estimated using an expression of the antenna diagram, the Fresnel reflection coefficient of the ground, and the divergence factor due to Earth's curvature which in Figure 26 is shown to be negligible for all but very low elevation angles. The Fresnel reflection coefficient is dependent on the relative permittivity $\varepsilon_r(f)$ and the conductivity $\sigma(f)$ of the surface at the operating frequency f. Curves for $\varepsilon_r(f)$ and $\sigma(f)$ for different surfaces are given in Rec. ITU-R P.527-3. The curves provided in Rec. ITU-R P.682-2 correspond to sea at 20°C ($\varepsilon_r = 80$ and $\sigma = 5$ S/m for $f = 1.5$ GHz). For ice (fresh water), the values are very different: $\varepsilon_r = 3$ and $\sigma \approx 4 \cdot 10^{-3}$ S/m. The difference in multipath power is illustrated in Figure 28. Depending on the elevation angle, the diffuse reflected path is 4-7 dB stronger over ice than over sea. It is therefore likely to assume that the multipath fading due to ground reflections over the polar cap will be more severe than over sea. Concerning the permittivity and conductivity over dry ground, the numbers are similar to those for ice. The corresponding numbers for wet ground are between those of sea and dry ground.

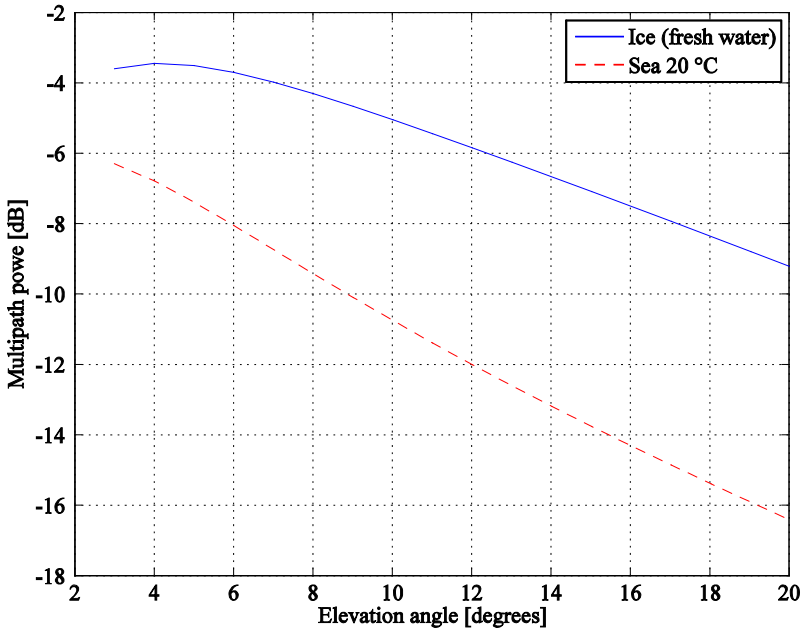

Figure 28 Mean multipath power as function of elevation angle. Aircraft altitude: 10 km.

In addition to the power level of the diffuse component it is of interest to get an insight in typical values for its delay and Doppler spreads, which can be derived from the delay power function $Q(\xi)$ and Doppler Power spectrum $P(\upsilon)$. Both of these are developed in a closed form using a series of approximations:

$$Q(\xi) = \frac{1}{4\alpha^2 H/c} \exp\left(-\left[\frac{\sin\theta + \frac{1}{\sin\theta}}{8\alpha^2 H/c} \right] \xi \right) I_0\left(\frac{\frac{1}{\sin\theta} - \sin\theta}{8\alpha^2 H/c} \xi \right)$$

and

$$P(\upsilon) = \frac{\sqrt{2}}{B_{rms}\sqrt{\pi}} \exp\left(-\frac{2\upsilon^2}{B_{rms}^2} \right), \quad B_{rms} = 4\alpha \left(\frac{f_0}{c} \right) \sqrt{\left(V_X \sin\theta + V_Z \cos\theta \right)^2 + V_Y^2 \sin^2\theta}$$

Note that the first equation is different from the erroneous version in [6]. The parameter α is the rms value of the surface slope. Another important quantity that is developed is the direct to diffuse power ratio:

$$\frac{P_S}{P_D} = |\Gamma_0|^2 A(H/\tan\theta, 0)$$

where H is the height of the airplane, θ is the observation angle (it is assumed to be the same as the grazing angle in Bello's derivations), and $A(x,y)$ is the combined gain of the transmitter and receiver antennas when looking at the surface-coordinate (x,y).

From our earlier assumptions Γ_0=1, which means that the rejection of the diffuse component is very much up to the antenna pattern. Alternatively, diversity techniques can be utilized. It should also be noted that the

approximations used to obtain the above solutions break down unless $\theta >> \alpha$. In other words, the results here should be used with caution for low elevation angles and/or very rough seas.

To give a graphical presentation of the delay power function and Doppler power spectrum we need an estimate of the rms surface slope α. Some values for various wind conditions are listed in [6]. Here we use $\alpha=0.1$, which corresponds to a wind speed of 10 knots, or 5 m/s. Figure 29 indicates that the delay spread of the diffuse component is in the order of 3 μs for all elevation angles, assuming a threshold of -10 dB. The two-sided Doppler power spectrum is about 300 Hz wide for all elevation angles. These values represent typical situations, although large variations of course may be encountered during operation.

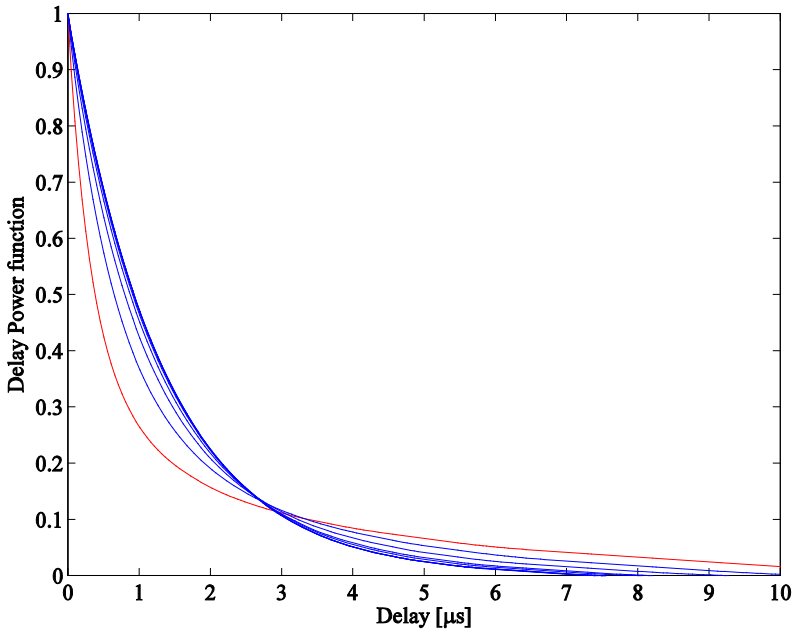

Figure 29 Delay Power Function for elevation angles from 10 (red) through 90 degrees.

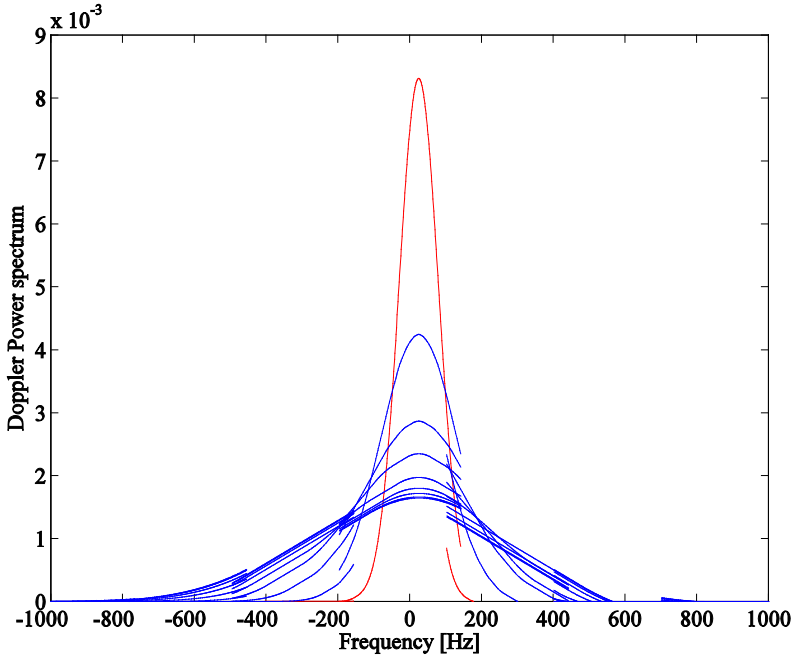

Figure 30 Doppler Power Spectrum for elevation angles from 10 (red) to 80 degrees.

4.4 Description of aeronautical tapped-delay channel model

For bit level simulation purposes, the propagation channel is often modelled using a tapped-delay model. The model incorporates the direct signal path between the transmitter and receiver, signal paths reflected by the surface of the aircraft, and ground reflections. The channel is normalised with respect to the direct signal path, which is generally the strongest one. This means that the channel does not incorporate slow variations in free space path loss due to aircraft and satellite movements and ionospheric and tropospheric effects.

Only the en-route scenario is included in this document due to several reasons. One reason is that other means of communications in most cases will be preferred during landing and take-off and on the ground. Another reason is that additional reflections from the surroundings when the aircraft is close to the ground are very dependent on the actual surroundings. Moreover, when the aircraft is close to or on the ground the delay of the reflected signal with respect to the direct signal will be so small that the reflected component may be incorporated in the direct signal. Finally, ref. [11] covers the landing and parking scenarios for geostationary satellites, and concerning the effects of reflections from buildings, other structures and terrain, the HEO case is no different than the GEO-case. The results are therefore not repeated in this document.

4.4.1 En-route scenario

In this scenario, the channel consists of the direct path, and reflections by the aircraft surface and the ground (specular and diffuse components).

The delay of the signal reflected by the surface of the aircraft is about 1.5 ns, which means that it for realistic signal bandwidths will not be extracted from the direct signal and lead to a Rice distributed direct path. The Rician factor K depends on the incidence angle, as shown in Figure 7 in [11]. The recommended worse case scenario is $K = 9$ dB.

The delay of the ground reflections (with respect to the direct path) depends on the altitude of the aircraft and on the elevation angle, and is in the order of 6-7 μs . The combined specular and diffuse component can be modelled using a Rice distribution. As shown in the previous section, the multipath power for the diffuse scattering is stronger over ice than over sea. For low elevation angles, the multipath power may be as high as -3 dB over ice and -6 dB over sea. It is however shown in the previous section that the delay spread of the diffuse component may be in the order of several μs and should be modelled using more than one tap. How many taps that should be included depends on how fast the channel is sampled. A sampling frequency of 1 MHz would give 4 taps assuming a delay spread of 3 μs. While the first ground reflection tap is Rice distributed, the others are Rayleigh distributed. Figure 29 could be used to find reasonable power values for each tap.

4.5 Conclusions

This study has investigated the effects of satellite and aircraft movements, atmospheric effects when a signal propagates through the ionosphere and troposphere, and multipath fading due to aircraft and ground reflections.

The variations in distance between aircraft and satellite due to the elliptical orbits of the satellites lead to variations in free space path loss, transmission delay and Doppler shift. The results of the study are given in Table 10. These parameters do not vary significantly with altitude and position of the aircraft for the areas considered in this study.

Table 10 Link parameters related to satellite movements

	Molniya orbit	Tundra orbit
Max free space path loss	186 dB	188 dB
Two-way delay	200 ms	270 ms
Maximum Doppler shift	9 kHz	2 kHz
Maximum Doppler rate	10 Hz/s	1 Hz/s

The most important atmospheric effects are Faraday rotation and scintillations in the ionosphere and attenuation by precipitation and clouds in the troposphere. The fades due to scintillations in the ionosphere are relatively slow (in the order of 0.1 – 1 Hz) and relatively deep (in the order of 5 dB in polar areas). Attenuation due to precipitations and clouds comes in addition and must be taken into account in the link budget calculations during system planning.

In addition to the direct path between aircraft and satellite the signal will be reflected by the aircraft surface and the ground, introducing multipath propagation. The delay of the received signal components reflected by the aircraft wings and fuselage will be small compared to the direct signal, in the order of 1.5 ns (corresponding to about 0.5 meter additional propagation length). For relevant bandwidths, the reflected signal component will be incorporated in the direct signal component, i.e. leading to so-called narrowband fading. This fading process can be modelled using a Rice distribution. The Rice factor will depend on the incidence angle of the signal. As a worst case value $K = 9$ dB is recommended. The delay of received signal reflected by the ground will be significantly longer, and will depend on the altitude of the aircraft and the satellite elevation angle. A recommended value to be used is 6-7 μs. The ground reflection will contain a specular component and a diffuse component. The diffuse component may have a delay spread in the order of 3 μs. The Rice factor of the first ground reflection tap will depend on the antenna diagram and on the topology and Fresnel reflection coefficient of the ground. The other ground reflection taps can be modelled as Rayleigh distributed. Ice and dry ground will lead to more severe fading than sea and wet ground.

4.6 References

[1] E. Vilar, J. Austin, “Analysis and correction techniques of Doppler shift for non-geostationary communication satellites,” International Journal of satellite Communications, Vol. 9, 123-136, 1991.

[2] Communications Operating Concepts and Requirements for the Future Radio System (COCR), Ver 2.0, EUROCONTROL/FAA.

[3] ITU-R P.531-9 Ionospheric propagation data and prediction methods required for the design of satellite services and systems.

[4] ITU-R P.618-9 Propagation data and prediction methods required for the design of earth-space telecommunication systems.

[5] Beckmann, Petr, and André Spizzichino. *The Scattering of Electromagnetic Waves from Rough Surfaces*. Pergamon Press, 1963.

[6] Bello, P. “Aeronautical Channel Characterization,” *Communications, IEEE Transactions on [legacy, pre - 1988]* 21, no. 5 (1973): 548- 563.

[7] Miller, A.R, R.M Brown, and E Vegh, “New derivation for the rough-surface reflection coefficient and for the distribution of sea-wave elevations,” *Microwaves, Optics and Antennas, IEE Proceedings H* 131, no. 2 (1984): 114-116.

[8] Steingass, A, A Lehner, F Perez-Fontan, E Kubista, M.J Martin, and B Arbesser-Rastburg. “A high resolution model for the aeronautical multipath navigation channel,” *Position Location and Navigation Symposium, 2004. PLANS 2004*, 2004: 357- 365.

[9] Rec. ITU-R P.682-2 Propagation data required for the design of earth-space aeronautical mobile telecommunication systems.
[10] Rec. ITU-R P.527-3 Electrical Characteristics of the surface of the earth.
[11] Aeronautical channel model, Iris Communication System Design Study Phase-A, ESTEC Contract No: 21364/08/NL/CLP.

5 Airport surface communications

AeroMACS is the new system under development within SESAR for airport surface communications. As this is written, the System Requirement Document (SRD) is in the process of being finalised. The next step will be to finalise the AeroMACS profile based on the IEEE802.16 standard and WiMAX. SINTEF is actively participating in the SESAR project 15.2.7 developing AeroMACS.

In Appendix A, a publication from the ICNS 2008 conference in Bethesda, Maryland, USA is included. The publication contains an evaluation of the use of WiMAX technology in general and multiple antenna techniques in particular at airports. The performance of the multiple antenna techniques Spatial Multiplexing (SM) and Space Time Coding (STC) is simulated using realistic channel models.

6 MIMO techniques for air ground communications

In Appendix B, it is shown that it is possible to use multiple-input multiple-output (MIMO) spatial multiplexing systems in aeronautical communications over an extended range even in the presence of a strong line-of-sight (LOS) component. Results originally derived to maximize the MIMO capacity in fixed range applications dominated by a LOS component is exploited to show that a high rank channel matrix may not only be offered for a fixed distance but can be maintained over an extended range and area in a MIMO ground-to-air communication system with $n_T = 2$ transmit antennas (ground terminal) and $n_R \geq 2$ receive antennas (aircraft). Numerical results are presented for an $n_R \times n_T$ MIMO system in a Ricean fading channel assuming communication between a ground terminal and an aircraft in the en-route domain.

7 MIMO techniques for aeronautical satellite communications

In Appendix C, a publication that analyses the spatial characteristics of the aeronautical satellite communication channel is included. The background for this work is the interest from geostationary satellite service providers to provide satellite services far to the north. The low elevation angles to the satellite do however create problems related to availability and reliability. By installing more than one antenna at the aircraft, increased availability and a diversity gain may be obtained. In the publication, specular and diffuse reflections off the sea surface are included.

Appendix A

Evaluation of downlink IEEE802.16e communication at airports

Jan Erik Håkegård, Tor Andre Myrvoll
SINTEF ICT
N-7465 Trondheim, NORWAY

Abstract

Mobile WiMAX technology is proposed for ATS and AOC communications in airport areas. This technology provides a large amount of flexibility, incorporating optional use of advanced communication techniques and signal processing. Of particular importance is the use of multiple antenna techniques.

In this paper the performance of Mobile WiMAX technology is assessed by means of simulations for communications over channel models suited for airport communications. The simulations include space time coding (STC) and spatial multiplexing (SM). The results illustrate the gain obtained using multiple antenna techniques in the case of non line-of-sight between transmitter and receiver, which may be exploited for increased cell size or increased throughput per cell. In addition, the effect of Weibull fading is illustrated for *b*-factors lower than 2. This leads to worse than Rayleigh fading, and should be taken into account when setting thresholds in the adaptive coding and modulation scheme.

Introduction

In order to support the requirements of future ATM services, it is recognised that the capacity of air ground communication systems must be increased. As a response to this demand, new frequency bands have recently been opened to aeronautical communications systems. One of these frequency bands is the 5091-5150 MHz MLS extension band, which will be used for communications at and around airports. As no communication system currently exists for airport communication occupying this frequency band, a new system must be developed. Adopting technologies conforming to commercial standards instead of developing a completely new and dedicated system will reduce cost related to development and purchase as well as maintenance and upgrade. The solution proposed by EUROCONTROL and FAA for communications at and near airports is to implement Mobile WiMAX technology[1, 2].

WiMAX technology is already in use in airports. In Aéroports de Paris, Alcatel and Hub télécom has have installed WiMAX networks to deliver public and private communication services to passengers and airport professionals. The system operates in the licensed 3.5 GHz band, and is based on the IEEE802.16-2004 standard. Proximetry's GateSync is another system developed to facilitate commercial airlines' need to update on board information and entertainment each time an aircraft land at an airport. This system is also based in the IEEE802.16-2004 standard.

Mobile WiMAX is based on the IEEE802.16e amendment of the IEEE802.16 standard. This standard is highly advanced in the sense that it incorporates state-of-the-art communication techniques such as Orthogonal Frequency division Multiplexing Access (OFDMA), adaptive coding and modulation, hybrid ARQ, smart antenna systems and iterative decoding (Turbo-codes, LDPC codes). Some of these techniques are mandatory in any equipment, others are optional. The standard is in addition flexible both with regards to operational frequency, bandwidth and type of physical interface (single carrier, OFDM, OFDMA). In order for a product to be WiMAX certified, it must be approved by the WiMAX forum. In April 2008 the first eight Mobile WiMAX products received the WiMAX Forum Certified Seal of Approval for use in the 2.3 GHz band. Products for use in the 2.5 GHz band will be certified in the coming months.

When developing a WiMAX profile for airport communications in the 5.1 GHz band, careful consideration must be given to the properties of the frequency band and to the particular characteristics of airport communications, such as the speed of aircrafts during taxing and during takeoff and

landing, communication distances, types and density of buildings and structures in the signal propagation path etc.

Several publications have already considered the use of Mobile WiMAX for communications at airports, but then typically only considering the OFDM physical layer[2] or OFDMA without Adaptive Antenna Systems (AAS)[3,4]. The physical layer adapted to airport environment is expected to be based on OFDMA and to take advantage of AAS to improve the performance and robustness against rapidly changing channel conditions. In this publication simulation results are given for communication over typical channel models using OFDMA and AAS. The channel models used are the standard Rayleigh model for non-line-of-sight (NLOS) communication and the "worse than Rayleigh" Weibull model considered suitable for airport environment. Both space time coding (STC) and spatial multiplexing (SM), which are the two main AAS techniques in the specifications, are included.

The paper is organized as follows: In the next section the properties and characteristics of the system are described more in detail. The simulation model is described in Sec 3, while simulation results are included in Sec. 4 together with an assessment of their consequences on system performance. Finally, the conclusions are drawn in Sec. 5.

System description

Figure 1 Airport communication

The WiMAX specifications contain three physical interfaces: single carrier, OFDM and OFDMA, and both Time Division Duplexing (TDD) and Frequency Division Duplexing (FDD). The WiMAX forum develops profiles for various usages of the WiMAX technology, including mobile usage. The release 1 of the WiMAX Forum Mobile System Profile[5] only considers OFDMA as physical interface and TDD as duplexing mode. It is reasonable to expect a future airport WiMAX profile to also be based on OFDMA and TDD, and only this mode is considered in this publication.

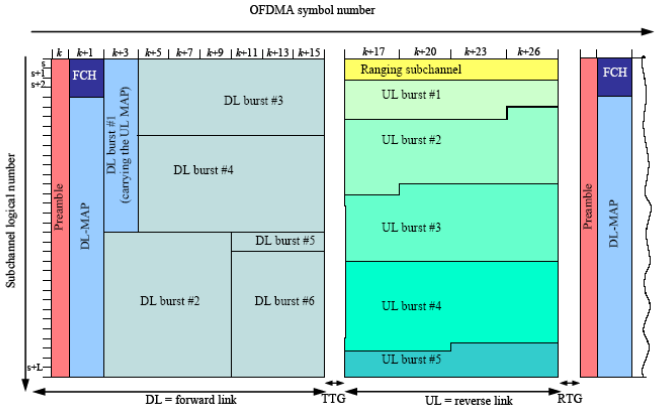

Figure 2 OFDMA frame structure

The OFDMA frame structure is illustrated in Figure 2. The main difference between OFDMA and the more traditional OFDM scheme is that the sub-carriers of the OFDMA symbols may be divided into groups, and that different groups of sub-carriers may be allocated to different mobile stations (MSs). In TDD mode, the base station (BS) transmits a block of OFDMA symbols first, and then, after a transmission gap, the MSs transmit a block of OFDMA symbols back to the BS. One burst, which is a group of sub-carriers within a number of OFDMA symbols is allocated to a communication link between the BS and one MS. Each burst has its proper coding and modulation scheme and other parameter settings adapted to the service requirements and to the quality of the channel between the BS and the particular MS. Information about downlink (DL) OFDMA resource allocation is provided in the DL-MAP field in the beginning of the OFDMA frame. Similarly, the resource allocation in the uplink (UL) is provided in the UL-MAP field. The distribution of resources between MSs both in DL and UL may be

changed dynamically between each OFDMA frame. Various frame durations are allowed. In the WiMAX Forum Mobile System Profile however, frame length of 5 ms is recommended.

Bandwidth - scalability

The Mobile WiMAX technology provides flexibility in signal bandwidth which may be selected from 1.25 MHz to 20 MHz. The sub-carrier spacing is fixed for all bandwidths, so that the varying bandwidth is obtained by varying the Fast Fourier Transform (FFT) size in the OFDMA modulator. The lowest bandwidth of 1.25 MHz corresponds to a FFT size of 128, and the largest bandwidth to a FFT size of 2048.

The duration of an OFDMA symbol is independent of the bandwidth and equal to 91.4 μs plus the length of the cyclic prefix. The allowed lengths of the cyclic prefix are 1/4, 1/8, 1/16 and 1/32 of the OFDMA symbol length. In the Mobile WiMAX Forum System Profile, cyclic prefix length equal to 1/8 of the OFDMA symbol length is recommended.

Sub-carrier allocation

For the downlink, there are two mandatory sub-channel allocation schemes: Full Usage of Sub-Carriers (DL-FUSC) and Partial Usage of Sub-Carriers (DL-PUSC). In addition there are a number of optional schemes. For the uplink, UL-PUSC is mandatory, while a number of permutation schemes are optional. In this publication we only consider DL-PUSC.

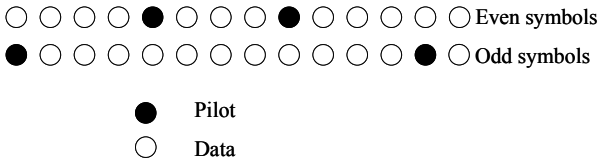

Figure 3 DL-PUSC cluster (SISO)

In DL-PUSC, the sub-carriers are allocated into clusters containing 14 contiguous sub-carriers and two OFDMA symbols. Each cluster contains four symbols which are known by the receiver and which are used by the channel estimation algorithm. The distribution of pilot symbols within each cluster is illustrated in Figure 3. The maximum number of clusters within the OFDMA symbol depends on the FFT size. For 128 FFT the number of clusters is 6 while it is 120 for 2048 FFT. Physical clusters are allocated into logical clusters using a renumbering sequence, logical clusters are divided into six major groups, and finally sub-carriers are partitioned into sub-channels containing 24 sub-carriers each. The result is that a data stream is spread over the physical sub-carriers and thus obtaining frequency diversity in the case of frequency selective fading.

Pilot symbols and channel estimation

In order to perform coherent detection of the received signal, the channel gains must be estimated. This is done using the pilot symbols embedded into the OFDMA block. The variations of the channel in both time and frequency domains and the strength of the additive white noise are factors determining how accurately the channel is estimated. The channel estimation error increases with the distance between pilot symbols. However, transmitting pilot symbols means spending power without transmitting information and leads to reduced spectral efficiency. Transmitting many pilot symbols is especially expensive in WiMAX systems, as pilot symbols are boosted 2.5 dB with respect to information symbols. Choosing the optimal density of pilot symbols is therefore a trade-off between estimation accuracy and spending energy on non-information bearing pilot symbols. The distribution of pilot symbols depends on the sub-channel allocation scheme. For DL-PUSC signals with one transmit antenna, the distribution of pilot symbols is given by Figure 3.

Coding and modulations

In the IEEE802.16 standards a number of coding and modulation schemes involving QAM modulation and convolutional coding are mandatory. These are listed in Table 1. By implementing link adaptation, the optimal mode providing the maximum number of information bits per symbol can be selected assuring sufficiently low bit error rate (BER) for reliable communication. In addition to convolutional coding, block and convolutional turbo coding and Low Density Parity Coding (LPDC) are optional schemes in the specifications. In this publication only the mandatory coding schemes listed in Table 1 are employed.

Table 1 Coding and modulation schemes

Mode	Modulation	Convolutional coding rate	Information bits per symbol
1	QPSK	1/2	1
2	QPSK	3/4	1.5
3	16QAM	1/2	2
4	16QAM	3/4	3
5	64QAM	1/2	3
6	64QAM	2/3	4
7	64QAM	3/4	4.5

Adaptive Antenna Systems (AAS)

The IEEE802.16e-2005 specifications include the optional use of several advanced multiple antenna techniques. Using multiple antennas in both ends of a transmission, and hence forming a multiple input-multiple output (MIMO) system, provides significant performance gain. This gain may be exploited to obtain extended range, extended capacity and/or better interference suppression depending on which MIMO technique that is employed in the system. In this publication, the focus is on Space-Time Coding (STC) and Spatial Multiplexing (SM).

The STC scheme included in the specifications is Alamouti's transmit diversity scheme and is referred to as matrix A. For DL transmission from 2-antenna BSs, matrix A is given by:

$$A = \begin{bmatrix} s_i & -s_{i+1}^* \\ s_{i+1} & s_i^* \end{bmatrix}$$

The procedure is as follows. For each sub-carrier in the transmitter, two and two consecutive symbols in the data stream are grouped in pairs (s_i, s_{i+1}). During the first symbol period t_i, transmit antenna 1 transmits symbol s_i and transmit antenna 2 transmits symbol s_{i+1}. During the second symbol period t_{i+1}, transmit antenna 1 transmits symbol $-s_{i+1}^*$ and transmit antenna 2 transmits symbol s_i^*, where $(^*)$ denotes complex conjugate. This transmit diversity scheme provides a diversity gain of order 2. In the receiver, the signals can be received by one or two antennas. With two receive antennas, maximum ratio combining is used (MRC). MRC provides an additional diversity gain of order 2, so that a 2×2 MIMO system employing STC obtains a total diversity gain of order 4.

The SM scheme included in the specifications is referred to as matrix B, and is given by:

$$B = \begin{bmatrix} s_i \\ s_{i+1} \end{bmatrix}$$

Transmit antenna 1 transmits the first symbol s_i and transmit antenna 2 transmit the second symbol s_{i+1} in parallel. The transmit side does not offer any diversity gain, but instead offers a coding gain of 2. If the signal is received by two receive antennas, the receive side offers a diversity gain of 2 provided that a maximal likelihood (ML) detector is used.

Adaptive MIMO switching (AMS) is included in the specifications. AMS implies that a transmitter can switch between STC and SM from block to block in the same way as the coding and modulation scheme may change. This provides additional flexibility in the system to efficiently distribute the frequency and time resources between BSs in dynamic environments.

Range

The range of a WiMAX BS will in most cases be limited by the required signal level at receivers. The length of the gaps between DL and UL blocks may also be a limiting factor (see Figure 2 for definition of the gaps TTG and RTG). The TTG must be so long that any MS does not start to transmit before it has received the total DL block. Similarly, the RTG must be so long that the BS does not start to transmit before it receives all of the preceding uplink data block. In the standard it is required that the both TTG and RTG must be longer than 5 μs. In the WiMAX Forum Mobile System Profile the values depend on the bandwidth. For 10 MHz channels TTG is 296 PS (106 μs) and RTG is

168 PS (60 μs), where PS is the Physical slot which is defined as $4/F_s$ where F_s is the sampling frequency. During 60 μs a signal propagates 18 km, well above the practical range of a BS. In systems conforming to the WiMAX profile the lengths of the gaps are therefore not a limiting factor. During 5 μs, which is the minimum value set in the IEEE802.16 standards, a signal propagates 1500 meters. Implementing such small gaps may therefore limit the range of some WiMAX networks.

Simulation model

The model used in the simulations is illustrated in Figure 4. It includes a transmitter chain, a 2×2 MIMO channel and a receiver chain.

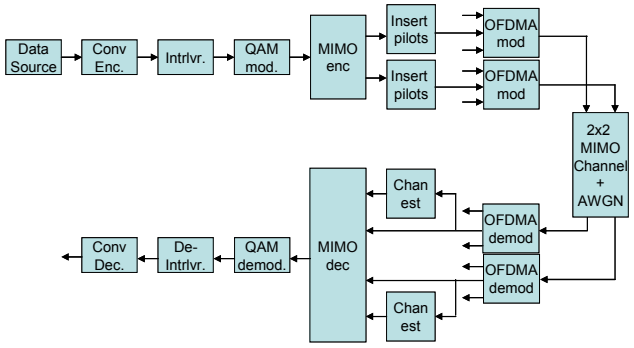

Figure 4 Simulation block diagram

Transmitter chain

Randomization, which is part of the standard, is not included in the simulation model as it will not have any impact on the BER performance. The convolutional encoder uses a rate 1/2 convolutional code. The code rates 2/3 and 3/4 are obtained by puncturing the basis code.

Two interleavers are defined in the specifications. In the simulations, the mandatory interleaver is implemented. It first assures that adjacent coded bits are mapped into non-adjacent subcarriers. It then assures that adjacent bits are mapped into less or more significant bits of the constellation. It is important to note that no interleaving is performed in the time domain, i.e. between OFDMA symbols. So in conditions with flat slow-varying fading, the results will most likely be bursts of errors that the decoder is not capable to recover from.

The interleaved bit stream is modulated into QPSK, 16QAM or 64 QAM symbols using Gray mapping. Then either STC or SM is used to provide signals to the two transmit chains of the 2×2 MIMO scheme. Pilot symbols are then inserted in the symbol stream as illustrated in Figure 3.

In the simulations, only one DL-PUSC cluster is used to transmit data. In frequency flat fading this will not have any impact on the results. In the case of frequency selective fading however, some improved performance must be expected when several clusters are used due to the effect of frequency diversity.

The smallest FFT size allowed in the specifications is used, i.e. 128. As only one cluster is used in the results included in this paper, there is no sense in implementing a larger FFT. In the case of several clusters, increased FFT size could provide enhanced performance as a larger FFT size implies larger bandwidth and hence better frequency selectivity.

Channel models

The airport environment is illustrated in Figure 1 and include communications between fixed installations, ground based vehicles and aircraft. In this publication only communication with aircraft is considered. Three different modes of the communication channel are considered: departing/approaching mode, taxing mode and terminal mode.

When an airplane is departing or approaching the airport, it is assumed that the propagation channel can be modeled as a line-of-sight (LOS) channel. The maximum speed of approaching or departing airplanes is set to 150 m/s. At 5.1 GHz this corresponds to a maximum Doppler shift of:

$$f_d = \frac{v}{c} f_c = 2530 \text{ Hz}$$

According to Ref. [6], this Doppler shift together with a symbol time T_s equal to 0.1 ms will give rise to Inter Channel Interference (ICI) of about -10 dB. Hence, ICI may in this case lead to significant performance loss.

In taxing mode, the channel is modeled as a specular non-line-of-sight channel (S-NLOS) channel, which means that there is line of sight between transmitter and receiver resulting in a noticeable and often dominant specular component in addition to significant amount of multipath fading. On the ground, the speed of airplanes is limited to 15 m/s, which corresponds to a maximum Doppler shift of:

$$f_d = \frac{v}{c} f_c = 253 \text{ Hz}$$

This Doppler shift will give rise to an ICI of about -30 dB, which may cause minor performance loss.

In terminal mode, the channel is assumed to be a NLOS channel. Hence, there is no line of sight between transmitter and receiver. In this case the maximum speed of the airplanes is set to 5.5 m/s, which corresponds to a maximum Doppler shift of:

$$f_d = \frac{v}{c} f_c = 93 \text{ Hz}$$

Such a Doppler shift will give rise to negligible ICI. The Doppler spread will however give rise to a significant coherence time that can be calculated using the following equation:

$$T_c = \sqrt{\frac{9}{16\pi f_d^2}} \approx 4.5 \text{ ms}$$

The OFDMA symbol rate is in the vicinity of 0.1 ms including the cyclic prefix, and each second OFDMA symbol contains pilot symbols. This should be sufficiently often for the impact of channel estimation error to be relatively low.

This work will focus on the taxing and parking scenarios under the assumption that the channel is NLOS. The NLOS channel is by far the most demanding environment, and also the one that is most likely to benefit from the added diversity offered by MIMO configurations.

As this publication is restricted to DL-PUSC only, the full high-resolution channel models described in Ref [7] can be replaced by a flat fading model. The reasoning is as follows; One DL-PUSC symbol has a total bandwidth of

$$BW = 14 \cdot 10600 \text{ Hz} = 148.4 \text{ kHz}$$

and will thus experience flat fading for coherence times significantly less than 6.7 μs. On the other hand, the model described in [7] is based on a bandwidth of 50 MHz and has a length of 50 taps, corresponding to a delay spread of 1 μs – well below 6.7 μs.

The entire OFDMA channel bandwidth may as mentioned above range from 1.25 MHz to 20 MHz. For these bandwidths a channel with delay spread of 1 μs will be frequency selective. The frequency selectivity will be particularly important for the wider channel bandwidth options as 10 MHz and 20 MHz. Not including the entire OFDMA bandwidth in the signal will fail to take advantage of the frequency diversity gained from randomizing the location of the sub-channels between OFDMA symbols. However, the goal of this study is not to estimate the full throughput of the channel, but rather to investigate the use of spatial diversity through space-time coding and spatial multiplexing.

Based on the findings in [7], both the well-known Rayleigh fading channel and the Weibull fading channel are investigated. The latter channel model is a two-parameter model considered to be "worse-than-Rayleigh" for shape parameters *b* less than two. For *b*=2 the Weibull channel is exactly identical to the Rayleigh fading channel. The following two shape parameters are considered:

$$b \in \{1.6, 1.8\},$$

Both these parameters describe channels with more severe fading than Rayleigh; lower numbers corresponding to worsening channel. The shape parameters have been chosen to represent the typical and extreme values found in [7].

Receiver chain

In the receiver, the signal goes through an OFDMA demodulator, and the relevant cluster of sub-carriers is extracted from the OFDMA symbols.

The channel estimators use the pilot symbols embedded on the received signal. There is a substantial literature on how to do pilot based channel estimation of OFDM signals. The channel

estimation algorithms employed in this publication first interpolate along the time dimension (between OFDMA symbols), and then in the frequency domain (between sub-carriers). The interpolation filters used are Finite Impulse Response (FIR) low-pass filters of variable length.

The received data symbols and the channel estimates are fed to the MIMO decoder, which is either space time coding or spatial multiplexing. In both cases MRC is used to obtain a receive diversity gain of 2. Hard QAM detection is then performed before deinterleaving and convolutional decoding.

Simulation results

In this publication simulation results for SISO, 2×1 STC, 2×2 STC and 2×2 SM are included. The figures illustrate the effect of the seven coding and modulation ratios, the effect of implementing MIMO techniques, and finally, the difference between the standard Rayleigh channel model and the Weibull channel model.

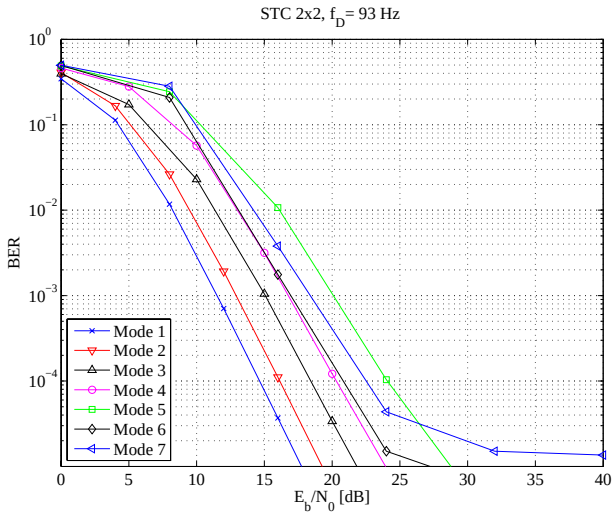

Figure 5 Simulated performance for 2×2STC, f_d= 93 Hz.

In Figure 5 and Figure 6, the performance of the seven coding and modulation modes is illustrated for 2×2 STC and for Doppler spreads 93 Hz and 253 Hz, respectively. The lower Doppler spread corresponds to the terminal channel mode. The higher Doppler spread corresponds to the taxing channel mode, but using the NLOS model instead of the S-NLOS model. This may therefore be considered as a worst case for the taxing channel when there is no line-of-sight between the BS and the MS. In the low E_b / N_0 region, the lowest mode corresponding to the lowest spectral efficiency generally obtains the best performance as expected. Mode 5 does however perform slightly worse than modes 6 and 7 for some reason. In the high E_b / N_0 region where the BER performance is limited by channel estimation errors, it becomes apparent how the higher modes are more sensitive to estimation errors than the lower modes. As expected the effect of channel estimation errors is more apparent for the higher Doppler spread case, resulting in severe error floors in particular for the higher modes. It is important to note, however, that in the high velocity case, the channel will in most cases contain a line-of-sight component, which will reduce the fading. The result will be smaller channel estimation errors and performance closer to that of a Gaussian channel. On the other hand, the effect of using MIMO techniques will be reduced.

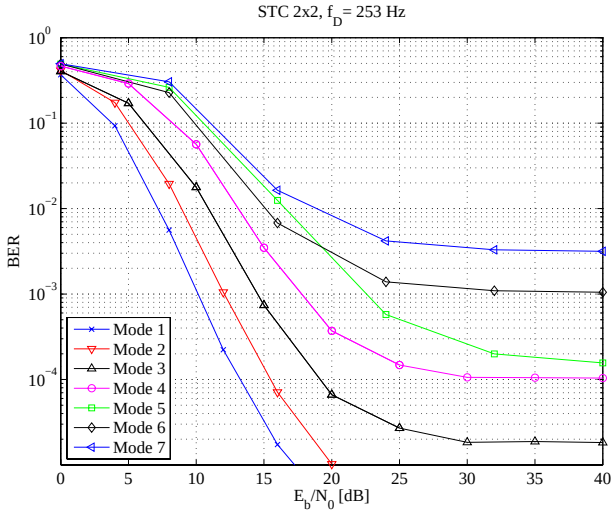

Figure 6 Simulated performance for 2×2STC, f_d= 253 Hz.

In Figure 7 and Figure 8 the performance of the different MIMO techniques are compared for mode 1 and mode 7, respectively. The curves illustrate the gain obtained by increased diversity. The SISO case have no diversity gain and performs worst, 2×1 STC provides a diversity gain of factor 2, while 2×2 STC provides a diversity gain of 4 and has the best performance. SM also provides a diversity gain of factor 2 in addition to a coding rate equal to 2. In particular for mode 7 SM performs

poorly, illustrating its sensitivity for channel estimation errors.

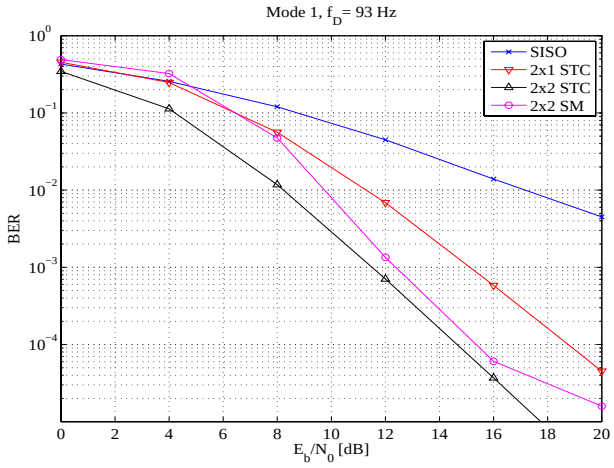

Figure 7 Simulated performance for mode 1.

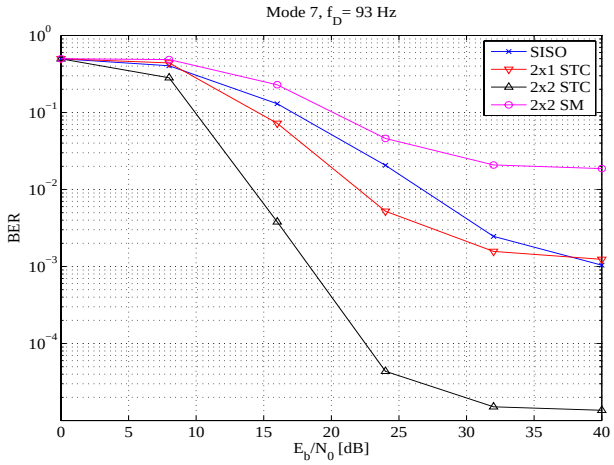

Figure 8 Simulated performance for mode 7.

In Figure 9, 2×2 STC and 2×2 SM are compared for modes providing similar number of information bits per symbol. The number of information bits per symbol for both 2×2 STC mode 3 and 2×2 SM mode 1 is 2, while 2×2 STC mode 6 and 2×2 SM mode 3 both have 4 information bits per symbol. The curves show that for the same number of information bits per symbol, SM performs slightly better than STC in the low E_b / N_0 region. SM is however more sensitive to channel estimation errors.

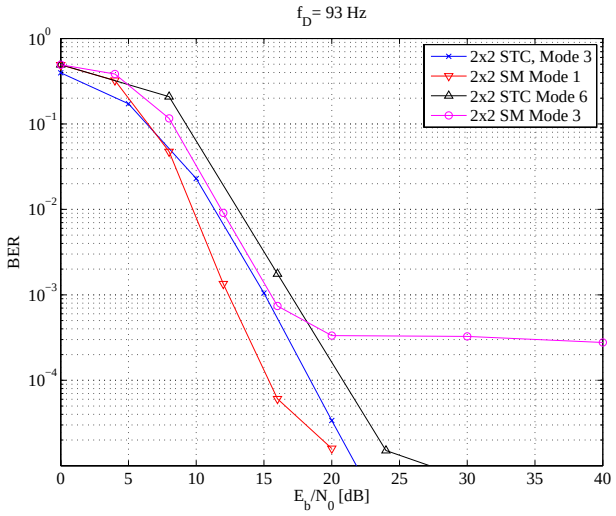

Figure 9 Comparison between STC and SM.

Only one DL-PUSC cluster within the OFDMA symbol is simulated, which means that only flat fading is captured by the simulator. A more realistic situation would be to simulate more clusters distributed over the OFDMA symbol. For typical channel lengths in airport environment, the signals would then experience frequency diversity. Together with forward error correction, this frequency diversity would lead to some diversity gain and hence improved performance in the lower E_b / N_0 regions compared to the results presented in this publication. In the high E_b / N_0 region where channel estimation errors are dominating the additive noise, the results would be similar.

Simulations results of communications over Weibull channels are in this publication limited to the 2×1 STC case, and to a maximum Doppler spread of 93 Hz. The Weibull channel is parameterized by the shape parameter *b*, and the selected values of *b* are 1.8 and 1.6. Lower values for *b* corresponds to increasingly worse channel conditions than a Rayleigh fading channel (a Weibull channel with $b = 2.0$ is identical to a Rayleigh channel). The choice of two values 1.8 and 1.6 are motivated by [7] where channel taps typically hovered around 1.8, with extremes at 1.6.

The curves in Figure 10 illustrate that the performance degrades when the channel conditions go from Rayleigh fading to increasingly severe Weibull fading. This is in accordance to theory, where the channel capacity decreases with *b*.

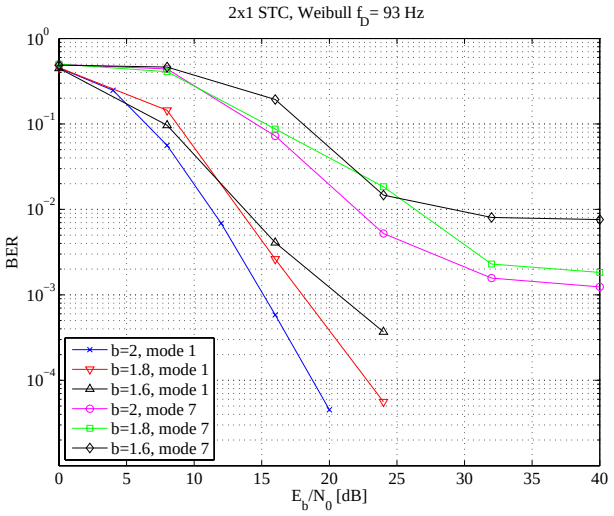

Figure 10 Simulated results with Weibull channel.

Conclusions

In this publication simulation results for different MIMO techniques included in the IEEE802.16e standard have been compared for typical channels models for airport environments. The results illustrate the gain that can be achieved in required E_b / N_0 at the receiver to obtain the required bit error rate for various services. This gain can be exploited to increase the size of a WiMAX cell or to increase the throughput within a call by choosing higher coding and modulation schemes for any given communication. The MIMO techniques are however best suited for the terminal channel mode, where the velocity of the aircraft is low and where there is generally no line-of-sight between the transmitter and the receiver.

Measurement campaigns reported in the literature indicate that the "worse than Rayleigh" Weibull channel may be a better model for the airport environment. As expected, the bit error rate for a given E_b / N_0 is worse for the Weibull channels than for the Rayleigh channel. A consequence is that the thresholds between the different rates of the adaptive coding and modulation should be adjusted compared to those given for communications over a Rayleigh channel to avoid too high bit error rates.

This publication contains simulations of DL-PUSC communication only including one cluster of 14 adjacent sub-carriers. In further studies, simulations including sub-carriers distributed over the complete OFDMA symbol will be included in order to capture the frequency diversity gain. Effects of the choices of FFT size, sub-carrier allocation schemes (PUSC, FUSC, TUSC, AMC) should be further assessed in order to select the optimal set of parameters for future Mobile WiMAX communication systems for aeronautical at airports.

Acknowledgements

This work done as part of the SECOMAS project, which is supported by the Norwegian Research Council and by the Norwegian ATM industry.

References

[1] SESAR Consortium, Jan. 2008, Deliverable D4: The ATM Deployment Sequence.

[2] Gilbert, Tricia, *et al.*, Oct. 2006, Identification of Technologies for Provision of future Aeronautical Communications," NASA/CR.

[3] Sen, Indranil, Beibei Wang, David W. Matolak, May 2007, Performance of IEEE802.16 OFDMA Standard Systems in Airport Surface Area Channels, ICNS 2007.

[4] Gheorghisor, Izabella, Yan-Shek Hoh, March 2006, Preliminary Analysis of the Spectral Requirements of Future ANLE Networks," The MITRE Corp.

[5] WiMAX Forum Mobile System Profile. Release 1.0 Approved Specifications (Revision 1.4.0: 2007-05-02)

[6] Li, Ye (Geoffrey), Leonard J. Cimini Jr., March 2001, Bounds on the Interchannel Interference of OFDM in Time-Varying Impairments, IEEE Trans. On Comms., Vol. 49, No. 3.

[7] Matolak, David W., May 2006, Wireless Channel Characterization in the 5 GHz Microwave Landing System Extension Band for Airport Surface Areas, Ohio University.

Appendix B

ENRI Int. Workshop on ATM/CNS. Tokyo, Japan (EIWAC2010)

[EN-028] On the use of MIMO in aeronautical communications

+ B. Holter J. E. Håkegård T. A. Myrvoll

Department of Communication Systems
SINTEF ICT
Trondheim, Norway
[bengt.holter|jan.e.hakegard|torandre.myrvoll]@sintef.no

Abstract In this paper, it is shown that it is possible to use multiple-input multiple-output (MIMO) spatial multiplexing systems in aeronautical communications over an extended range even in the presence of a strong line-of-sight (LOS) component. Results originally derived to maximize the MIMO capacity in fixed range applications dominated by a LOS component is exploited to show that a high rank channel matrix may not only be offered for a fixed distance but can be maintained over an extended range and area in a MIMO ground-to-air communication system with $n_T = 2$ transmit antennas (ground terminal) and $n_R \geq 2$ receive antennas (aircraft). Numerical results are presented for an $n_R \times n_T$ MIMO system in a Ricean fading channel assuming communication between a ground terminal and an aircraft in the en-route domain.

Keywords MIMO, Aeronautical communications, Chebyshev polynomials

1. INTRODUCTION

The introduction of multiple-input multiple-output (MIMO) systems has contributed to vast improvements in capacity and reliability in wireless communications. MIMO systems thrive in rich multipath environments, since it leads to antenna decorrelation and a high rank channel matrix.[1] In these conditions, a MIMO system can offer a linear increase in capacity that is proportional to the minimum number of transmit and receive antennas. As a result, the majority of research on MIMO communications have been focused on systems operating in a rich multipath environment.

MIMO signalling techniques are currently been considered for future aeronautical communication systems within Europe and the United States. In particular, the future airport datalink system AeroMACS will be based on IEEE802.16 technology involving MIMO, and aeronautical satellite communications consider introducing MIMO techniques for use in high latitudes and for low satellite elevation angles.

A more theoretical approach to improve the performance of future aeronautical communication systems by increasing the capacity and reliability in air-to-ground links has been proposed in [1]. Aeronautical channels are typically Ricean fading channels, characterized by the presence of a strong line-of-sight (LOS) component. A LOS component will usually reduce the performance of a MIMO system, since there is a large probability that all the signals will be conveyed through the same channel. Effectively, it means that the MIMO channel matrix in a LOS environment becomes rank-deficient (not full rank). This reduces the spatial multiplexing gain of the system since several data streams can be separated by an equalizer only if the fading processes of the spatial channels are (nearly) independent.

A possible solution to this challenge was indicated in [2], stating that a linear increase in capacity could be achieved by increasing the distance between the antennas at the transmitter to produce antenna patterns with nulls on all but one receiver antenna. By this approach, independent channels on the same carrier frequency could be established. A similar technique was indicated in [3, Sec. III].

Motivated by the results in [2] and [3], the authors in [4] and [5] propose a design methodology to achieve a full-rank MIMO channel matrix in a LOS environment. It is shown that orthogonality between subchannels of the channel matrix can be related to the product of the inter-element spacings of the antennas at the transmitter and receiver, assuming uniform linear array (ULA) antennas at both ends. They both introduce more general geometrical models than that applied in earlier works to gain additional insight, in particular to quantify a reduction from optimal performance caused by misalignment between the transmitter and receiver antenna arrays. In [4], the performance is evaluated with respect to both ergodic and outage capacity using a Ricean fading channel model. The results show that even with some deviations from an optimal design, a LOS MIMO system may outperform a system operating on independent and identically distributed (i.i.d.) Rayleigh fading channels in terms of Shannon capacity.

[1] In some cases, the channel matrix may still be of rank one even though the antennas at both ends are uncorrelated. Such a MIMO channel is commonly called a ”pinhole” channel.

The results presented in [4] and [5] have contributed to create new interest in the use of spatial multiplexing in environments with a strong LOS component. Notably, results have been presented in recent publications on fixed wireless access schemes [6], indoor communication [7], and vehicle-to-roadside communication [8]. However, to the author's knowledge, no one has yet looked into the use of the results for aeronautical communications. Hence, in this paper, the theoretical results in [4] are re-visited but viewed from an aeronautical perspective, where the range now is variable rather than fixed. Note however that the particular view of a variable range is not original to this paper, since it has been addressed to some extent in small range applications [7–9]. In particular, it is shown in [7] that a MIMO system operating in a LOS environment may be used over a larger set of ranges by using optimized nonuniform antenna arrays rather than uniform antenna arrays.

In this paper, a MIMO system which involves a ground terminal with 2 antennas and a ULA antenna mounted on the aircraft wings is proposed. The channel capacity of such a system is quantified and presented as a function of range and angle between the ground antenna array and the aircraft antenna array. Numerical results show that the channel matrix may be kept at full rank in a LOS environment over an extended range, which is essential to accommodate MIMO communication in the en-route domain.

The paper is organized as follows. In Section 2, the system and channel model is presented. Then, for clarity, information theoretic results on the channel capacity of a MIMO system are reviewed in Section 3. In Section 4, numerical and analytical results that quantify the performance of a MIMO system operating in a LOS environment are presented. The conclusions of the paper are presented in Section 5.

2. CHANNEL MODEL

Using complex baseband vector notation, the input/output relations of a narrowband single user MIMO link with n_T transmit antennas and n_R receive antennas can be written as

$$\mathbf{y} = \sqrt{\Omega}\mathbf{H}\mathbf{x} + \mathbf{n}, \tag{1}$$

where $\mathbf{y} \in \mathbb{C}^{n_R \times 1}$ is the received signal vector, $\mathbf{x} \in \mathbb{C}^{n_T \times 1}$ is the transmitted signal vector, $\mathbf{H} \in \mathbb{C}^{n_R \times n_T}$ is the channel matrix, Ω is the common power attenuation factor for all the channels in the channel matrix, and $\mathbf{n} \in \mathbb{C}^{n_R \times 1}$ is an additive noise vector containing i.i.d. circularly symmetric Gaussian elements with zero mean and variance σ^2 (in short $\mathcal{CN}(0, \sigma^2)$).[2] As in [10], $\mathbf{H}$ represents a *normalized* channel matrix, which means that all entries of the matrix have unit average power. The path loss for all subchannels is accounted for by the common parameter Ω. This normalization is convenient since it makes the average signal-to-noise ratio (SNR) independent of $\mathbf{H}$.

A general entry in $\mathbf{H}$ is denoted $h_{m+1,n+1}$, representing the complex channel gain between transmit antenna $n \in \{0, 1, \ldots, n_T - 1\}$ and receive antenna $m \in \{0, 1, \ldots, n_R - 1\}$. The channel matrix may then be written as

$$\mathbf{H} = \begin{bmatrix} h_{1,1} & h_{1,2} & \ldots & h_{1,n_T} \\ h_{2,1} & h_{2,2} & \ldots & h_{2,n_T} \\ \vdots & \vdots & \ddots & \vdots \\ h_{n_R,1} & h_{n_R,2} & \ldots & h_{n_R,n_T} \end{bmatrix}. \tag{2}$$

For simplicity (and later reference), it can also be presented in terms of its individual column vectors $\mathbf{h}_n$ as

$$\mathbf{H} = \begin{bmatrix} | & | & & | \\ \mathbf{h}_0 & \mathbf{h}_1 & \ldots & \mathbf{h}_{n_T-1} \\ | & | & & | \end{bmatrix}. \tag{3}$$

In the en-route domain, the aeronautical channel is commonly characterized as a fast fading (rapidly time varying) channel where the amplitude of the received signal follows a Rice distribution [11]. In this case, the MIMO channel matrix in (2) may be written as a sum of two parts, a deterministic part (LOS component) and a Rayleigh fading part (Non-LOS (NLOS) component):

$$\mathbf{H} = a\mathbf{H}_{\text{LOS}} + b\mathbf{H}_{\text{NLOS}}. \tag{4}$$

The power ratio of the two matrix components defines the Rice factor as $K = a^2/b^2$, which commonly is expressed in decibels as $K = 10\log_{10}\left(\frac{a^2}{b^2}\right)$dB. In the following, it is assumed that the sum power of the components is normalized, i.e. $a^2 + b^2 = 1$. With this assumption, a and b can be expressed in terms of the Rice factor as $a = \sqrt{K/(K+1)}$ and $b = \sqrt{1/(K+1)}$.

For simplicity, a flat fading channel is assumed, which means that the channel impulse response of each subchannel in the channel matrix consists of one tap only (thus no inter-symbol interference). In addition, since the channel capacity subsequently is used as a measure to quantify the performance, coherent detection with perfect channel knowledge at the receiver is assumed throughout the paper. In practice, perfect channel knowledge is not possible in a rapidly time varying channel, so the results of this paper will only serve as performance upper bounds.[3]

[2] A circularly symmetric complex Gaussian random variable with zero mean and variance σ^2 is a complex random variable $x + jy$, where x and y are independent and normally distributed with zero mean and variance $\sigma^2/2$.

[3] In [12], performance degradation of basic modulation schemes in a rapidly time varying channel using a first order autoregressive channel model is presented.

2.1. LOS channel

The matrix $\mathbf{H}_{\text{LOS}}$ represents the transfer function for signals that have traveled from the transmitter to the receiver by a direct path. As a result, it is a deterministic matrix since all the entries only depend on the distance between the transmit and receive antenna elements. The entries of $\mathbf{H}_{\text{LOS}}$ can then in general be expressed as

$$h_{m+1,n+1} = \exp\left(\jmath\beta r_{mn}\right), \tag{5}$$

where $\beta = 2\pi/\lambda$ is the wave number, λ is the wavelength of the transmitted signal, and r_{mn} is the direct path length between transmit antenna n and receive antenna m. In this paper, the expression for r_{mn} is identical to [4, Eq. (7)], which is based on the geometrical model depicted in Fig.1. It shows a general MIMO system with ULA antennas at both ends of the link. This means that the inter-element distance between adjacent antennas in each of the arrays is fixed. The antenna inter-element distance at the transmitter and receiver are denoted d_t and d_r, respectively. With n_T transmit antennas and n_R receive antennas, the total length of the transmitter array becomes $(n_T-1)d_t$, while the length of the receiver array becomes $(n_R-1)d_r$. The distance (or range) between the transmitter and receiver is denoted R, and it is defined to be the distance between the lower end of the two arrays. Finally, the ULAs are not restricted to be parallel, and the angles θ_t, θ_r, and ϕ_r are used to model the impact of arbitrary orientations. Based on the geometry in Fig.1, the distance r_{mn} in (5) can be expressed as [4, Eq. (7)]

$$\begin{aligned} r_{mn} &\approx R + md_r\sin\theta_t\cos\phi_r - nd_t\sin\theta_t \\ &+ \frac{(md_r\sin\theta_r\sin\phi_r)^2}{2R} \\ &+ \frac{(md_r\cos\theta_r - nd_t\cos\theta_t)^2}{2R}. \end{aligned} \tag{6}$$

The approximation sign in (6) is used as a reminder that the result is valid only when R is much larger than the transmit and receive antenna dimensions.

2.2. NLOS channel

The matrix $\mathbf{H}_{\text{NLOS}}$ represents the transfer function for signals that are received as a result of reflection, diffraction and scattering from the environment. The combined reception of such signals are commonly modeled by a stochastic process. As in [10], the entries of $\mathbf{H}_{\text{NLOS}}$ are modeled as circular symmetric complex Gaussian random variables with zero mean and variance σ_h^2. Hence,

$$h_{m+1,n+1} \sim \mathcal{CN}\left(0, \sigma_h^2\right). \tag{7}$$

Since the individual channel gains in this case will be Rayleigh distributed, $\mathbf{H}_{\text{NLOS}}$ is commonly referred to as a Rayleigh fading matrix. To keep the matrix normalized, it is assumed that $\sigma_h^2 = 1$. Since the aeronautical channel is a rapidly time varying channel, it is assumed that $\mathbf{H}_{\text{NLOS}}$ is memoryless, i.e. for each use of the channel and independent realization of $\mathbf{H}_{\text{NLOS}}$ is drawn.

3. CHANNEL CAPACITY

The channel capacity is a measure of the amount of information which can be transmitted and received with a negligible probability or error. With a uniform power distribution among the transmit antennas, the channel capacity of a MIMO system is equal to

$$C = \log_2\left[\det\left(\mathbf{I}_M + \frac{\overline{\gamma}}{n_T}\mathbf{W}\right)\right] \text{ bit/s/Hz}, \tag{8}$$

where $M = \min\{n_R, n_T\}$, $\mathbf{I}_M$ is the $M \times M$ identity matrix, $\overline{\gamma} = \frac{\Omega P_T}{\sigma^2}$ is the average received SNR, P_T is the total average transmit power,[4] and

$$\mathbf{W} = \begin{cases} \mathbf{H}\mathbf{H}^{\text{H}}, & n_R < n_T \\ \mathbf{H}^{\text{H}}\mathbf{H}, & n_R \geq n_T \end{cases} \tag{9}$$

is the channel covariance matrix. The superscript $^{\text{H}}$ in (9) denotes Hermitian transpose. Note that (8) is valid only for a given channel realization. When $\mathbf{H}$ is stochastic, C becomes a random variable and the *ergodic* channel capacity (mean capacity over all channel realizations for a given average SNR) can be obtained as $\overline{C} = E_H(C)$.[5]

Using the matrix notation introduced in (3) and assuming $n_R \geq n_T$, the covariance matrix $\mathbf{W}$ can be expressed as

$$\mathbf{W} = \begin{bmatrix} \mathbf{h}_0^{\text{H}}\mathbf{h}_0 & \mathbf{h}_0^{\text{H}}\mathbf{h}_1 & \dots & \mathbf{h}_0^{\text{H}}\mathbf{h}_{n_T-1} \\ \mathbf{h}_1^{\text{H}}\mathbf{h}_0 & \mathbf{h}_1^{\text{H}}\mathbf{h}_1 & \dots & \mathbf{h}_1^{\text{H}}\mathbf{h}_{n_T-1} \\ \vdots & \vdots & \ddots & \vdots \\ \mathbf{h}_{n_T-1}^{\text{H}}\mathbf{h}_0 & \mathbf{h}_{n_T-1}^{\text{H}}\mathbf{h}_1 & \dots & \mathbf{h}_{n_T-1}^{\text{H}}\mathbf{h}_{n_T-1} \end{bmatrix}. \tag{10}$$

Using eigenvalue decomposition on $\mathbf{W}$, (8) may alternatively be written as [14]

$$\begin{aligned} C &= \sum_{i=1}^{r_\omega}\log_2\left(1 + \frac{\overline{\gamma}}{n_T}\omega_i\right), \\ &= \log_2\left(\prod_{i=1}^{r_\omega}\left(1 + \frac{\overline{\gamma}}{n_T}\omega_i\right)\right), \end{aligned} \tag{11}$$

where $\{\omega_i\}_{i=1}^{M}$ are the eigenvalues of $\mathbf{W}$, and $r_\omega \leq M$ is the rank of $\mathbf{W}$ (or $\mathbf{H}$).

[4] For a pure Rayleigh fading channel, an uniform power distribution is optimal in the sense that it maximizes the capacity, but this is generally not the case for a Ricean fading channel. However, a uniform power distribution is asymptotically optimal as the SNR tends to infinity if $n_R \geq n_T$ [13].

[5] $E_H(\cdot)$ denotes the expectation over all channel realizations.

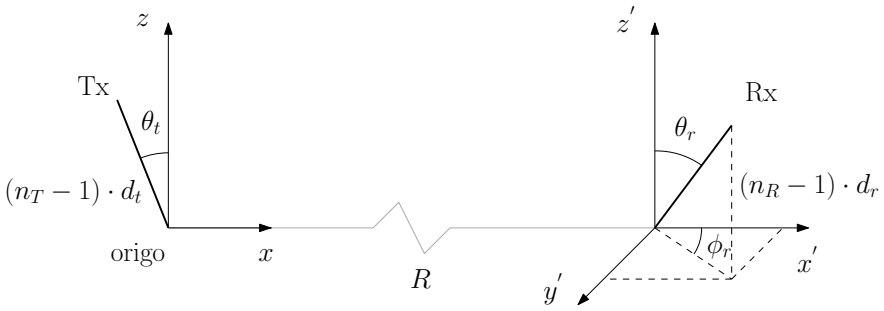

Figure 1 A general MIMO system with uniform linear arrays at both the transmitter and the receiver [4, Fig. 1].

Table 1 List of the eight first Chebyshev polynomials of the second kind.

n_R	$U_{n_R-1}(\cos x)$
1	1
2	$2\cos x$
3	$4\cos^2 x - 1$
4	$8\cos^3 x - 4\cos x$
5	$16\cos^4 x - 12\cos^2 x + 1$
6	$32\cos^5 x - 32\cos^3 x + 6\cos x$
7	$64\cos^6 x - 80\cos^4 x + 24\cos^2 x - 1$
8	$128\cos^7 x - 192\cos^5 x + 80\cos^3 x - 8\cos x$

In the following, it will be focused on the matrix $\mathbf{H}_{\text{LOS}}$ since the overall rank of $\mathbf{H}$ in a strong LOS environment in general will be dominated by the rank of $\mathbf{H}_{\text{LOS}}$. As such, it is convenient to define the associated LOS version of (9) as $K \to \infty$ (pure LOS channel). In this case, the channel covariance matrix can be defined as

$$\mathbf{M} = \begin{cases} \mathbf{H}_{\text{LOS}}\mathbf{H}_{\text{LOS}}^{\text{H}}, & n_R < n_T \\ \mathbf{H}_{\text{LOS}}^{\text{H}}\mathbf{H}_{\text{LOS}}, & n_R \geq n_T \end{cases}. \tag{12}$$

The capacity may then be expressed as

$$C = \log_2\left(\prod_{i=1}^{r_\lambda}\left(1 + \frac{\overline{\gamma}}{n_T}\lambda_i\right)\right), \tag{13}$$

where $\{\lambda_i\}_{i=1}^{M}$ are the eigenvalues of $\mathbf{M}$, and $r_\lambda \leq M$ is the rank of $\mathbf{M}$ (or $\mathbf{H}_{\text{LOS}}$).

From (13), it is observed that the rank of $\mathbf{M}$ plays an important part in maximizing the capacity of a MIMO system. A MIMO system thrives in a rich multipath environment since it contributes to realize a high rank channel matrix. However, when a strong LOS component is present, $\mathbf{H}_{\text{LOS}}$ becomes rank deficient since all the signals then are conveyed through the same channel. Hence, in order to exploit MIMO spatial multiplexing techniques in a LOS channel, methods that can contribute to increase the rank of $\mathbf{M}$ must be employed. Note that the rank of a matrix usually is defined as the number of non-zero singular values. However, when the rank of $\mathbf{M}$ is maximized, the rank of $\mathbf{H}_{\text{LOS}}$ is also maximized since the squared singular values of $\mathbf{H}_{\text{LOS}}$ are equal to the eigenvalues of $\mathbf{M}$. As mentioned in the introduction, the authors in [4] and [5] have proposed a design methodology to achieve a full rank MIMO channel matrix in a LOS environment. With the assumption of ULA antennas at both ends, the technique is to use an optimized inter-element distance at both the transmitter and the receiver to obtain a full rank channel matrix at a given fixed range R. In [4], the key design parameter is presented as the product of d_t and d_r, referred to as the *antenna separation product* (ASP). The optimal ASP which maximizes (13) for a pure LOS channel is equal to [4, Eq. (12)]

$$d_t d_r = \frac{\lambda R}{N\cos\theta_t\cos\theta_r}, \tag{14}$$

where $N = \max(n_R, n_T)$. When the ASP is equal to (14), the rank of $\mathbf{M}$ (and $\mathbf{H}_{\text{LOS}}$) is maximized and equal to $r_\lambda = M$.

In the following, a MIMO system with $n_T = 2$ and $n_R \geq n_T$ will be assumed. In this case, the maximum rank of $\mathbf{M}$ (or $\mathbf{H}_{\text{LOS}}$) is $r_\lambda = 2$. The eigenvalues of $\mathbf{M}$ for a $n_R \times 2$ MIMO system can then be expressed compactly as (see Appendix)

$$\lambda_1 = n_R + U_{n_R-1}(\cos x), \tag{15}$$
$$\lambda_2 = n_R - U_{n_R-1}(\cos x), \tag{16}$$

where $x = \frac{\pi}{n_R\eta}$, $\eta = \frac{\lambda R}{N\cos\theta_t\cos\theta_r d_t d_r}$, and $U_{n_R-1}(\cdot)$ is a Chebyshev polynomial of the second kind. The eight first Chebyshev polynomials of the second kind as a function of n_R are listed in Table 1.

The symbol η is called the *deviation factor*, and it is defined in [4, Eq. (13)] as the ratio between the optimal ASP in (14) (in the following denoted ASP_{opt}) and the actual ASP, i.e.

$$\eta = \frac{\mathrm{ASP}_{opt}}{\mathrm{ASP}} = \frac{\lambda R}{N \cos\theta_t \cos\theta_r d_t d_r}. \qquad (17)$$

In [4], η is used as a measure (in dB) for how far the actual ASP is from the optimal ASP for a fixed range R. Hence, if $\eta > 1$, the actual ASP is too small compared to the optimal value in (14). If $\eta < 1$, the actual ASP is too large. However, once the optimal d_t and d_r have been established for a fixed range denoted R_{opt}, deviations from R_{opt} will cause η to deviate from its optimal value of one as well. Hence, in this paper, $\eta > 1$ is used to signify a system that operates at $R > R_{opt}$. Similarly, $\eta < 1$ signifies a system that operates at $R < R_{opt}$. As such, η is in this paper used as a measure for the performance of a MIMO system as the range deviates from its optimal fixed value.

Finally, ρ is defined as the normalized correlation coefficient between the receive array responses from the lth and kth transmit element (l,$k \in [0, 1]$)

$$\rho \triangleq \frac{|\mathbf{h}_l^{\mathrm{H}} \mathbf{h}_k|}{\| \mathbf{h}_l \| \cdot \| \mathbf{h}_k \|} = \frac{\left| U_{n_R-1}(\cos x) \right|}{n_R}. \qquad (18)$$

With the aid of (15), (16) and (18), the capacity in (13) for an $n_R \times 2$ MIMO system can then be expressed compactly in closed form as

$$C = \log_2 \left(1 + \overline{\gamma} n_R + \left(\frac{\overline{\gamma} n_R}{2} \right)^2 \left(1 - \rho^2 \right) \right). \qquad (19)$$

For $n_R = 2$, (19) reduces to [15, Eq. 20].

4. GROUND-TO-AIR COMMUNICATION

This section is divided into two parts. In the first part, numerical and analytical results of a ground-to-air MIMO communication system are presented for a pure LOS channel, i.e. for $\mathbf{H}_{\mathrm{LOS}}$ only. In the second part, similar results are presented for the complete channel matrix $\mathbf{H}$, which is a stochastic channel. The numerical results in the second part are therefore obtained by averaging over many channels realizations. In both parts, it is assumed that the transmitter (ground terminal) is equipped with $n_T = 2$ antennas and the receiver (aircraft) is equipped with $n_R \geq 2$ antennas. The distance between the two ground terminal antennas is denoted d_t, whereas the aircraft antenna array is assumed to be an ULA with inter-element distance d_r. In the aircraft, the antennas are assumed to be conformal antennas evenly distributed along the aircraft wings.

For a given channel realization and a fixed number of antennas, the capacity is a function of the SNR. The SNR is again a function of the range, since the signal level naturally decreases as a function of range which then effectively also reduces the SNR. However, in all the numerical results presented in this paper, the SNR is kept fixed as a function of range in order to isolate the impact of the range from the impact of the SNR. Otherwise, it would be difficult to know whether a change in the capacity is caused by a change in the range or by a change in the SNR if they both vary at the same time. Hence, to better visualize the impact of a variable range on the capacity of the system, the SNR is kept fixed as a function of range.

4.1. Part 1 - Deterministic channel

4.1.1. 2×2

As a reference, the capacity of a 2×2 MIMO system is used. In Fig.2, (19) is depicted as a function of R when d_t and d_r are selected to maximize the capacity at $R_{opt} = 150$km. In order to maximize the capacity at such a long range, either d_t, d_r or both must be quite large. For this reason, the inter-element distance at the ground terminal is in this paper selected to be fixed at $d_t = 1500$m. This makes it possible to maximize the capacity using a comparatively small inter-element distance in the aircraft, which is assumed to be a commercial passenger jet. With $d_t = 1500$m, the capacity is maximized at $R_{opt} = 150$km with $d_r = 15$m.

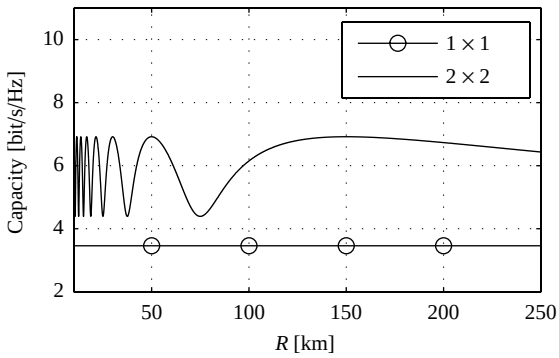

Figure 2 Capacity of a 2×2 system as a function of R when $\lambda = 0.3$m (f=1.0GHz), $d_t = 1500$m, $d_r = 15$m, $K \to \infty$, $\overline{\gamma} = 10$dB, and $\theta_t = \theta_r = 0^o$.

In Fig.2, it is observed that the capacity indeed is maximized at $R_{opt} = 150$km, but it oscillates between two extremes for $R < R_{opt}$.[6] The oscillation stems from ρ in (19), which for $n_R = 2$ is equal to $\rho = |\cos\frac{\pi}{2\eta}|$. Hence, for $R \leq R_{opt}$ ($\eta \leq 1$), it can be deduced that ρ is equal to

$$\rho = \begin{cases} 0 & \text{for } \eta = \frac{1}{(2q-1)} \\ 1 & \text{for } \eta = \frac{1}{2q} \end{cases}, \; q \in \mathbb{Z}^+, q \neq 0. \quad (20)$$

At maximum capacity, the channel matrix is a full rank matrix ($r_\lambda = 2$) since the columns of the channel matrix are uncorrelated ($\rho = 0$). The capacity is then exactly twice the capacity of a 1×1 system. Denoting the distances where the channel matrix is full rank as $R_{\rho=0}$, it occurs at

$$R_{\rho=0} = \frac{2\cos\theta_r \cos\theta_t d_t d_r}{(2q-1)\cdot\lambda}, \; q \in \mathbb{Z}^+, q \neq 0. \quad (21)$$

At minimum capacity, the channel matrix is rank deficient ($r_\lambda = 1$) since the columns of the channel matrix are completed correlated ($\rho = 1$). Denoting the distances where the channel matrix is rank deficient as $R_{\rho=1}$, it occurs at

$$R_{\rho=1} = \frac{\cos\theta_r \cos\theta_t d_t d_r}{q\cdot\lambda}, \; q \in \mathbb{Z}^+, q \neq 0. \quad (22)$$

In general, the distances related to a given correlation value between zero and one can be expressed as

$$R_\rho = \frac{\pi\cos\theta_r \cos\theta_t d_t d_r}{\lambda(\theta+\pi q)} = \frac{\pi}{2(\theta+\pi q)} R_{opt}, \quad (23)$$

where $q \in \mathbb{Z}^+$, $\rho = |\cos(\theta+\pi q)|$, and

$$\theta = \begin{cases} 0 < \theta < \frac{\pi}{2} & R > R_{opt} \\ \frac{\pi}{2} \leq \theta \leq \frac{3\pi}{2} & R \leq R_{opt} \end{cases}. \quad (24)$$

In Fig.3, the result of Fig.2 is reproduced but presented as function of both θ_r and R to visualize how the capacity varies with respect to range and misalignment between the ground and aircraft antenna. As such, Fig.3 can be viewed as an illustration of the capacity region covered by the ground antenna for an incoming aircraft at range R and angle θ_r relative to the ground antenna. It is assumed that $\theta_t = 0^o$. Once again, it is observed that the capacity fluctuates between two extremes given by either no correlation ($\rho = 0$) or complete correlation ($\rho = 1$). A relatively large area with a full rank matrix (red areas) is observed in the area 100km $\leq R \leq$ 250km and $-50^o \leq \theta_r \leq 50^o$. For distances closer than 100km, it is necessary to change the inter-element distance in the aircraft in order exploit MIMO spatial multiplexing techniques, since the correlation between the subchannels of the channel matrix becomes too high (blue areas).[7]

An option is to mount more than two antennas at the aircraft and use a switch-based system to select the optimal two antennas for a given range and angle. Assuming that d_r is optimal (maximizes the capacity) at R_{opt} and $\theta_r = \theta_1$, the new optimal inter-element distance d_r^* at range R and $\theta_r = \theta_2$ is equal to

$$d_r^* = \frac{R\cos\theta_1}{R_{opt}\cos\theta_2} d_r. \quad (25)$$

By adjusting the inter-element distance close to d_r^* in a switch-based fashion as the aircraft closes in on the ground terminal, it is possible to stay in the vicinity

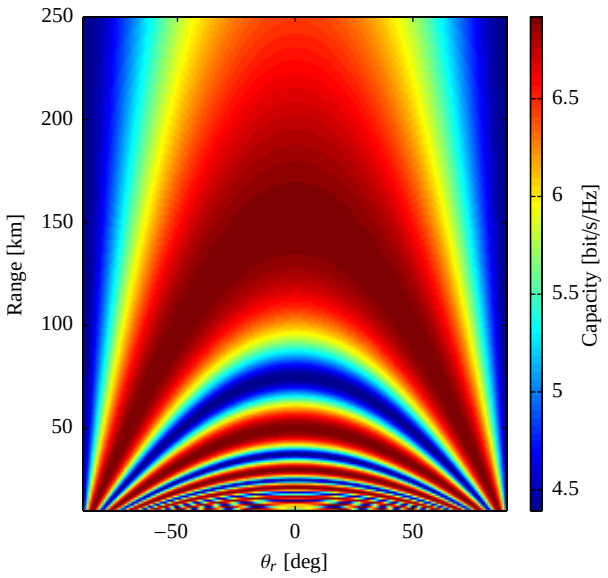

Figure 3 Capacity region of a 2×2 in a deterministic LOS channel ($K \to \infty$) as a function of θ_r and R.

[6] A similar result is presented in [5, Fig. 2], but then as a function of d_t and d_r when R is fixed.

[7] An additional ground terminal with a different coverage area could be used to give coverage for $\theta_r > \pm50^o$ if antennas also could be placed along the fuselage of the aircraft. The combined coverage of two ground terminals will then ensure that θ_r in any case will be less than $\pm50^o$.

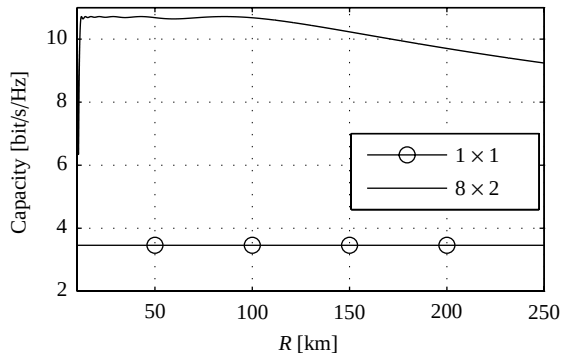

Figure 4 Capacity of a 8×2 system as a function of R when $\lambda = 0.3$m (f=1.0GHz), $d_t = 1500$m, $d_r = 2.14$m, $K \to \infty$, $\overline{\gamma} = 10$dB, and $\theta_t = \theta_r = 0^o$.

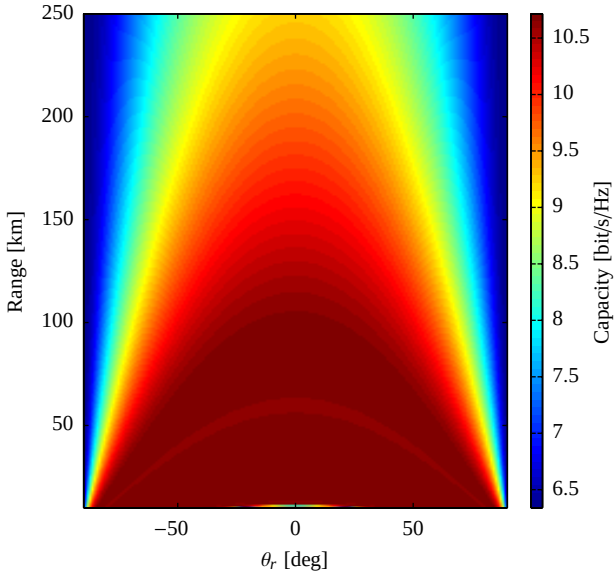

Figure 5 Capacity region of a 8×2 system in a deterministic LOS channel ($K \to \infty$) as a function of θ_r and R.

of the maximum of the capacity curve over an extended range. However, as the aircraft comes closer and closer to the ground terminal, the switching must be performed faster and faster to be in correlation with the fluctuation of the capacity curve. Hence, such an approach is not well suited when the aircraft comes at close range. A remedy to this challenge is explored in the next subsection.

4.1.2. $n_R \times 2$

A simple yet effective way to increase the robustness of the link in a strong LOS environment is simply to use more antennas at the receiver than at the transmitter and exploit all available antennas at the receiver at the same time rather than using a switched-based approach between a small subset of antennas.[8] To illustrate this fact, Fig.4 shows the capacity of a 8×2 MIMO system. Compared to the 2×2 case, it is observed that the capacity has increased as a result of the increased number of antennas in the system. However, more importantly, the capacity curve does not contain the oscillations observed in the 2×2 system. Hence, the general condition $n_R > n_T$ has a stabilizing effect on the capacity curve as a function of range, and the effect resembles the stabilizing effect which antenna diversity has on the SNR level in a fading channel. Note that the receiver antenna length is assumed to be fixed at the reference length of 15m. Hence, in the 2×2 case, $d_t = 15$m, whereas in the 8×2 case, $d_t \approx 2.14$m. As a result of the increased number of antennas and the reduced inter-element distance, R_{opt} is reduced to approximately 86km in the 8×2 case compared to 150km in the 2×2 case.

In Fig.5, the capacity region of the 8×2 system is depicted. It clearly shows the improvement from the 2×2 case, as there are no fluctuations of the capacity curve in the entire range $10\text{km} \leq R \leq 250\text{km}$. The angle range is almost unchanged from the 2×2 case, i.e. $-50^o \leq \theta_r \leq 50^o$.

The increased stability of the capacity curve as a function of range can also be observed by examining the condition number $\kappa_{\mathbf{M}}$ of $\mathbf{M}$ (and $\mathbf{H}_{\text{LOS}}$). The condition number is a measure of stability or sensitivity of a matrix (or the linear system it represents) to numerical operations, and matrices with a condition number close to one is said to be well-conditioned. The condition number of $\mathbf{M}$ is equal to

$$\kappa_{\mathbf{M}} = \frac{\lambda_{\max}}{\lambda_{\min}} \triangleq \frac{n_R + \left|U_{n_R-1}(\cos x)\right|}{n_R - \left|U_{n_R-1}(\cos x)\right|} = \frac{1+\rho}{1-\rho}. \quad (26)$$

The condition number of $\mathbf{H}_{\text{LOS}}$ may be obtained from $\kappa_{\mathbf{M}}$ by the following relation

$$\kappa_{\mathbf{M}} = \frac{\lambda_{\max}}{\lambda_{\min}} = \frac{\sigma^2_{\max}}{\sigma^2_{\min}} = \kappa^2_{\mathbf{H}_{\text{LOS}}}, \quad (27)$$

[8] The motivation for this particular approach comes from [7], where numerical results illustrate the relationship between the channel quality and the relative positions of a transmit and receiver node in a mm-wave MIMO architecture.

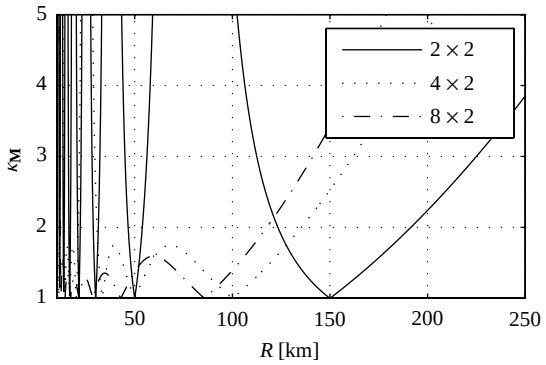

Figure 6 Condition number $\kappa_{\mathbf{M}}$ as a function of R and $n_R \in \{2, 4, 8\}$ with $\theta_t = \theta_r = 0^o$.

where $\sigma_{\max}$ and σ_{min} denote the maximum and minimum singular values of $\mathbf{H}_{\text{LOS}}$, respectively. Hence, when $\mathbf{M}$ is well-conditioned, $\mathbf{H}_{\text{LOS}}$ is well-conditioned. Using (15) and (16), the normalized correlation coefficient ρ can be expressed in terms of the condition number as

$$\rho = \frac{\kappa_{\mathbf{M}} - 1}{\kappa_{\mathbf{M}} + 1}. \tag{28}$$

From (28), it can be seen that a condition number close to one ensures that ρ is close to zero. In Fig.6, (26) is depicted as a function of n_R and R. It is observed that the range over which the condition number of $\mathbf{M}$ (and hence $\mathbf{H}_{\text{LOS}}$) is close to one increases as n_R increases. Basically, this means that by increasing the number of receive antennas, $\mathbf{H}_{\text{LOS}}$ may be kept at full rank over an extended range.

4.2. Part 2 - Stochastic channel

In this part, the capacity region results of the previous section obtained with the deterministic channel matrix $\mathbf{H}_{\text{LOS}}$ are compared to simulation results obtained with the complete Rice fading channel matrix $\mathbf{H}$. Since $\mathbf{H}$ is a stochastic matrix, the simulation results in this part are obtained by averaging over a number of channel realizations. According to [11], a typical Rice factor for the aeronautical channel in the en-route domain is $K = 15$dB. Hence, all the simulations are obtained for a Rice factor of $K = 15$dB. In Fig.7 and Fig.8, the capacity regions of a 2×2 and a 8×2 system are depicted, respectively. They both do not differ much from Fig.3 and Fig.5 obtained in a pure LOS channel.

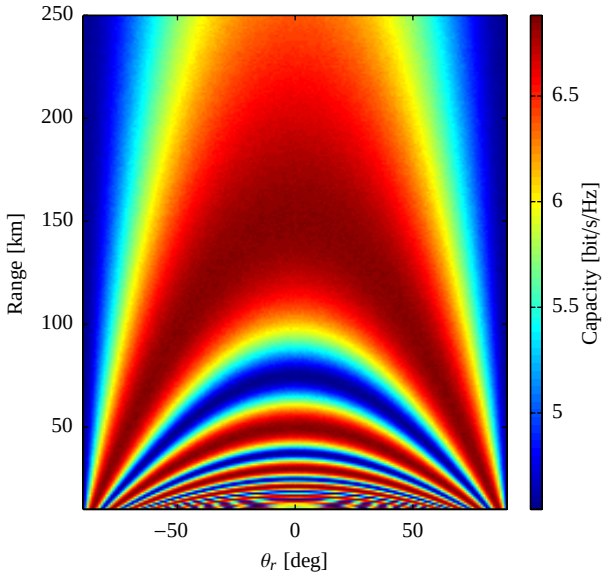

Figure 7 Capacity region of a 2×2 system in a Rice fading channel (averaged of 1000 channel realizations) as a function of θ_r and R with $\overline{\gamma} = 10$dB and $K = 15$dB.

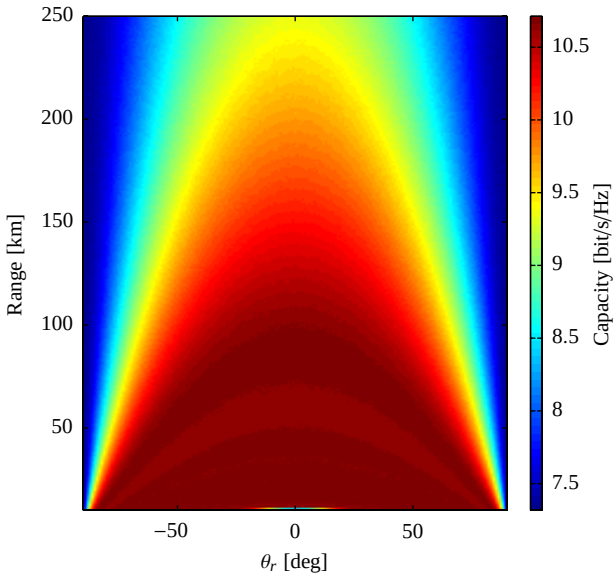

Figure 8 Capacity region of a 8×2 system in a Rice fading channel (averaged of 1000 channel realizations) as a function of θ_r and R with $\overline{\gamma} = 10$dB and $K = 15$dB.

5. CONCLUSIONS

The results of this paper indicate that it is possible to exploit MIMO spatial multiplexing techniques in aeronautical communications over an extended range even in the presence of a strong LOS component. Numerical results are presented for a MIMO ground-to-air communication system with $n_T = 2$ transmit antennas (ground terminal) and an ULA antenna with $n_R \geq 2$ receive antennas (aircraft). The results show that a high rank channel matrix may be offered over an extended range (and area) when $n_R > n_T$, where the range improves as n_R increases. For an $n_R \times 2$ MIMO system with $n_R \geq 2$, the maximum number of spatial data pipes offered is two, and the n_R receive antennas contributes to stabilize the two data pipes in a LOS environment. Additional data pipes may be offered by increasing the number of transmit antennas but due to the large inter-element distance needed to obtain a large range, systems with more than two antennas in the ground terminal may not be very practical.

6. APPENDIX

Eigenvalues of $\mathbf{M}$ for an $n_R \times 2$ MIMO system

For a $n_R \times 2$ system, using [4, Eq. (7)], the difference in path length from transmit antennas $l \in [0, 1]$ and $k \in [0, 1]$ to receive antenna $m \in [0, 1, \ldots, n_R - 1]$ can be expressed as

$$\begin{aligned} r_{m,k} - r_{m,l} &= (l-k)d_t \sin\theta_t - (l^2 - k^2)\frac{(d_t \cos\theta_t)^2}{2R} \\ &+ \frac{d_t d_r \cos\theta_t \cos\theta_r}{R}(l-k)m \\ &= \alpha + \frac{d_t d_r \cos\theta_t \cos\theta_r}{R}(l-k)m, \quad (29) \end{aligned}$$

where $\alpha = (l-k)d_t \sin\theta_t - (l^2 - k^2)\frac{(d_t \cos\theta_t)^2}{2R}$. The channel matrix in (2) is simplified to

$$\mathbf{H} = \begin{bmatrix} h_{1,1} & h_{1,2} \\ h_{2,1} & h_{2,2} \\ \vdots & \vdots \\ h_{n_R,1} & h_{n_R,2} \end{bmatrix} \quad (30)$$

The individual terms of the matrix product $\mathbf{M} = \mathbf{H}_{\text{LOS}}^{\text{H}}\mathbf{H}_{\text{LOS}}$ can then be expressed as

$$\mathbf{M} = \begin{bmatrix} \mathbf{h}_0^{\text{H}}\mathbf{h}_0 & \mathbf{h}_0^{\text{H}}\mathbf{h}_1 \\ \mathbf{h}_1^{\text{H}}\mathbf{h}_0 & \mathbf{h}_1^{\text{H}}\mathbf{h}_1 \end{bmatrix}, \quad (31)$$

where

$$\mathbf{h}_0 = \left[e^{\jmath\beta r_{0,0}}, \ldots, e^{\jmath\beta r_{n_R-1,0}}\right]^{\text{T}}, \quad (32)$$

$$\mathbf{h}_1 = \left[e^{\jmath\beta r_{0,1}}, \ldots, e^{\jmath\beta r_{n_R-1,1}}\right]^{\text{T}}. \quad (33)$$

The inner product of the two channel vectors in (32) and (33) can in general by written as

$$\begin{aligned} \mathbf{h}_l^{\text{H}}\mathbf{h}_k &= \sum_{m=0}^{n_R-1} e^{\jmath\beta(r_{m,k} - r_{m,l})} \\ &= \sum_{m=0}^{n_R-1} e^{\jmath\beta\left(\alpha + \frac{d_t d_r \cos\theta_t \cos\theta_r}{R}(l-k)m\right)} \\ &= e^{\jmath\beta\alpha} \cdot \sum_{m=0}^{n_R-1} e^{\jmath\left(2\pi\frac{d_t d_r \cos\theta_t \cos\theta_r}{\lambda R}(l-k)m\right)} \\ &= e^{\jmath\beta\alpha} \cdot \sum_{m=0}^{n_R-1} e^{\jmath mu} \\ &= e^{\jmath\beta\alpha} \cdot \frac{1 - e^{\jmath n_R u}}{1 - e^{\jmath u}} \\ &= e^{\jmath\beta\alpha} e^{\jmath(n_R-1)\frac{u}{2}} \cdot \frac{\sin\left(\frac{n_R u}{2}\right)}{\sin\left(\frac{u}{2}\right)} \\ &= e^{\jmath\psi} \cdot \frac{\sin(n_R x)}{\sin x} \\ &= e^{\jmath\psi} \cdot U_{n_R-1}(\cos x), \quad (34) \end{aligned}$$

where $u = 2\pi\frac{d_t d_r \cos\theta_t \cos\theta_r}{\lambda R}(l-k)$, $x = u/2 = \frac{\pi}{n_R\eta}(l-k)$, and $\psi = \beta\alpha + (n_R - 1)x$.[9] Since $\mathbf{h}_0^{\text{H}}\mathbf{h}_1 = (\mathbf{h}_1^{\text{H}}\mathbf{h}_0)^*$, the matrix $\mathbf{M}$ may be written compactly as

$$\mathbf{M} = \begin{bmatrix} n_R & e^{-\jmath\psi}U_{n_R-1}(\cos x) \\ e^{\jmath\psi}U_{n_R-1}(\cos x) & n_R \end{bmatrix}, \quad (35)$$

where $x = \frac{\pi}{n_R\eta}$.[10] The eigenvalues of the matrix in (35) are derived from the characteristic equation, and they are equal to

$$\lambda_1 = n_R + U_{n_R-1}(\cos x), \quad (36)$$

$$\lambda_2 = n_R - U_{n_R-1}(\cos x). \quad (37)$$

7. ACKNOWLEDGEMENTS

This work has been funded by the Norwegian Research Council through the SECOMAS project (180018/S10).

[9] For the last equal sign in (34), see [16, Identity 4].

[10] In general, for an $n_R \times n_T$ system, x can be defined as $x = \frac{\pi}{n_R\eta}|(l-k)|$. The absolute value is introduced for simplicity since $\cos x = \cos(-x)$. Hence, if $(l-k) < 0$, $U_{n_R-1}(\cos(-x)) = U_{n_R-1}(\cos x)$.

8. COPYRIGHT

9. REFERENCES

[1] J. Rasool, G. E. Øien, J. E. Håkegård, and T. A. Myrvoll, "On multiuser MIMO capacity benefits in air-to-ground communication for air traffic management," *in Proc. 6th International Symposium on Wireless Communication Systems*, pp. 458–462, September 2009.

[2] P. F. Driessen and G. J. Foschini, "On the capacity formula for multiple input-multiple output wireless channels: A geometric interpretation," *IEEE Transactions on Communications*, vol. 47, no. 2, pp. 173–176, February 1999.

[3] D. Gesbert, H. Bölcskei, D. A. Gore, and A. J. Paulraj, "Outdoor MIMO wireless channels: Models and performance prediction," *IEEE Transactions on Communications*, vol. 50, no. 12, pp. 1926–1934, December 2002.

[4] F. Bøhagen, P. Orten, and G. E. Øien, "Construction and capacity analysis of high-rank line-of-sight MIMO channels," *in Proc. IEEE Wireless Communications and Networking Conference*, vol. 1, pp. 432–437, March 2005.

[5] I. Sarris and A. R. Nix, "Design and performance assessment of maximum capacity MIMO architectures in line-of-sight," *in Proc. IEE Commun*, vol. 153, no. 4, pp. 482–488, August 2006.

[6] B. T. Walkenhorst and M. A. Ingram, "Repeater-assisted capacity enhancement (RACE) for MIMO links in a line-of-sight environment," *in Proc. IEEE International Conference on Communications*, pp. 1–6, June 2009.

[7] E. Torkildson, C. Sheldon, U. Madhow, and M. Rodwell, "Millimeter-wave spatial multiplexing in an indoor environment," *in Proc. First International Workshop on Multi-Gigabit MM-Wave and Tera-Hz Wireless Systems*, November 2009.

[8] M. Matthaiou, D. I. Laurenson, and C.-X. Wang, "Capacity study of vehicle-to-roadside MIMO channels with a line-of-sight component," *in Proc. IEEE Wireless Communications and Networking Conference*, pp. 775–779, April 2008.

[9] E. Torkildson, C. Sheldon, U. Madhow, and M. Rodwell, "Nonuniform array design for robust millimeter-wave MIMO links," *in Proc. 28th IEEE Conference on Global Telecommunications*, pp. 4826–4832, December 2009.

[10] F. Bøhagen, P. Orten, and G. E. Øien, "Design of optimal high-rank line-of-sight MIMO channels," *IEEE Transactions on Wireless Communications*, vol. 6, no. 4, pp. 1420–1425, April 2007.

[11] E. Haas, "Aeronautical channel modeling," *IEEE Transactions on Vehicular Technology*, vol. 51, no. 2, pp. 254–264, 2002.

[12] K. S. Gomadam and S. A. Jafar, "Modulation and detection for simple receivers in rapidly time varying channels," *IEEE Transactions on Communications*, vol. 55, no. 3, pp. 529–539, 2007.

[13] D. Hösli and A. Lapidoth, "How good is an isotropic Gaussian input on a MIMO Ricean channel?" *in Proc. International Symposium on Information Theory*, p. 291, 2001.

[14] B. Holter, "On the capacity of the MIMO channel: A tutorial introduction," *in Proc. IEEE Norwegian Symposium on Signal Processing*, pp. 167–172, 2001.

[15] B. T. Walkenhorst, T. G. Pratt, and M. A. Ingram, "Improving MIMO capacity in a line-of-sight environment," *in Proc. IEEE Global Telecommunications Conference*, pp. 3623–3628, 2007.

[16] A. T. Benjamin, L. Ericksen, P. Jayawant, and M. Shattuck, "Combinatorial trigonometry with Chebyshev polynomials," *Journal of Statistical Planning and Inference*, vol. 140, pp. 2157–2160, 2010.

Appendix C

ENRI Int. Workshop on ATM/CNS. Tokyo, Japan (EIWAC2010)

[EN-027] Aeronautical satellite propagation channel characteristics using multiple antennas

+ T. A. Myrvoll * J. E. Håkegård * B. Holter *

* Communication Systems, SINTEF ICT,
Trondheim, Norway.
[Tor.Andre.Myrvoll | Jan.E.Hakegard | Bengt.Holter]@sintef.no

Abstract In this work we have investigated the use of multiple antennas for satellite-aircraft communications. In particular, we have looked at how signals received by antennas attached to the aircraft are correlated as a function of their separation distance. The signal correlation is an important factor when determining how effective a multiple antenna scheme will be. We have limited ourselves to reflections from sea surfaces due to the relatively simple analytical properties as opposed to land surfaces. The aeronautical channel is well described in the literature and analytical results exist for communications parameters like delay and Doppler spreads. There does not however, seem to be a simple analytical model to describe the correlation between signals as observed at different points in space. We therefore used Monte Carlo methods combined with electromagnetic scattering theory to obtain numerical estimates of the correlations. Due to the computational complexity we reduced the problem to a two-dimensional representation. That is, the sea surface is a one dimensional function, and the aircraft is positioned at an altitude h above the surface. Although this is a simplification, we still believe that the insights we gain with respect to changes aircraft altitude, elevation angles and sea surface roughness, are valid.

Keywords ATM, CNS, CARATS

1 INTRODUCTION

Systems providing communications between aircraft and ground play a vital role for the security, safety and efficiency of air traffic. As most of the earth surface is covered by water or ice, flights over these areas will often be out of reach of terrestrial communication systems and must therefore rely on satellite communication.

Several satellite communication systems, such as Inmarsat, provide aeronautical services in the so-called ORP (ocean, remote, polar) domain. A drawback related to geostationary satellite systems such as Inmarsat is that the polar coverage is poor, as the satellite will be located below the horizon for latitudes above 82°. Moreover, reliable communication is often difficult above 65° - 70° due to low satellite elevation angles. For polar routes, and some intercontinental routes, this implies long time spans without reliable communication means.

A propagation channel with low satellite elevation angle will generally be affected by multipath propagation, as the receiver antenna will receive signals reflected by the earth surface and the fuselage, as well as the direct signal. An efficient strategy to combat multipath propagation is to use multiple antennas. By implementing diversity schemes such as maximum ratio combining (MRC), the inherent diversity in multipath propagation channels can be exploited to obtain significant performance gains. A condition for obtaining diversity gain is however that the signals received by the different antenna elements are uncorrelated. If the correlation coefficient is close to one, the signals are close to correlated and no diversity gain is obtained. If however the correlation coefficient is close to zero, the signals are close to uncorrelated and diversity gains can be obtained.

In this publication, the correlation coefficient of the signal reflected by the earth surface is explored for low elevation angles and for flights over sea. Due to the waves of the sea surface, the receiver antennas will receive signals reflected by not only one point but from a surface area. The size of the area depends among others on the sea state and the flight altitude.

2. SCATTERING THEORY

This section describes the use of Monte Carlo simulations of scattering from a one dimensional (1D) rough sea surface. The goal of the simulations is to investigate the correlation between points in the diffuse component of the scattered electro-magnetic field. The first subsection will give a brief overview of the underlying theory and the approximations that need to be made to facilitate the numerical simulations. Later subsections will present the simulation results as well as interpretations and discussions.

2.1. The theory of scattering of electromagnetic waves from rough surfaces

Research into the effect of scattering from rough surfaces, be it e.g. acoustic or electro magnetic waves, has been conducted for more than a century. Our work will be based on [1] and [2].

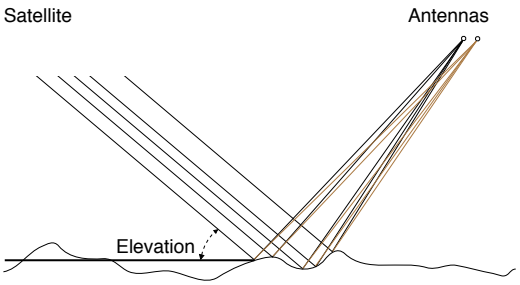

Figure 1: Geometry of satellite-aircraft communications. The elevation angle is measured between the satellite and the horizon.

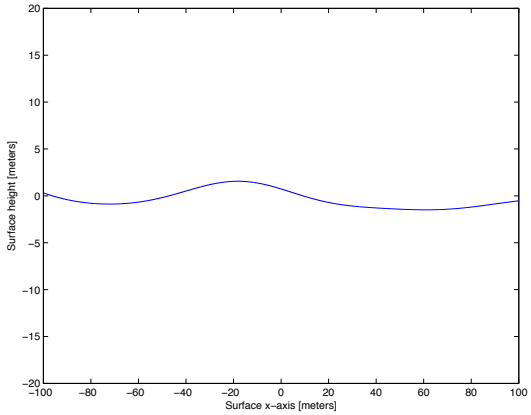

Figure 2: Random surface example. Rms height is 1.25 m, rms slope 0.07 and the resulting correlation length is 25 meters.

2.1.1. *Modeling the sea surface*

Before we can get into the scattering theory, we need a model for a rough sea surface. Although there is a rich theory of models for spectra of sea waves, it has been shown that a simple Gaussian process described by the root-mean-square (rms) height σ and the spatial correlation distance L is a sufficient model for many applications. There is a third parameter, α, that describes the rms slope of the waves. When the waves have a Gaussian spectrum it can be shown that:

$$\alpha = \sqrt{2}\frac{\sigma}{L} \tag{1}$$

This relation is useful when one wants to chose reasonable values for σ and L, as α has been determined empirically for various weather conditions.

2.1.2. *Approximations and conditions*

The Kirchhoff approximation states that the field existing on a point of a surface is the same as if the surface was a plane coinciding with the tangent plane. This approximation is stated to be valid whenever

$$\kappa \gg \frac{\lambda}{4\pi \sin\gamma} \tag{2}$$

where κ is the radius of curvature of the surface, λ is the carrier wavelength and γ is the elevation angle, that is, the angle between the horizon and the direction of observation. Clearly, care must be taken at low elevation angles as not to violate this assumption.

2.1.3. *The scattered field E(p)*

The scattered field off a surface S as seen from a point p in free space, is given by the Helmholtz integral:

$$E(p) = \iint_S \left(E\frac{\partial \psi}{\partial n} - \psi \frac{\partial E}{\partial n} \right) dS \tag{3}$$

where the constituents are as follows in the one-dimensional case:

- Under the Kirchhoff approximation the electric field is equal to $E = (1 + \Gamma)E_1$. Here $E_1 = \exp i\mathbf{k_1} \cdot \mathbf{r}$ where $\mathbf{k_1}$ is the wave-number and $\mathbf{r}$ is a directional vector from the origin to the point $(x, \zeta(x))$, $\zeta(x)$ being a realization of the Gaussian surface. Γ is the reflection coefficient of a smooth plane-wave on a flat surface.
- $\psi = \frac{\exp(ikR)}{R}$ is the reflected wave. R is the distance from the point of observation, p, and the point of reflection $(x, \zeta(x))$. The scalar k is equal to the wave number, $k = \frac{2\pi}{\lambda}$.
- $\frac{\partial E}{\partial n}$ is shorthand for $\nabla E \cdot \mathbf{n}$, $\mathbf{n}$ being the surface normal. Under the Kirchhoff approximation it can be shown that $\frac{\partial E}{\partial n} = i(1 - \Gamma)E_1\mathbf{k_1} \cdot \mathbf{r}$.
- The same goes for $\frac{\partial \psi}{\partial n}$. Computing the derivative yields $\frac{\partial \psi}{\partial n} = \phi\frac{(ik_2R-1)\nabla R}{R}$
- dS is the infinitesimal length of a surface segment at some point x.

2.2. Numerical simulations

This section describes the Monte Carlo simulations. The geometry of the simulations is given in the Figure 1.

Here the assumption is that the satellite is at infinity while the airplane antennas are at a much closer distance. The non-flatness of the earth is not considered, as it will only be an issue at very low angles at which the Kirchhoff approximation is invalid anyway.

The Monte Carlo simulation is performed as follows:

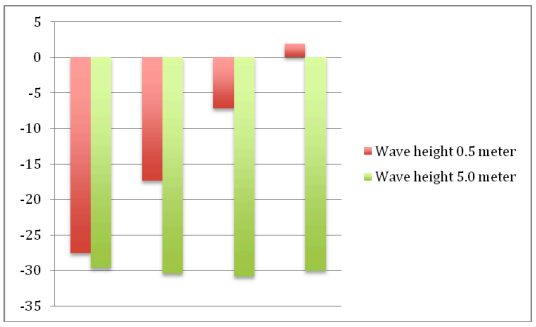

Figure 3: Specular-to-diffuse power ration [dB]. From left to right the bars represent the elevation angles 20, 15, 10 and 5 degrees.

1. Filtering white Gaussian noise using a spatial correlation filter having a Gaussian shape and correlation length L creates a series of surfaces. An example of a surface is shown in Figure 2 for rms height 1.25 meters, and rms slope 0.07 – which corresponds to a wave correlation distance of 25 meters.

2. For each surface the Helmholtz integral is evaluated. We use a mesh size of $dx = \frac{\lambda}{10}$, and assume that the aircraft is at height h and x-position zero. The antennas are placed at 0, a, $2a$, $3a$, and so on, where a typically is some multiple of a wavelength.

3. For each antenna position a series of complex channel gains are now available, and we can compute their correlation.

3. EXPERIMENTAL RESULTS

3.1. Prelimenary simulations

The experiments are performed for a carrier frequency of 1.5 GHz, which corresponds to a wavelength of 0.2 meter. This means that the integration resolution is 2 cm, or 50 points per meter. Clearly, integration domains in the order of tens of kilometers make for very intensive simulations, motivating the use of smaller domains. On the other hand, using too small domains result in a less rich scattering environment and consequently more correlation between antennas.

As an initial experiment we will focus on a low altitude aircraft scenario with h=1000 meter and a domain of integration equal to -30000 to 5000 meters. Here x-coordinate equal to zero corresponds to the point right below the aircraft. The satellite is assumed to be at minus infinity. We then compute the average power of the specular and diffuse components per surface area for several elevation angles. The results are shown in Figure 4a through Figure 4h for elevation angles 20, 15, 10 and 5 degrees above the horizon, as well as wave heights of 0.5 and 5.0 meters[1]. The immediate interpretation of these results is as follows:

- The effective surface area contributing to the reflected power increases with decreasing elevation angles.
- The ratio between specular and diffuse power increases with decreasing elevation angles.
- The main contribution to the specular reflection comes from the area around the glistening point – the surface point where the elevation angle is equal to the observation angle to the aircraft.
- For an elevation angle equal to five degrees and wave height 0.5 meters, the surface seems to be effectively flat and the specular component dominates.

All of the above observations are consistent with theory. Based on the above observations we can adjust our domain of integration. The parameters used are summarized in Table 1.

Finally, the specular-to-diffuse power ratio is shown in Figure 3. Clearly, for the 0.5 meter wave height scenario, the specular component becomes relatively stronger when the elevation angle decreases. For the 5.0 meter wave height scenario this effect is not seen, which indicates that the surface roughness is sufficient to completely annihilate the specular component for elevations at least down to 5 degrees.

3.2. Antenna correlations

The correlation between antennas on an aircraft traveling at an altitude of 1000 meters is estimated for several elevation angles: 5, 10, 15 and 20 degrees. The wave heights are 0.5 and 5.0 meters. For each combination of elevation angle and wave height, 1000 random surfaces were generated and the electric field at each of the antennas was computed.

All simulations are summarized in the graphical representations in Figure 5 and 6. We make the following conclusions from these figures:

- The correlation between antennas increases as the elevation angle decreases.
- Larger wave heights results in less correlation between antennas for all elevations.
- The correlation is more dependent on the elevation angle than the wave height.

[1] When wave heights are specified without the explicit use of the term rms, it is assumed that the wave height corresponds to four standard deviations. This means that there is a 95% likelihood of any wave to be below the wave height when measured from trough to crest.

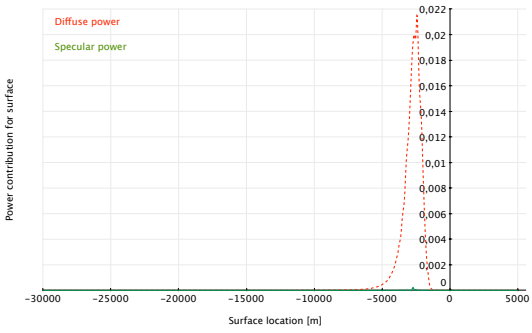

(a) Elevation 5 degrees, wave height 0.5 m

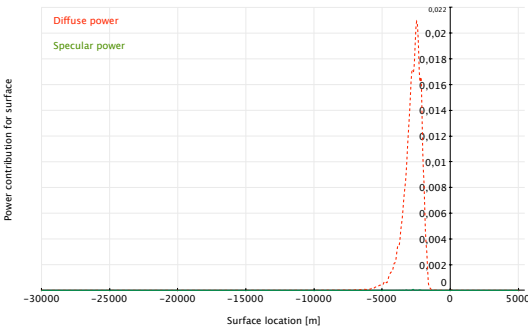

(b) Elevation 5 degrees, wave height 0.5 m

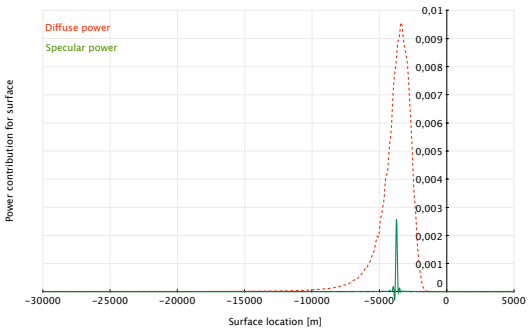

(c) Elevation 5 degrees, wave height 0.5 m

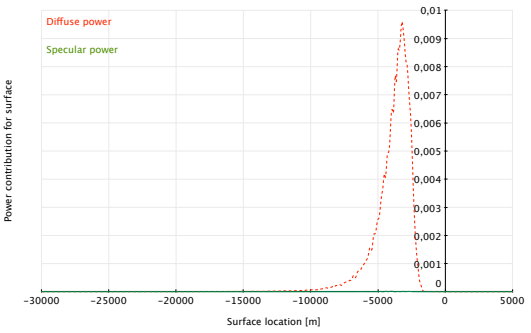

(d) Elevation 5 degrees, wave height 0.5 m

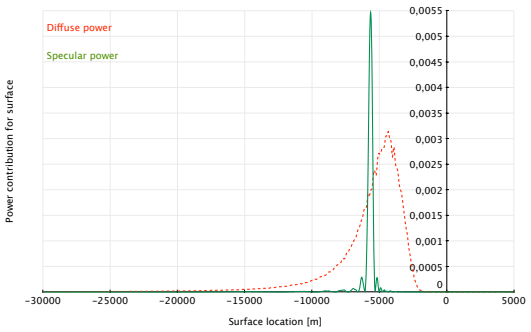

(e) Elevation 5 degrees, wave height 0.5 m

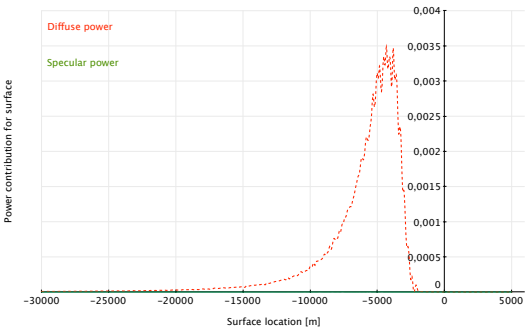

(f) Elevation 5 degrees, wave height 0.5 m

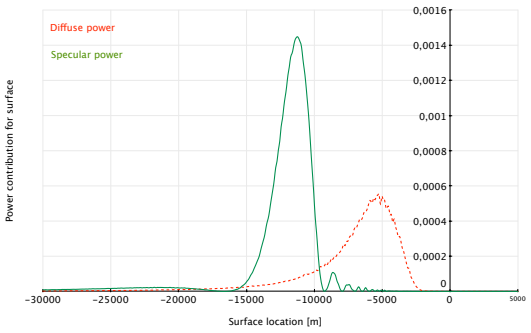

(g) Elevation 5 degrees, wave height 0.5 m

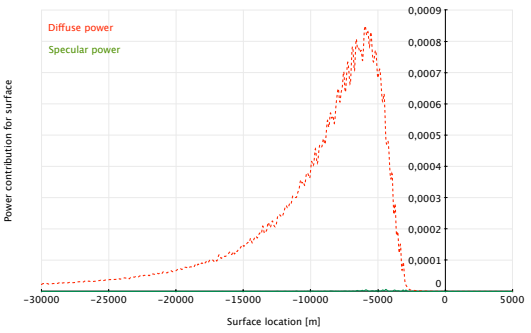

(h) Elevation 5 degrees, wave height 0.5 m

Figure 4: Specular (solid green) and diffuse (dashed red) power contributions from surface.

Table 1: Simulation parameters for the various scenarios

Physical parameters			Integration range	
Elevation	Waveheight	RMSSlope	Lower bound	Upper bound
5	0.5	0.07	-30000	0
5	5.0	0.07	-30000	0
10	0.5	0.07	-15000	0
10	5.0	0.07	-15000	0
15	0.5	0.07	-10000	0
15	5.0	0.07	-10000	0
20	0.5	0.07	-7500	0
20	5.0	0.07	-7500	0

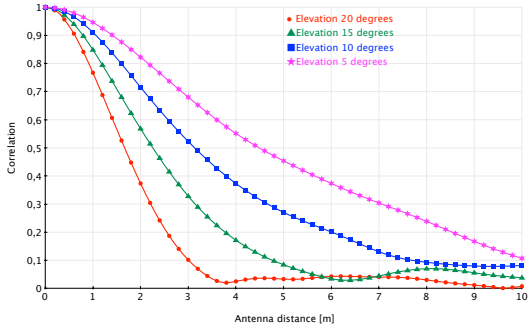

Figure 5: Correlation between antennas as a function of distance. Wave height 0.5 meters.

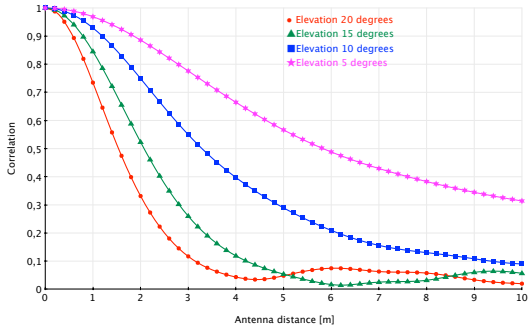

Figure 6: Correlation between antennas as a function of distance. Wave height 5.0 meters.

It may seem counter-intuitive that the correlation increases with the surface area contributing to the reflection. A larger surface implies a richer scattering environment, which should result in less, not more correlation. The explanation for this observation may be found by considering the effective wavelength of the incoming signal at low elevations (see Figure 7). For a wave height of 0.5 meters and a wavelength of 0.2 meters, the effective wavelength will be larger than the wave height when the elevation angle is less that arcsin(0.2/0.5) = 23.6 degrees. For low angles the phase variations will no longer be uniformly random over 0 to 2π, but rather narrowly distributed.

Why the larger wave height is showing more correlation than the small wave height is less clear. Since both scenarios use the same rms slope, the correlation lengths are different and makes them difficult to compare. Using the same rms slope as in the 0.5 meter model will lead to very choppy waves, which in turn leads to blocking at low elevations.

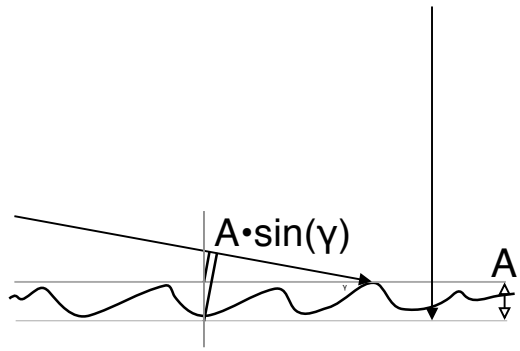

Figure 7: The effective wavelength of an incoming EM wave. Given a surface with a total variation A, the observed variation at an angle γ is $A \sin\gamma$. Equivalently, the effective wave length of the EM wave is $\frac{\lambda}{\sin\gamma}$.

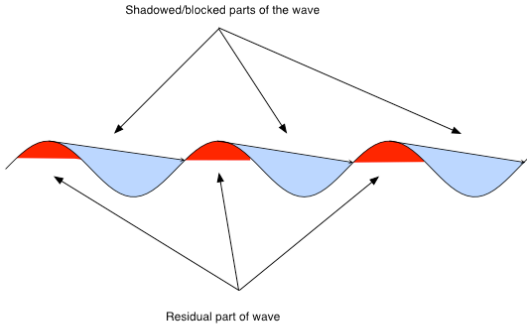

Figure 8: Shadowing/blocking of EM wave by sea surface. The figure shows the blocking of incoming waves from the satellite.

4. CONCLUSIONS

Using a simple one-dimensional representation of a rough sea surface we have investigated the antenna diversity corresponding to the signal reflected from the surface. Depending on the elevation angle and surface roughness, the channel gain correlation is less than 0.2 when the antennas are 3-10 meters apart. Finally, we want to discuss some of the shortcomings of this model and how they may impact the results:

1D vs. 2D: A 2D model will on one hand have a richer scattering environment, but on the other hand, the scattered field will attenuate as r^{-2} as opposed to r^{-1}. As the fastest decorrelation occurs for high elevation angles with smaller effective reflective surface areas, the attenuation may not be very important given that a "sufficiently" large area of the surface contributes. In that respect, the richer scattering environment should imply that the 1D simulations are an upper bound on the decorrelation.

Backscattering and shadowing: These effects have not been considered in this work. The backscattering effect is believed to be of little importance as it mostly affects the overall attenuation of the reflected signal. The shadowing or blocking effect may impact our results in theory, at least for large wave heights and low elevation angles. See Figure 9 where part of the surface is blocked by waves. The figure indicates that the effective surface wave height may be reduced, which in turn could increase correlation.

Polarization: Polarization has only been considered in the sense that a horizontally polarized EM wave is reflected perfectly from the surface. This is according to theory when considering plane waves and surfaces. A vertically polarized wave would see an elevation angle dependent attenuation. For a 1D surface this is sufficiently accurate, but for a 2D surface the full modeling of polarization effects should be undergone.

COPYRIGHT

5. REFERENCES

[1] P. Beckmann and A. Spizzichino, *The scattering of electromagnetic waves from rough surfaces*. Norwood, Mass.: Artech House, c1987.

[2] P. Bello, "Aeronautical channel characterization," *Communications, IEEE Transactions on*, vol. 21, no. 5, pp. 548–563, 1973.

Technology for a better society

www.sintef.no